Design and Operation of the Synthesis Gas Generator System for Reformed Propane and Glycerin Combustion

By

Derek Kyle Pickett

Submitted to the graduate degree program in Mechanical Engineering and the Graduate Faculty of the University of Kansas in partial fulfillment of the requirements for the degree in Master of Science.

_____

Chair: Dr. Christopher Depcik

_____

Dr. Bedru Yimer

_____

Dr. Edward Peltier

_____

Dr. Susan Williams

Defended: December 18, 2013

Design and Operation of the Synthesis Gas Generator System for Reformed Propane and Glycerin Combustion

By

Derek Kyle Pickett

The Thesis Committee for Derek Pickett certifies that this is the approved version of the following thesis:

_____

Chair: Dr. Christopher Depcik

_____

Acceptance Date

Abstract

Due to an increased interest in sustainable energy, biodiesel has become much more widely used in the last several years. Glycerin, one major waste component in biodiesel production, can be converted into a hydrogen rich synthesis gas to be used in an engine generator to recover energy from the biodiesel production process. This thesis contains information detailing the production, testing, and analysis of a unique synthesis generator rig at the University of Kansas.

Chapter 2 gives a complete background of all major components, as well as how they are operated. In addition to component descriptions, methods for operating the system on pure propane, reformed propane, reformed glycerin along with the methodology of data acquisition is described. This chapter will serve as a complete operating manual for future students to continue research on the project.

Chapter 3 details the literature review that was completed to better understand fuel reforming of propane and glycerin. This chapter also describes the numerical model produced to estimate the species produced during reformation activities. The model was applied to propane reformation in a proof of concept and calibration test before moving to glycerin reformation and its subsequent combustion.

Chapter 4 first describes the efforts to apply the numerical model to glycerin using the calibration tools from propane reformation. It then discusses catalytic material preparation and glycerin reformation tests. Gas chromatography analysis of the reformer effluent was completed to compare to theoretical values from the numerical model. Finally, combustion of reformed glycerin was completed for power generation. Tests were completed to compare emissions from syngas combustion and propane combustion.

Table of Contents

Chapter 4: Investigation of Glycerin Reforming and Syngas Combustion

Table of Figures

Table of Tables

Nomenclature

Abbreviation	Description
A/F	Air to Fuel Ratio
AFV	Air Fuel Valve
ATDC	After Top Dead Center
BTDC	Before Top Dead Center
C_3H_8	Propane
CEA	Chemical Equilibrium with Applications
CH_4	Methane
CI	Compression Ignition
CO	Carbon Monoxide
CO_2	Carbon Dioxide
cRIO	Compact RIO
DC	Direct Current
DoE	Department of Energy
ECU	Engine Control Unit
EGR	Exhaust Gas Recirculation
EPA	Environmental Protection Agency
FID	Flame Ionization Detector
GC	Gas Chromatograph
GM	General Motors
H_2	Hydrogen
H_2O	Water
HC	Hydrocarbons
KU	University of Kansas
LFE	Laminar Flow Element
LHV	Lower Heating Value
N_2	Nitrogen
NI	National Instruments
NO_x	Nitrogen Oxides
O_2	Oxygen
PP	Pure Propane
REG	Renewable Energy Group
RFS	Renewable Fuel Standards
RG	Reformed Glycerin
RP	Reformed Propane
RPM	Revolutions Per Minute
SM	Steam Methanation
TCD	Thermal Conductivity Detector

TDC	Top Dead Center
TV	Throttle Valve
VAC	Voltage Alternating Current
VDC	Voltage Direct Current
WGS	Water Gas Shift

Variable	Description	Units
A_s	Reformer Surface Area	[m^2]
a	Moles Carbon Dioxide	[mol]
b	Moles Hydrogen	[mol]
c	Moles Carbon Monoxide	[mol]
d	Moles Water	[mol]
e	Moles Nitrogen	[mol]
f	Moles Fuel	[mol]
g	Moles Methane	[mol]
h	Molar Enthalpy	[J/g]
h_c	Convective Heat Transfer Coefficient	[$W/m^2/K$]
K_{WGS}	Water Gas Shift Equilibrium Constant	[ ]
K_{SM}	Steam Methanation Equilibrium Constant	[ ]
m	Mass Flow Rate	[g/s]
MW_{Sample}	Species Molecular Weight	[g/mol]
n	Molar Flow Rate	[mol/s]
p	Pressure	[Pa]
Q	Heat Transfer Rate	[J/s]
Q_{LHV}	Mass Based Lower Heating Value	[MJ/kg]
R_u	Universal Gas Constant	[J/mol/K]
X	Volume Fraction	[ ]
Y	Mass Fraction	[ ]
$[Sample]$	Species Concentration	[mol/m^3]
ϕ	Equivalence Ratio	[ ]
α	Fuel Source Carbon Atom Count	[ ]
β	Fuel Source Hydrogen Atom Count	[ ]
γ	Fuel Source Oxygen Atom Count	[ ]

1.1 Introduction

As petroleum prices continue to rise, there is an increasing need for non-petroleum based fuels. The current amount of crude oil consumption is around 86 million barrels per day and is predicted to reach 110.6 million barrels per day by 2030 [1]. One possible source of alternative fuel, biodiesel, can be derived from biomass feedstocks (e.g., soybean). This bio-based diesel can augment or replace petroleum based diesel with little to no modifications needed for most diesel engines [2]. Currently, biodiesel is already being blended with traditional petroleum fuels and is used in many countries around the world [3]. Of importance, biodiesel is the only commercially available fuel for compression ignition (CI) engines in sufficient quantities that meets the Renewable Fuel Standards (RFS) set by the Environmental Protection Agency (EPA) [4]. Upcoming mandates surrounding biofuels (including bio-based ethanol) in the United States requires a dramatic increase in the supply of these alternative fuels. The EPA requires that by 2022 at least 36 billion gallons of renewable fuels are to be used each year [4]. Tax breaks and subsidies are already in place to motivate an increased production of biodiesel; however, the development of improved technologies is required to make biodiesel an economic solution to petroleum-based diesel. A sustainable solution to the monetary feasibility of biodiesel involves the analysis of its production methods.

The most common method to produce biodiesel is through transesterification. This process refers to the catalyzed chemical reaction of a renewable lipid feedstock, such as vegetable oil or animal fat, and an alcohol, most commonly methanol, to yield fatty acid alkyl esters (biodiesel) and glycerin [5]. In the United States, canola and soybean oil are the most common feedstocks for biodiesel production. Other feedstock oils include rapeseed, jatropha, castor, and palm oils that all have different compositions and fatty acid profiles [3]. Differences in composition affect the yield and quality of the biodiesel produced; however, a study of this dissimilarity is not part of this effort. There are some downsides to biodiesel production using vegetable oil as a feedstock even though it is a renewable

resource. There has been some debate regarding this option because the use of fertile lands needed to produce biofuels reduces the available land area for food crops [6]. In addition to this competition with food, the use of land for biodiesel feedstock also increases the destruction of natural habitats [7]. However, assessments of biodiesel production have shown that it is an economic solution to the United States dependence on oil [8]. Similar to the petroleum industry, it is as important to investigate the downstream components (aka byproducts) of biodiesel production when considering costs.

One significant byproduct of biodiesel production is crude glycerin. Glycerin is a colorless, odorless, nontoxic, highly viscous liquid that is widely used in the food and pharmaceutical industry, as well as in the production of soaps. Of importance to this effort, glycerin is considered one of the leading sources of hydrogen production because of its naturally renewable derivation, as well being carbon dioxide (CO_2) neutral [9]. Crude glycerin can be refined into pure glycerin by refining (e.g., distillation) and purification.

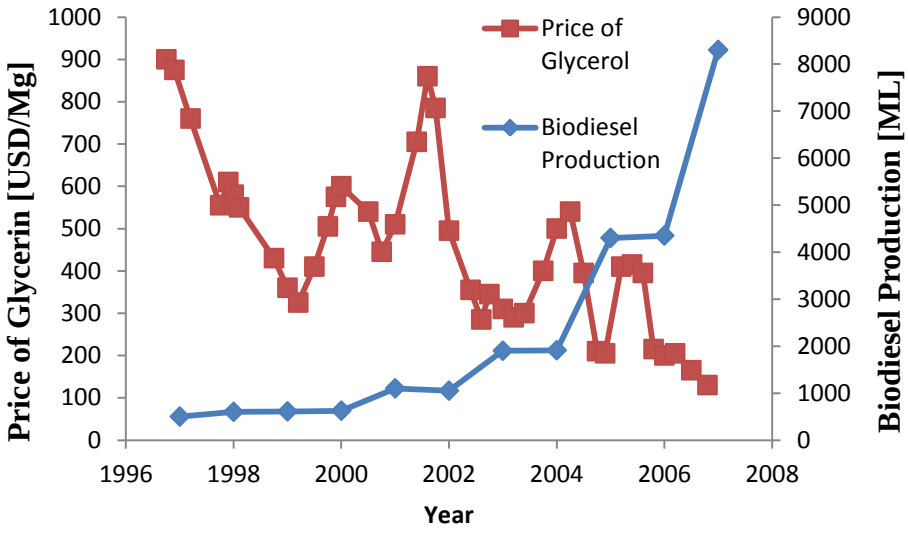

Figure 1 – Price of glycerin and biodiesel production as a function of year [10, 11].

With respect to the economic feasibility of biodiesel, it was found that as EPA mandates promoted the dramatic growth of biodiesel production, the increased volume of glycerin saturated the

market and the price of crude glycerin dropped dramatically [12]. Figure 1 indicates the increase in biodiesel production and drop in glycerin cost as a function of time.

Initially, biodiesel plants were able to purify and sell the glycerin, but as prices continued to drop it became necessary for plants to simply discard the crude glycerin. Nearly all small facilities were forced to dispose of this by-product as a waste stream, subsequently making biodiesel less economically competitive with traditional fuels [13]. At low costs of crude glycerin, the viability of it as a commodity becomes a concern for the biodiesel industry. In order to provide an illustration of the magnitude of the issue, the Department of Energy (DoE) estimates that further displacing 2% of petroleum usage with biodiesel will result in an additional 800 million pounds of glycerin produced each year [14]. Some large-scale biodiesel facilities continue to purify and sell glycerin, but as prices continue to fall it is becoming less economically feasible [13]. As a result, it is necessary to find an inexpensive use for crude glycerin.

One possible option is to convert glycerin into a hydrogen rich synthesis gas through partial oxidation and steam reforming techniques. The synthesis gas can be used in hydrogen fuel cells, hydrocracking, upgrading to other fuels (e.g., methanol), or with an internal combustion engine. Glycerin cannot be used directly as a fuel because it is subject to caking or settling and solidifying in the fuel lines [15]. Researchers have attempted to use glycerin as a fuel additive, but they are unable to get the fuel mixture to atomize and burn properly at high glycerin concentrations because of its relatively large viscosity. Studies completed using glycerin at low concentrations as a fuel additive have shown that rising glycerin content causes hydrocarbons (HC), carbon monoxide (CO), and nitrogen oxides (NO_x) concentrations to increase while brake thermal efficiency (i.e., fuel economy) decreases. This is because the greater fuel viscosity, even at low glycerin concentrations, causes a reduction in fuel atomization resulting in an increased ignition delay [15-19].

As a result, for combustion purposes, glycerin should first be converted into a hydrogen rich gaseous mixture (syngas) through catalytic methods. This hydrogen rich fuel can be then burned in an

engine to create power and potentially coupled to a generator in order to produce direct energy. With respect to hydrogen, it is expected to play a major role in energy supply in the future because of its clean burning nature [20, 21]. A secondary reason why reforming is beneficial is to reduce emissions. Although glycerin is non-toxic, the acrolein fumes created from directly burning glycerin are extremely toxic [17]. A catalytic aftertreatment system could help reduce these fumes, but the syngas produced from glycerin reforming has the potential to burn significantly cleaner in an engine.

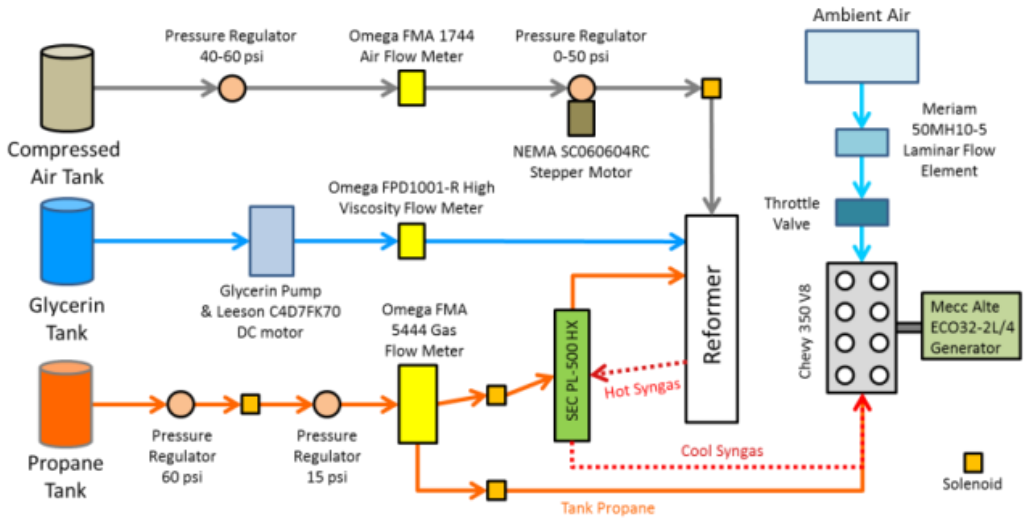

Figure 2 – Flow structure of the synthesis gas generator rig at the University of Kansas

At the University of Kansas (KU), a unique experimental setup includes a full-scale reformer and Chevy 350 in^3 V-8 engine used to reform glycerin and create power from its subsequent syngas. A glycerin/water mixture is supplied to the reformer and is converted to a hydrogen rich gas over a nickel catalyst. The resulting syngas is sent to the engine for combustion and power generation with the generator. It is also possible to supply pure propane to the engine as a way to calculate required energy content of the fuel at all generator loads. A numerical model was written to calculate the flow rates of the glycerin/water mixture and air that needs to be supplied to the reformer to produce syngas with matching energy content. Before reformed glycerin combustion was achieved, the model was first used for reformed propane combustion. This effort proved that combustion of a reformed fuel is possible, as

well as providing a tool to validate and calibrate the numerical model. Figure 2 indicates the different flow patterns of the rig including pure propane combustion, reformed propane combustion, and reformed glycerin combustion.

1.2 Thesis Efforts

Chapter 2 gives a complete description and background of the unique experimental setup, hereto referred as the "syngas rig", at the University of Kansas. The first part of this chapter provides a complete description of each major device on the rig, as well as an explanation of data acquisition components. The second section of Chapter 2 consists of control and operation of the rig including propane combustion in the engine, fuel reformation, reformed propane combustion, reformed glycerin combustion, data collection, and shutdown procedures. This chapter will serve as an operating manual for the entire syngas rig for future students so they may continue research using this system.

The third chapter discusses the process of propane reforming and its subsequent combustion as a precursor to the final goal of glycerin reforming. Literature research was completed to fully understand the reactions taking place during conversion of glycerin. This literature study was completed to describe the derivation of a numerical model used and its application in the experimental section. Also described in this chapter is a discussion about calibration of the model in order to apply it directly to glycerin reforming and its subsequent combustion.

The fourth and final chapter discusses glycerin reforming and its subsequent engine combustion including the use of the generator. This chapter provides additional background of glycerin reforming with respect to the fundamental reactions taking place, specifically the water gas shift reaction. Detailed in this chapter is an application of the numerical model developed in Chapter 3 to predict the glycerin-water mixtures that produce the syngas with the highest hydrogen content. A parametric study was completed that calculates the products of glycerin reformation and is compared to experimental findings. Additionally, this chapter describes the catalytic material preparation that is necessary for

glycerin reforming. Finally, this chapter indicates the experimental side of glycerin reforming and the combustion of the syngas produced that includes the electrical power created by the engine and generator system. This includes a complete emissions analysis, as well as coupling the energy generated through the syngas system with the requirements for biodiesel production.

Chapter 2: Detailed Description and Operating Procedure of the Syngas Rig

2.1 Background and Description of Syngas Rig Equipment

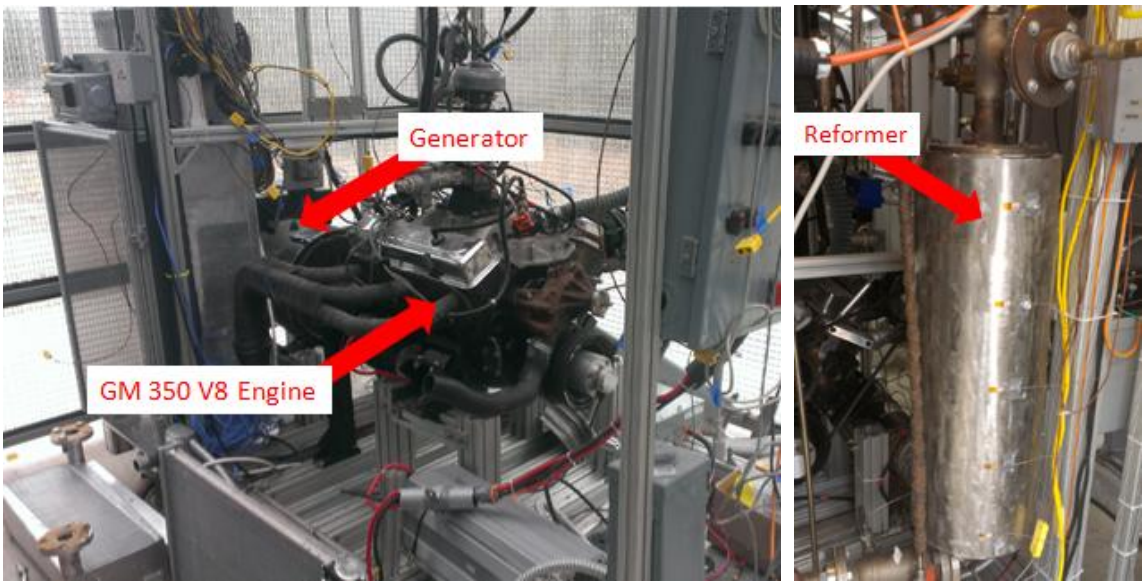

Figure 3 – Synthesis gas generator with important features indicated.

The syngas rig at KU consists of four major components: reformer, engine, generator, and data acquisition system. Successful operation of the syngas rig requires a detailed description of all components along with how they operate. Figure 3 shows the unique syngas rig with the major items indicated.

2.1.1 Reformer Background and Description

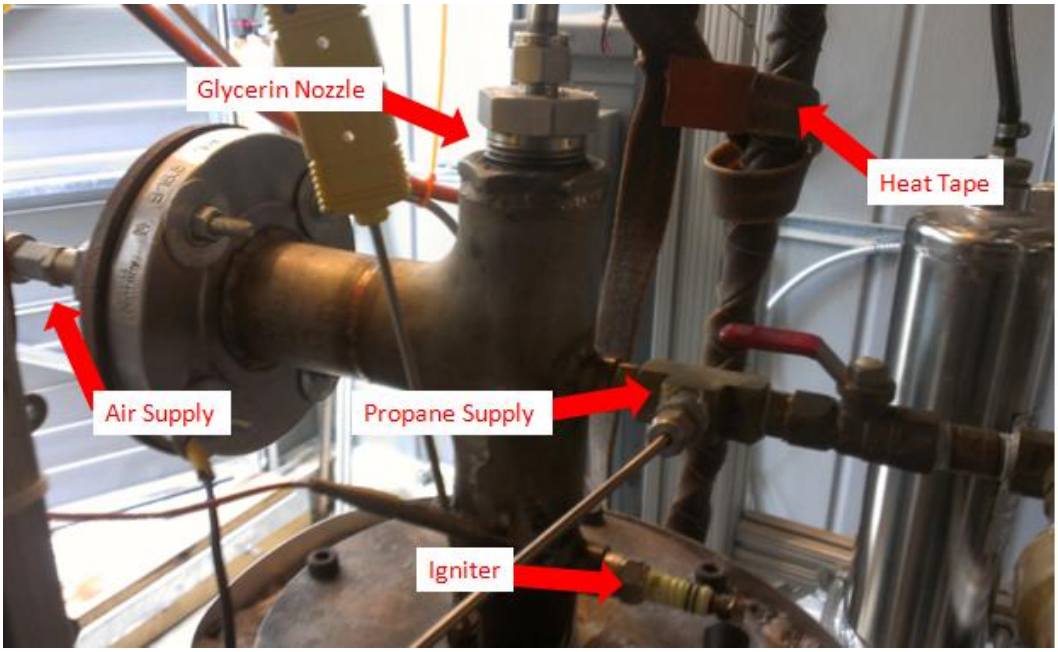

Figure 4 - Top section of reformer with important components indicated

The first major piece to be discussed is the reformer. The reformer, indicated in Figure 4, is where partial combustion of the different fuels (e.g., propane and glycerin) takes place resulting in the production of syngas. There are connections to the reformer for the two types of input fuel (gaseous and liquid phase). A quarter inch hose line connection allows bottled gas to be supplied to the reformer, primarily propane as configured. Propane is supplied at approximately 15 psi from a 60-gallon propane tank. The combustion of propane serves to preheat the reformer, as well as calibrate the numerical model as discussed in Chapter 3. Typically, the air-to-fuel ratio for propane is significantly rich in order to keep temperatures relatively low in the reformer while producing a significant amount of hydrogen and carbon monoxide for running the engine.

Once preheating of the reformer is completed, the second fuel input source (glycerin) can be utilized. There is a Delavan DLN WDB 30 degree nozzle with 120 mesh strainer at the top of the reformer where glycerin can be supplied. A custom direct current (DC) motor and pump setup was created to transport the glycerin to the reformer through a quarter inch hose from a 60-gallon tank that stores a

glycerin and water mixture. Note that the use of water with glycerin will be discussed later in this thesis. Partial combustion of glycerin is typically more difficult than that of propane; hence, in order to make combustion happen more readily, the glycerin is preheated through the pumping line by a heat exchanger with Omegalux HTWC101-006 heating tape wrapped around the line. Glycerin requires a temperature greater than 554 degrees Fahrenheit to vaporize [22], and the heat exchanger and heat tape pre-heats the mixture to around 300 degrees F before reaching the nozzle. The energy supplied to the heat exchanger is from the outlet heat of the reformer. Hence, the glycerin-water mixture is not vaporized prior to entering the reformer; however, pre-heating this mixture does help facilitate the two-phase (liquid & gaseous) reactions occurring within the reformer.

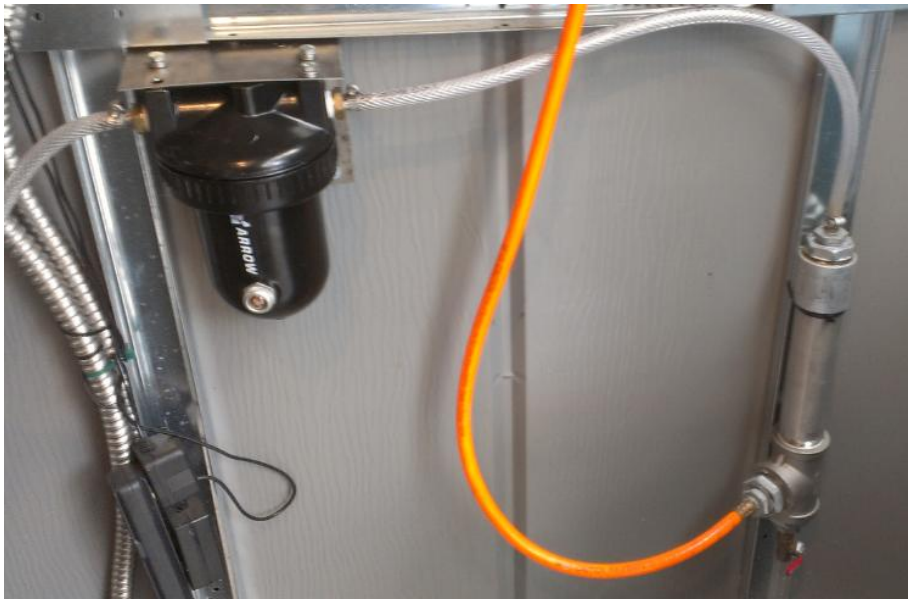

Figure 5 - Air dryer (left) and custom flow separator (right) in line before air controller

In addition to the two fuel sources, there is a connection to a compressed air line on the reformer. Air is supplied between 80 and 150 psi by an Industrial Air Super Hi-Flo Single-Stage compressor. Since there is a tendency for water to condense in the line before an air flow meter, an in-line custom flow separator was created where wet air enters, dry air leaves, and any condensed water can be drained periodically. In addition to the custom flow separator, a 4370K5 high pressure steel bowl

air dryer with desiccant material was purchased and placed in line before the flow meter. Both of these devices are shown in Figure 5. The compressed air line is essential in controlling partial combustion in the reformer. In order to maximize the production of hydrogen, combustion must take place in a rich environment. This compressed air line allows for complete control of this process when reforming either propane or glycerin.

Figure 6 – Franceformer 9030 P4 neon transformer used for spark plug igniter.

Upon entering the reformer, the gaseous fuel is ignited by a Bosch Platinum +4 spark plug (note: glycerin ignition occurs through catalytic means as discussed later). The spark plug is powered by a 9000 V Franceformer (9030 P4) neon transformer shown in Figure 6. A transformer converts a given input voltage into either a higher or a lower voltage through modification of the electrical current. This transformer converts 120 VAC to 9000 VDC. Control of the spark plug igniter for partial combustion will be discussed later in the data acquisition and control section.

2.1.2 Engine Background and Description

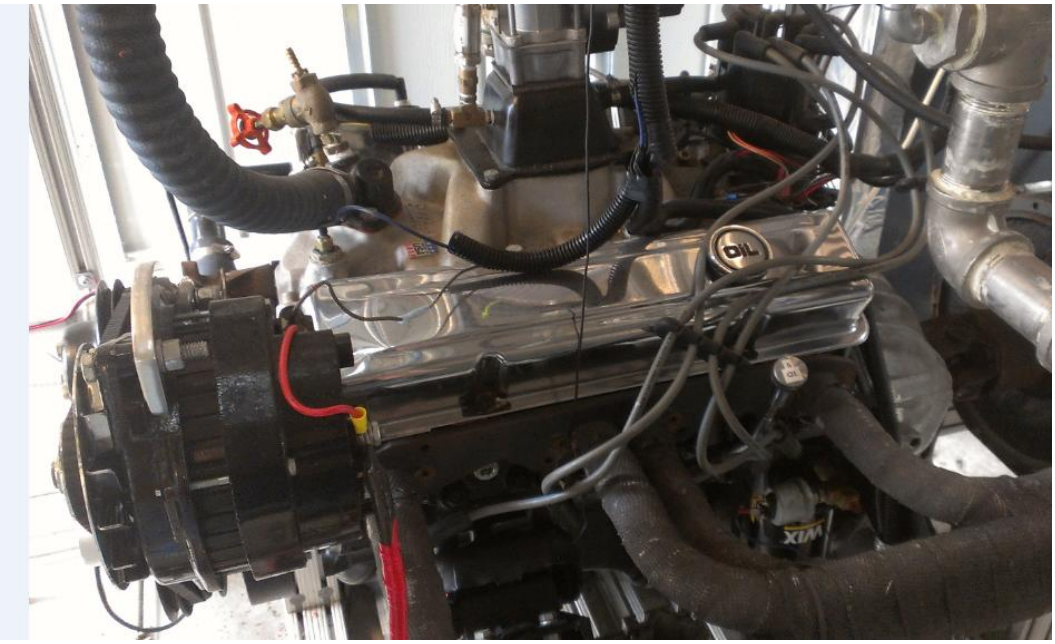

Figure 7 - General Motors engine used in the syngas rig

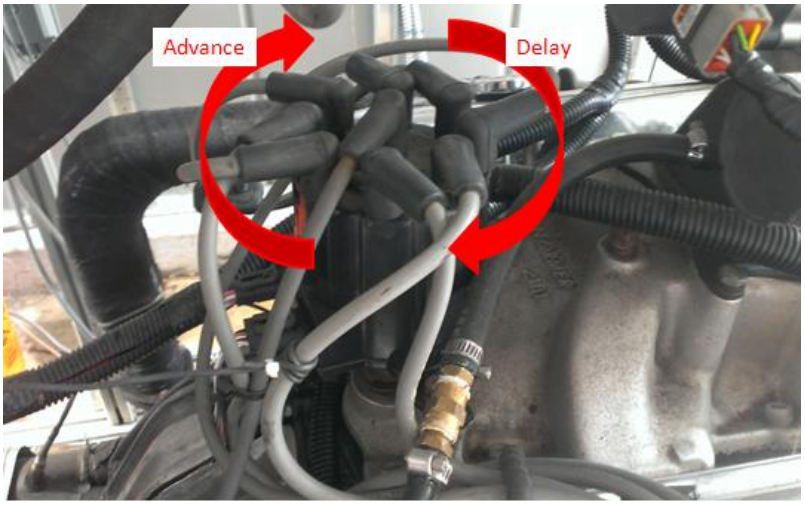

Figure 8 - Engine distributor cap and how to advance or delay the spark

The engine used in this setup is a General Motors (GM) 350 cubic inch V-8 with a compression ratio of 8.2:1. Figure 7 shows the engine used in the syngas rig. The engine is naturally aspirated and has the capabilities of adjusting spark timing, as well as engine speed. The initial spark timing was set for gasoline combustion at 12 degrees after top dead center (ATDC). This spark timing was found not to be

ideal for either propane combustion or syngas combustion. Therefore, in order to reduce fuel consumption and increase engine performance, the idle spark timing was adjusted. In particular, the distributer cap was loosened and rotated while monitoring spark timing in real time, as shown in Figure 8.

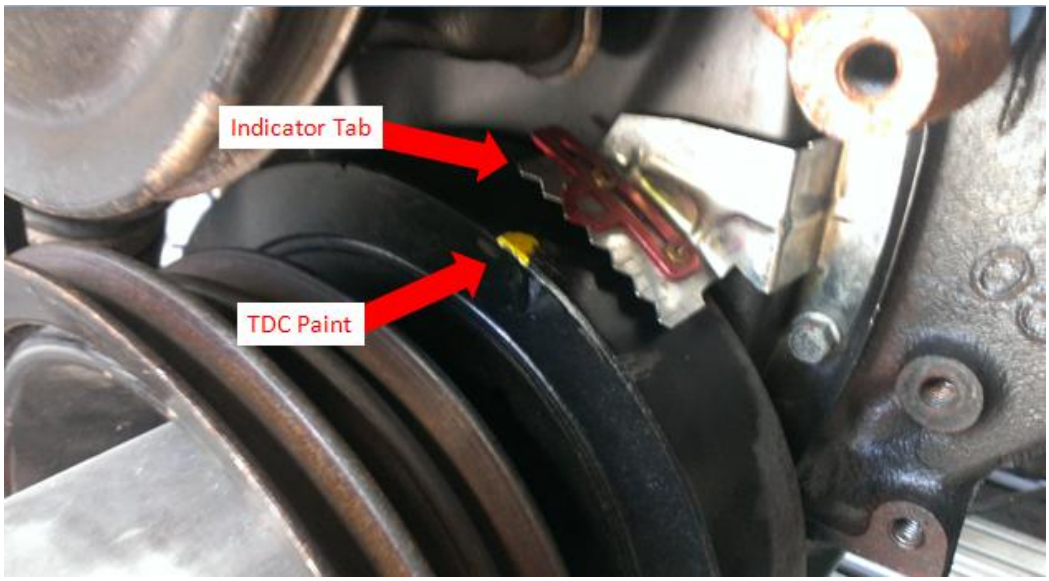

Figure 9 - Crank shaft indicator tab with TDC position indicated

Determination of spark timing in real time occurred by removing the spark plug of the first cylinder of the engine and the engine was manually rotated until the piston head reached the top dead center (TDC) position. At this point, paint was applied to the crankshaft timing indicator tab. Figure 9 shows the indicator tab when the piston of the first cylinder is at TDC.

Then, a spark timing light was used to monitor the spark timing at different distributor cap adjustments. In addition to watching the spark timing on the crankshaft indicator, in-cylinder pressure traces were monitored in order to ensure safe engine performance. In particular, as spark timing is advanced, the pressure rises and must stay within a safe threshold to reduce the tendency for engine knock or excessive combustion pressures [23]. The result is that the new spark timing was set mechanically at 18 degrees BTDC for combustion of pure propane. This timing remained the same for the duration of this effort. Findings demonstrate that fuel consumption was drastically reduced after the

spark timing changes were made. Table 1 indicates fuel flow rates before and after spark optimization at three different loads.

Table 1 - Fuel optimization before and after spark timing adjustments

	Propane Flow Rate Before Spark Optimization [lb/min]	Propane Flow Rate After Spark Optimization [lb/min]
No Load	0.6376	0.2403
One Load	0.7242	0.3404
Two Loads	0.8068	0.4288

Additional spark timing adjustments can be made digitally through use of an aftermarket Dynamic EFI EBL Flash System Engine Control Unit (ECU) employed in the setup. Correct spark timing is essential when operating on reformed fuels in order to ensure the most efficient combustion can take place in the engine. Adjustments made to spark timing for syngas will be discussed further in Chapter 4.

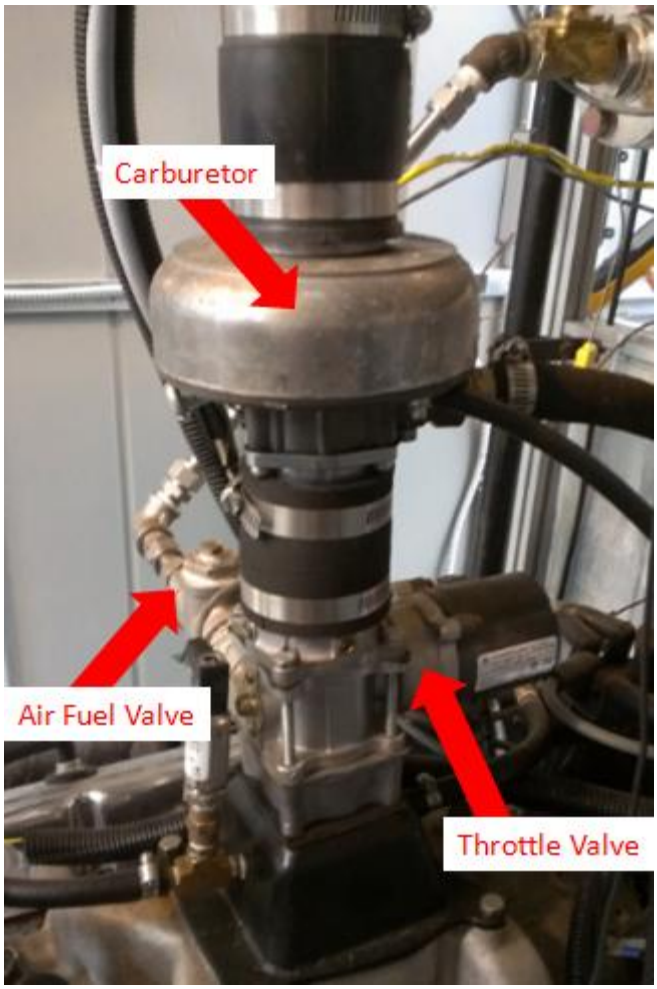

Figure 10 - Air fuel valve, throttle valve and carburetor

A Woodward 8404-3002 Air-Fuel Valve (AFV) and Woodward 8404-4009 Throttle Valve (TV) regulate the air to fuel ratio and air supplied to the engine, respectively and are shown in Figure 10. These components allow adjustments to account for engine speed. Initially, the engine speed was set at 1800 revolutions per minute (RPM) as this speed is necessary for operating the generator at the correct frequency. The engine speed was lowered temporarily to 1200 RPM for reformed propane combustion in the proof of concept test discussed in Chapter 3. In addition to engine speed settings, the throttle valve allows modifications for engine speed ramping. Changes to this setting allow a smoother transition from zero RPM to idle speed. This speed ramp needs to be adjusted periodically throughout the year as ambient air temperature changes. In particular, as the ambient temperature warms during the summer,

a more aggressive speed ramp is necessary compared to when ambient temperature is cooler in the winter.

Initial tests of combustion with pure propane indicated engine overheating issues that needed to be alleviated. This was caused by two primary problems: lack of air flow to the radiator and spark timing. When operating in a vehicle, sufficient air is supplied to the radiator due to movement of the vehicle and overheating issues are not usually a problem. With a stationary engine, this issue was fixed by implementing a large fan to draw air from the environment and into the radiator. Moreover, as mentioned prior, the initial spark timing set for gasoline combustion was much later than that of propane. As a result, advancing the spark timing greatly reduced the engine temperature. When spark timing is set too late, a significant amount of the fuel is still burning when the exhaust valve opens. Moreover, more fuel is used to provide a required generator power reducing the efficiency of the engine (see Table 1) while also increasing the operating temperatures [23]. Thermocouples were placed in the coolant lines before and after the radiator, and upon making the changes mentioned previously, it was found that the operating temperature was reduced by around 15%. Table 2 indicates the drop in engine temperature at all of the different generator loads.

Table 2 - Engine temperature before and after spark timing adjustments

	Engine Temperature Before Spark Optimization [F]	Engine Temperature After Spark Optimization [F]
No Load	224.3	210.4
One Load	245.6	210.7
Two Loads	250.2	215.6

2.1.3 Generator Background and Description

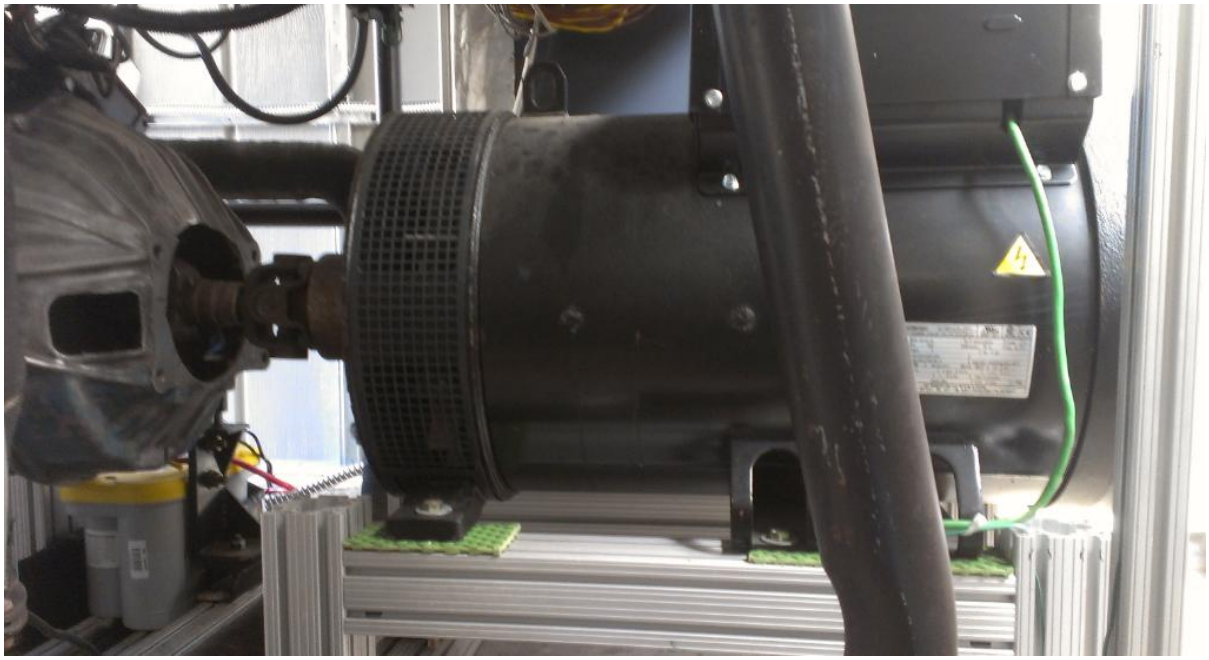

Figure 11 - Mecc Alte ECO32-2L/4 generator used in the syngas rig

The generator used in this system is a Mecc Alte ECO32-2L/4 alternator shown in Figure 11. The generator is equipped with two 240 VAC, 50 amp power outlets in which devices can draw an electrical load. Electric heaters were used to draw power from the system at three different loads. When no heaters are connected, a baseline can be calculated for the engine fueling (i.e., energy) requirements to be used in reformed fuel combustion tests. Adding one heater draws approximately 3.0 kW from the generator and a second heater draws approximately 6.5 kW. The generator is capable of achieving a power output up to 50 kW, but the majority of all tests described are significantly less.

Figure 12 - GCP 20 generator controller

A GCP 20 generator controller, as shown in Figure 12, governs the output. This allows the generator engine speed and power output to be monitored in real time. This controller is directly coupled to the National Instruments (NI) data acquisition device as described in the next section.

2.1.4 Data Acquisition and Control Background and Description

Data acquisition and control of the syngas rig is essential for efficient operation of the setup. There are multiple types of data acquisition and control devices for the rig including thermocouples, pressure transducers, humidity sensors, solenoids, and flow controllers. All of these devices are necessary for collecting data during testing with additional experimental features that will be discussed. The majority of all data acquisition and control is accomplished using NI hardware.

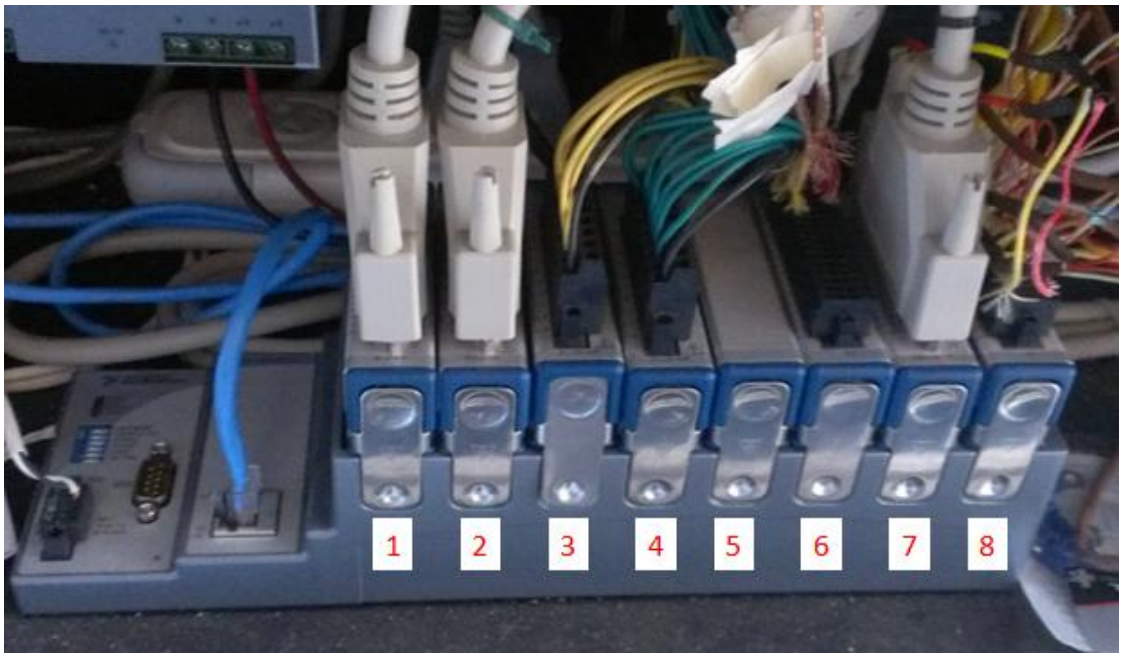

Figure 13 - NI hardware chassis used for primary data acquisition

Figure 13 shows the NI cRIO-9073 chassis, the primary data acquisition port for the entire system. It consists of eight different modules with specific data acquisition capabilities. In port one there is an NI 9205 that is a 32-channel analog voltage input module. This module receives a voltage input from 200 mVDC to 10 VDC for devices such as flow meters. Port two has an NI 9264, a 16-channel analog output module. This module sends up to 10 VDC to various sensors, such as the flow controllers. Both ports three and four have NI 9203 eight channel analog current input modules. These modules read the current supplied by various sensors, such as pressure transducers and humidity sensors. Port five currently is open for any future needs and any style of module could easily be added. Ports six and eight are both using NI 9213 thermocouple modules that read all thermocouples employed in the syngas rig. The last type of module is the NI 9403 located in port seven. This is a 32-channel 5 VDC bidirectional digital input/output module. It is used to control all of the components on the rig that are either “on” or “off”. Examples of this are the various solenoids, engine starter, reformer igniter, and glycerin heat tape. The cRIO is connected to a desktop computer in the control room via an Ethernet cable where all of the data can be monitored and controlled in real time, as well as saved for further calculations and analysis.

Figure 14 - Standard Omegaclad K-Type thermocouple probe used on the syngas rig

Thermocouples (Figure 14) are primarily used in the reformer; however, additional probes are mounted in other locations. The system can collect data for the flame temperature inside the reformer, as well as the catalytic material. It is important to monitor the reformer temperature when partial combustion takes place with the operating temperatures of the reformer to be discussed in more detail in Chapter 3. In addition to the thermocouples in the reformer, there are also probes along the reformer outlet line and on the surface of the reformer to monitor how the syngas cools and to calculate heat loss to the environment. Along with other probes measuring ambient temperature, engine air temperature, propane temperature and others, all of the thermocouple wires meet at the two 16-channel NI 9213 thermocouple input modules. This allows data acquisition for all temperatures in real time.

Figure 15 - PX 319 pressure transducer used on the syngas rig

Pressure transducers (Figure 15) are also an essential data acquisition tool used throughout the setup. The majority of all pressure transducers are Omega PX 319 models; these transducers were chosen due to the relatively low pressures in the reformer lines. All of the transducers used in the system send an analog current signal of 4-20 mA to the 9203 module in ports three and four. Similar to many of the other sensors in the rig, pressure measurements can also be monitored in real time with the LabVIEW software.

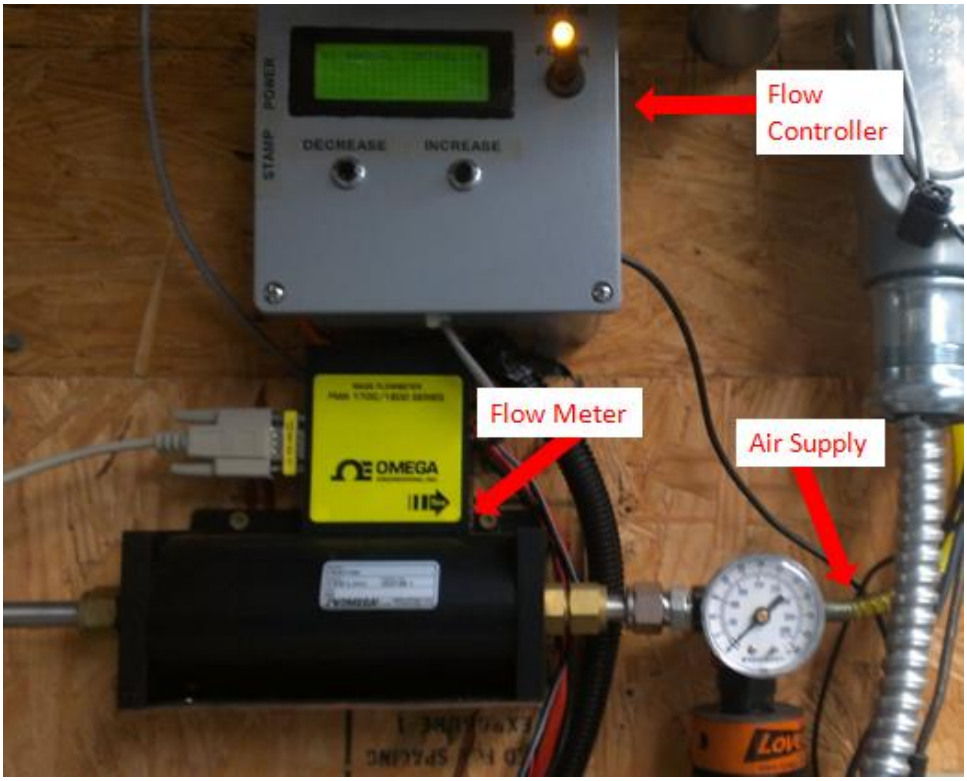

Figure 16 - Air control system with important features indicated

There are three flow controllers in this system, all essential for accurate operation of the syngas rig. The first is used to control air flow from the compressed air line. An Omega FMA 1744 air flow meter is used in line with a custom-built controller operated by a BASIC stamp microprocessor. The controller allows compressed air to be supplied to the reformer at a flow rate up to 12.1 g/s. The limiting factor on maximum air supply is the compressor that is unable to produce pressures above 150 psi. Adjustments to air flow rates can be made by pressing the “increase “ or “decrease” buttons as shown in Figure 16.

Figure 17 - Omega gas flow controller for propane (or other combustible gasses)

The second flow controller is an Omega FMA 5444 gas flow controller and meter shown in Figure 17 used for the bottled gas line. Tests completed by this author used propane for analysis described in Chapter 3, but other combustible gasses could potentially be used. The flow controller is placed before the heat exchanger in order to stay within the operating temperatures of the controller. The original design of the syngas rig had the controller placed after the heat exchanger, but the high temperature of the propane reduced the accuracy of the meter causing limited repeatability and lowering the precision of the tests. Both of these flow meters send a 0-10 VDC signal to the NI 9205 analog input module so that flow rates can also be monitored in real time.

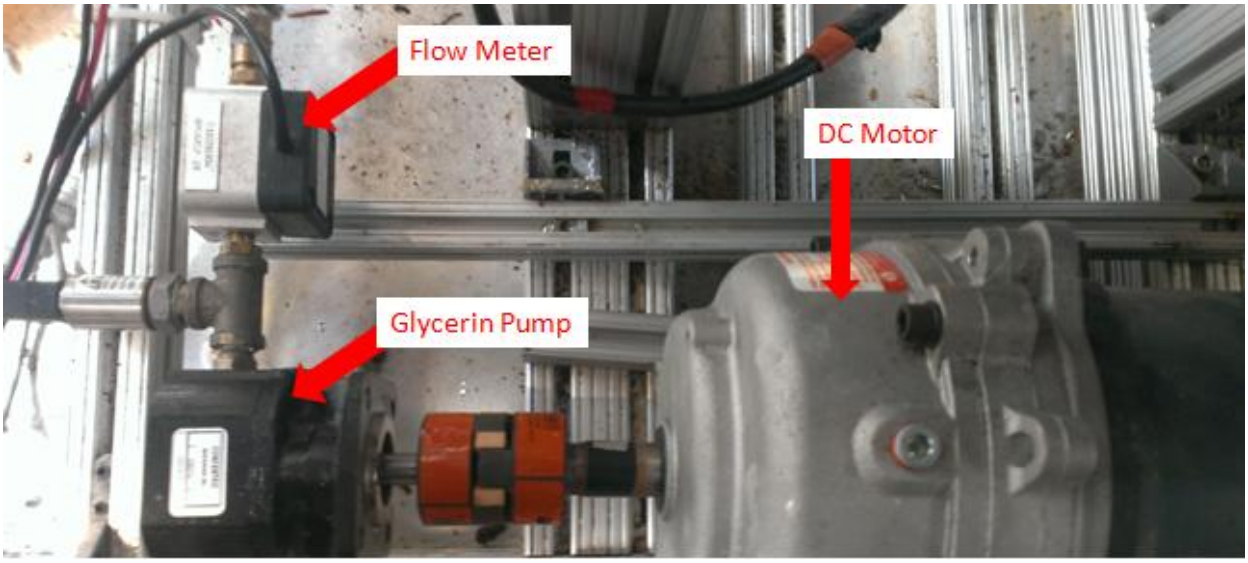

Figure 18 - Glycerin control with important components indicated

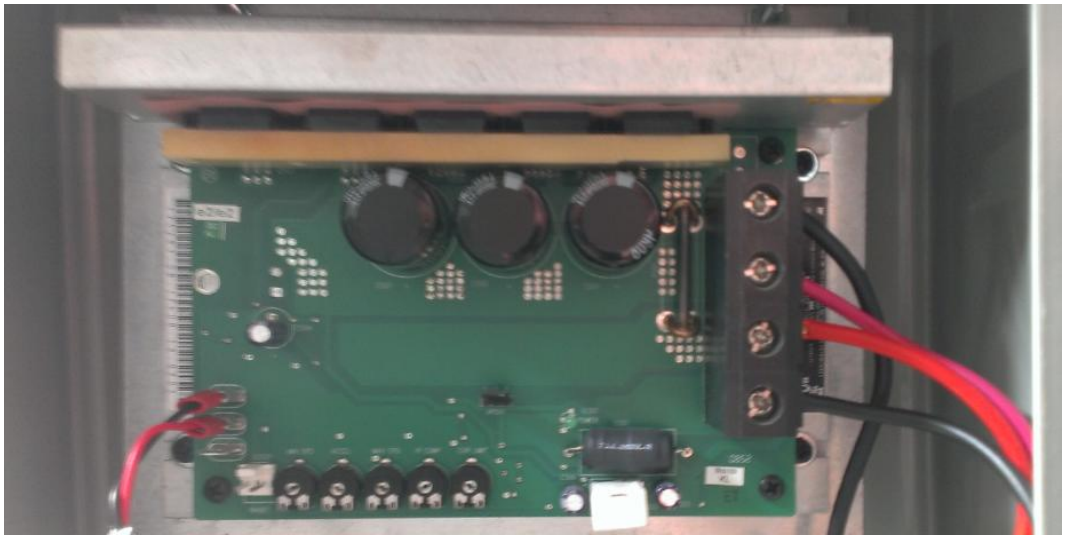

Figure 19 - Glycerin DC motor controller

The final flow control device used is the glycerin flow meter, pump, and control system. A Leeson C4D7FK70 DC motor and 0.46 gallon per minute 4F17 hydraulic pump are used to supply the glycerin as shown in Figure 18. Minimum and maximum speed, torque, and acceleration of the pump are controlled by the Leeson 175291.00 C09 low voltage motor controller shown in Figure 19.

Figure 20 - Glycerin control converter from pulse input to analog input

An Omega FPD 1001-R high viscosity flow meter is used to monitor glycerin flow. This device has a pulse output signal that cannot be monitored by the data acquisition system in place. The solution was to convert this pulse output to an analog 4-20 mA output as shown in Figure 20. This device was calibrated by holding the 4 and 20 mA buttons when no flow and maximum flow occur respectively.

All of the components connected to the cRIO chassis are listed in Table 3. This table indicates what type of signal is being sent, where it is sent, and where the component is found on the syngas rig.

Table 3 - Syngas sensors with location and use described

	Pin	Signal	Location
Port 1 - NI 9205	VI0	0-10 V DC Input	Environmental Pressure
	VI1	0-10 V DC Input	Environmental Temperature
	VI2	0-10 V DC Input	Environmental Relative Humidity
	VI3	0-10 V DC Input	Laminar Flow Element Pressure
	VI4	0-5 V DC Input	Engine Water Temperature
	VI5	0-5 V DC Input	Engine Oil Pressure
	VI6	0-5 V DC Input	Throttle Valve Position
	VI7	0-5 V DC Input	Air/Fuel Valve Position

	VI8	0-10 V DC Input	Reformer Air Flow Meter
	VI9	0-10 V DC Input	Battery Voltage
Port 2 - NI 9264	VO1	0-10 V DC Output	Glycerin DC Motor Controller
	VO2	0-10 V DC Output	Air Flow Controller
	VO3	0-10 V DC Output	Propane Flow Controller
	VO4	0-10 V DC Output	Propane Flow Controller
Port 3 - NI 9203	AI0	4-20 mA Analog Input	Laminar Flow Element Pressure
	AI1	4-20 mA Analog Input	Glycerin Flow Meter
	AI2	4-20 mA Analog Input	Post Glycerin Pump Pressure
	AI3	4-20 mA Analog Input	Glycerin Pre Reformer Pressure
	AI4	4-20 mA Analog Input	Air Pressure Pre Flow Meter
	AI5	4-20 mA Analog Input	Syngas Post Cyclone Pressure
	AI6	4-20 mA Analog Input	Engine Intake Pressure
	AI7	Open	-
Port 4 - NI 9203	AI0	4-20 mA Analog Input	GCP 20 Controller
	AI1	4-20 mA Analog Input	GCP 20 Controller
	AI2	Open	-
	AI3	4-20 mA Analog Input	Post Reformer Pressure
	AI4	Open	-
	AI5	Open	-
	AI6	Open	-
	AI7	Open	-
Port 5 - Open	-	-	-
Port 6 - NI 9213	TC0	Thermocouple Input	Reformer Surface Thermocouple 1
	TC1	Thermocouple Input	Reformer Surface Thermocouple 2
	TC2	Thermocouple Input	Reformer Surface Thermocouple 3
	TC3	Thermocouple Input	Reformer Surface Thermocouple 4
	TC4	Thermocouple Input	Reformer Surface Thermocouple 5
Port 7 - NI 9403	DIO0	Digital Input/Output	Main Propane Solenoid
	DIO1	Digital Input/Output	Engine Propane Solenoid
	DIO2	Digital Input/Output	Syngas to Engine Solenoid
	DIO3	Digital Input/Output	Syngas Propane Solenoid
	DIO4	Digital Input/Output	Heat Wrap Relay
	DIO5	Digital Input/Output	Reformer Igniter Relay
	DIO6	Digital Input/Output	Back Pressure Close Relay
	DIO7	Digital Input/Output	Back Pressure Open Relay
	DIO8	Digital Input/Output	Engine Starter
	DIO9	Digital Input/Output	Air Fuel Valve Increase Value
	DIO10	Digital Input/Output	Air Fuel Valve Decrease Value
	DIO11	Digital Input/Output	Reformer Air Valve Open
	DIO12	Digital Input/Output	Reformer Air Valve Close

Port 8 - NI 9213	TC0	Thermocouple Input	Syngas Inlet
	TC1	Thermocouple Input	Glycerin Pre Glycerin Heat Exchanger
	TC2	Thermocouple Input	Glycerin Post Glycerin Heat Exchanger
	TC3	Thermocouple Input	Glycerin Intake
	TC4	Thermocouple Input	Upper Reactor Temperature
	TC5	Thermocouple Input	Reformer Catalyst Temperature
	TC6	Thermocouple Input	Syngas Post Reformer
	TC7	Thermocouple Input	Propane Reformer Supply
	TC8	Thermocouple Input	Propane Tank Supply
	TC9	Thermocouple Input	Syngas Pre Cyclone
	TC10	Thermocouple Input	Syngas Post Cyclone
	TC11	Thermocouple Input	Syngas Pre Intercooler
	TC12	Thermocouple Input	Syngas Post Intercooler
	TC13	Thermocouple Input	Syngas Engine Intake
	TC14	Thermocouple Input	Reformer Air Supply
	TC15	Thermocouple Input	Engine Air Supply

Figure 21 - Shielded input block for in-cylinder pressure measurements

In addition to the components mentioned above, there is another data acquisition device not coupled to the NI cRIO system. In-cylinder pressure measurements are recorded using a standalone NI

SCB-68 shielded input/output connector block shown in Figure 21. Three signals are sent to the NI SCB-68 shielded input/output connector block; pressure, TDC trigger, and an encoder square wave. A Kistler 6052C piezoelectric transducer is used to measure the pressure in the engine along with a Kistler 2614B optical encoder to indicate engine crank angle position.

Figure 22 - Power supply (left) and charge amplifier (right) for in-cylinder pressure measurements

The pressure transducer was implemented in the third cylinder spark plug port. The third cylinder was chosen because it is located between cylinders one and five allowing fewer fluctuations in heat loss than alternative cylinders (i.e., less exposed to ambient). The output of the pressure transducer is a linear change in voltage as the pressure inside the cylinder fluctuates. However, this output voltage is relatively small when compared to the 10 VDC measurement capabilities of the NI system. Therefore, Kistler manufactures a charge amplifier to scale the output voltage of the transducer to a 0-10 VDC signal that can be used with the NI system. In particular, the 5011B charge amplifier shown in Figure 22 scales the output of 1 VDC to 2 bar such that 10 bar of pressure would be represented as 5 VDC.

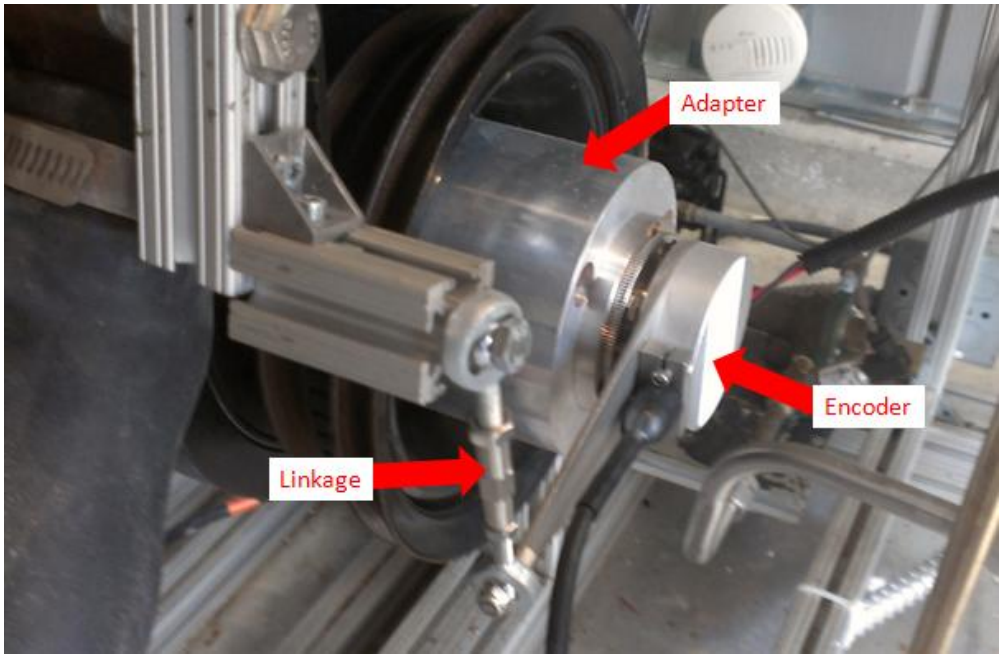

Figure 23 - Encoder adapter and linkage for in-cylinder pressure measurements with important components indicated

In order for the in-cylinder pressure traces to represent useful information, it is important that the pressures be recorded with a corresponding reference to the crankshaft position in the engine. This is accomplished with the Kistler 2614B optical encoder. A reference location is set by manually moving the crankshaft until cylinder three is in its top dead center position (TDC) and adjusting the linkage shown in Figure 23 to the encoders' appropriate TDC signal position. Every time the encoder reaches the TDC position, a pulse signal is sent to the NI SCB-68 shielded input/output connector block. Additionally, a square wave representing incremental change in the encoder position is sent. Finally, the digital signals can be analyzed by the NI hardware for crank angle and pressure signal recording.

Attachment of the encoder to the engine required the production of an adapter from the crankshaft to the encoder as shown in Figure 23. The adapter was machined out of a 6-inch piece of 5-inch diameter aluminum. Shoulder-bolt, counter-bore through holes were drilled with a matching bolt pattern to that of the flywheel, as well as M5X0.8 tap connections for the encoder flange.

2.2 Control and Operation of the Syngas Rig

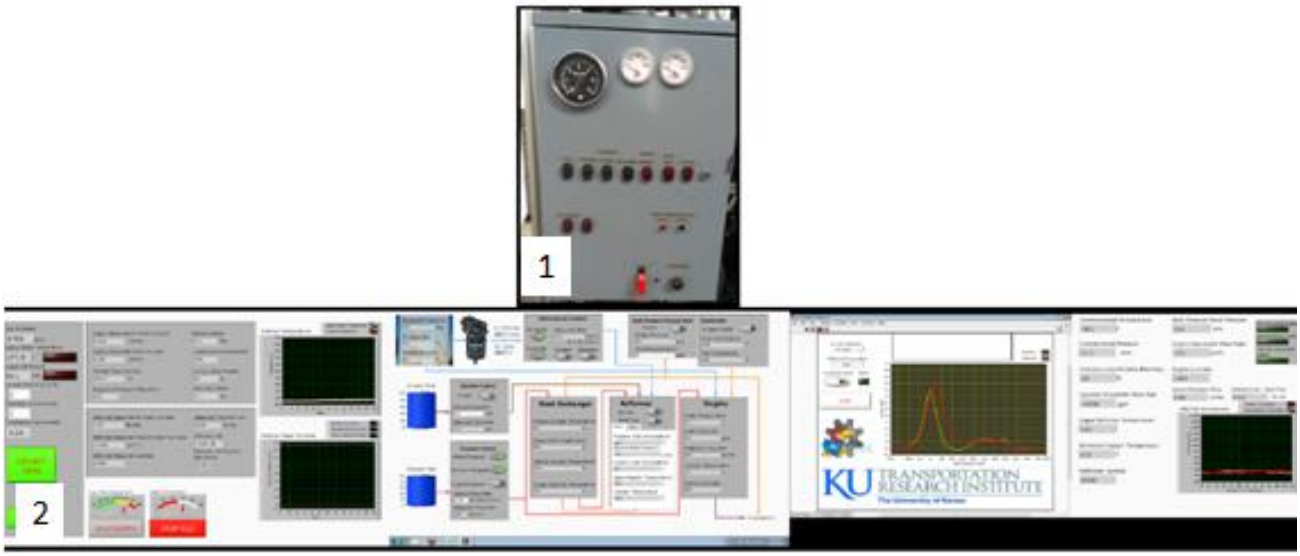

Figure 24 – Control panel in testing area (1) and computer control in control room (2).

There are two ways in which the syngas rig system can be operated; manually in the testing area, or electronically via LabVIEW software in the control room. Although more control and data acquisition is capable when using just the computer software, it is generally more useful to operate with both manual controls and the software working together. Figure 24 shows the control panel in the testing area and computer control in the control room.

This section will give a description on how to operate the four different options of the rig. First of which is engine combustion using propane as a fuel source. The next topic described is partial combustion of propane in the reformer followed by reformed propane combustion in the engine. Finally, this segment will provide a description of the procedure of glycerin reforming and its subsequent combustion.

2.2.1 Operating Procedure for Propane Combustion in the Engine

Figure 25 - Syngas control panel for engine combustion using pure propane

Propane combustion in the engine has two benefits; heating the engine before reformed fuels can be used and finding a baseline for fuel (i.e., energy) requirements in an engine map. This engine map will be discussed further in Chapter 3. In order for combustion to take place, several steps must be taken. After turning on and ensuring that all of the data acquisition systems are running, the master propane solenoid must be opened. This can be done by either flipping the "Master Propane" switch on the control panel in Figure 25 or clicking the "Master Propane" button in the LabVIEW program shown in Figure 24. Once master propane is activated, propane can be sent to the engine by flipping the "Engine Propane" switch on the control panel or clicking the "Engine Propane" button in LabVIEW.

Next, a setpoint must be provided for the propane flow level. This can only be accomplished by inputting a value into the LabVIEW software. The desired setpoint must be greater than the required fuel for combustion at idle, usually around 0.75 lb/min. The carburetor on the setup only allows the required amount of fuel into the engine, and if the set point is lower than this value, combustion will be

difficult to achieve. As long as the controller is set to a higher flow rate than that required by the engine, no excess propane will be supplied since the carburetor is self-correcting.

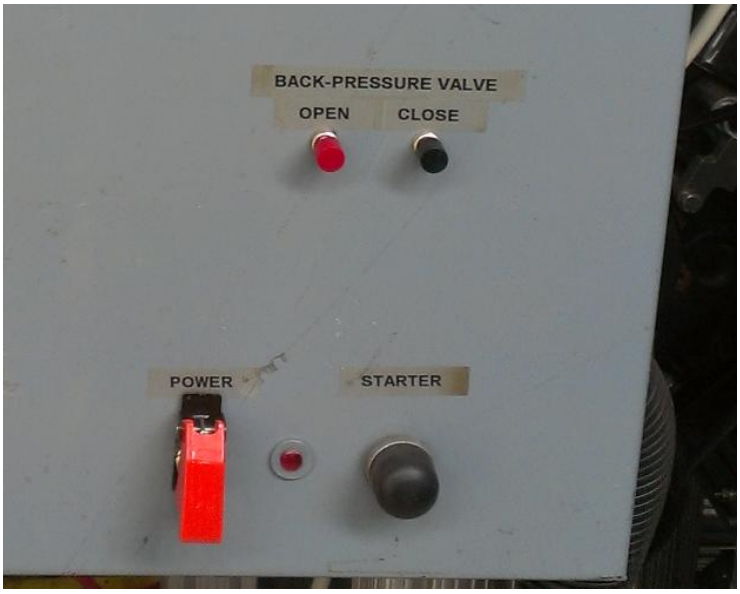

Figure 26 - Control panel showing power and starter button

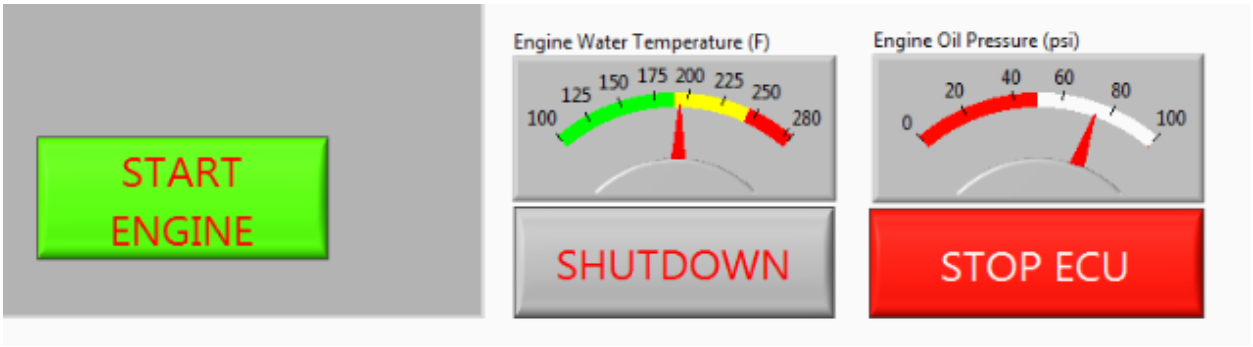

Figure 27 - LabVIEW screenshot showing start engine button and engine dials

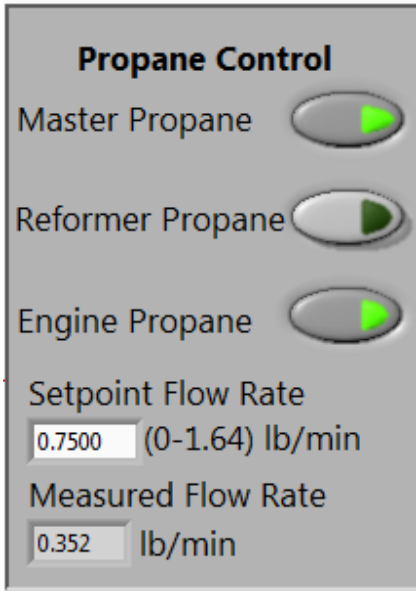

Figure 28 - Propane control window showing engine combustion at no load and 1800 RPM

At this point, it is possible to start the engine by either pressing the "Starter" button on the control panel or clicking "Start Engine" in LabVIEW both shown in Figures 26 and 27 respectively. Once the engine is running, data can be saved or monitored in real time with the computer program. Figure 28 shows the propane control section of the LabVIEW program when the engine is operating at no load and 1800 RPM.

When the engine is running, it is possible to add an energy load to the generator. This is accomplished using two electric heaters (previously mentioned) that are physically plugged into the generator. When the heaters are turned on, the engine will become loaded and the fuel flow rates to the engine will automatically increase (i.e., carburetor will add more fuel). It is essential that the setpoint for the flow rate of propane is still greater than the required fuel flow rate at maximum load (approximately 0.5 lb/min).

2.2.2 Operating Procedure for Partial Combustion in the Reformer

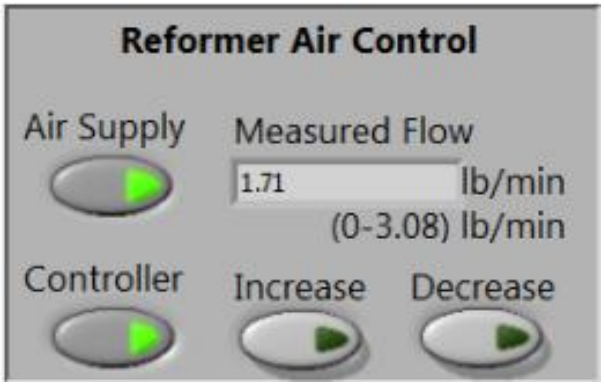

Figure 29 - Air control window during reforming operations

Reforming operations are an important feature of the syngas rig. Similar to propane combustion in the engine, partial combustion in the reformer requires the master propane to engage in the same way as mentioned prior. However, now before sending propane to the reformer, one must ensure that air is supplied first. This is accomplished by pressing the "Air Supply" button in the program and then turning on the controller. The air supply can be set to any desired value with the reformer air control window shown in Figure 29.

In addition, before propane is supplied, it is important to turn on the spark plug in the reformer by flipping the "Igniter" switch on the control panel (Figure 25) or clicking the "Igniter" button in the program. Adding propane before turning on the igniter can result in unwanted combustion in the reformer and cause a potential safety issue.

In order for reforming to take place, the flow rates of air and propane must be set so that combustion takes place in a rich environment; more fuel than air as compared to stoichiometry. Stoichiometry can be calculated using the fundamental molar balance of the combustion equation for propane:

$$C_3H_8 + 5(O_2 + 3.76N_2) \rightarrow 3CO_2 + 4H_2O + 18.8N_2 \quad (1)$$

Equation 1 provides a way to calculate the number of moles required for complete combustion to take place with one mole of propane. Completing the molar balance of this equation shows that for every mol of propane provided, 23.8 moles of air are required. Using the molar weight of propane and air (44.10 g/mol and 28.97 g/mol respectively) the mass air to fuel ratio (A/F) of 15.6 can be found for stoichiometry (i.e., perfect combustion). This means that in order for partial combustion to take place, the A/F ratio must be less than 15.6.

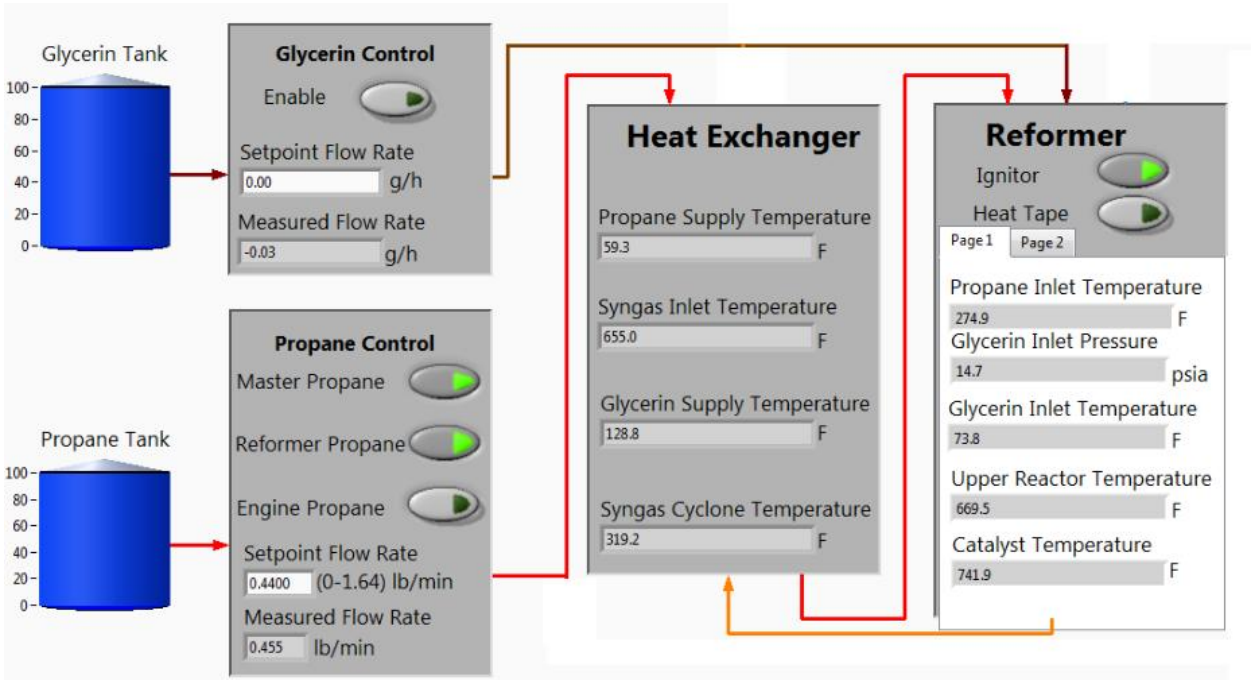

Figure 30 - LabVIEW window during proper reforming operations

Finally, the desired flow rate of propane can be supplied by either flipping the "Reformer Propane" switch or clicking the same button in LabVIEW. When partial combustion is taking place, the upper reactor temperature, as well as catalyst temperature will begin to increase. These temperatures should be monitored at all times to ensure safe operational settings (discussed in Chapter 3). A screenshot of the LabVIEW program during proper partial combustion of propane is shown in Figure 30.

2.2.3 Operating Procedure for Syngas Combustion in the Engine

Syngas combustion in the engine is the primary goal of this effort and a detailed understanding of how it is accomplished is essential. The previous section describes how to achieve partial combustion of propane in the reformer to produce syngas. This step must be completed first before engine operation on syngas is possible.

Figure 31 - Backpressure valve with open position indicated

Figure 32 - Control panel during reformed propane combustion

When just reforming is taking place, the backpressure valve located in Figure 31 is fully open. This allows the syngas to travel through the exhaust lines to the environment bypassing the engine. When the operator is ready to run the engine on syngas, the syngas to engine solenoid must be activated by flipping the “Syngas Engine” switch on. This allows the syngas to travel to the engine intake rather than to the environment. An image of the control panel during propane syngas combustion is shown in Figure 32.

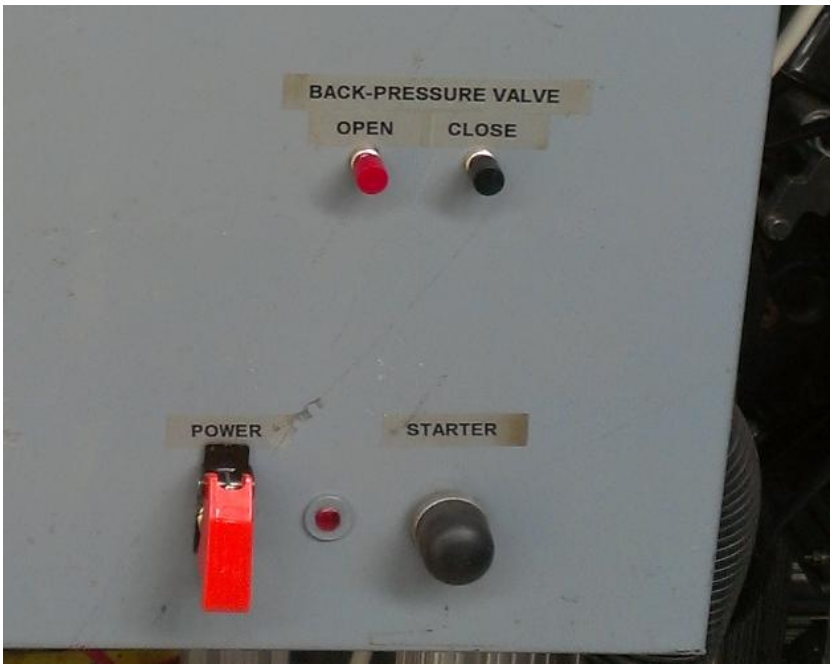

Figure 33 - Control panel showing backpressure valve control and starter location

At this point, it is necessary to push the “Starter” button on the control panel while simultaneously closing the backpressure valve. It is important to note that if the backpressure valve is closed before attempting to start the engine, the pressure in the reforming lines will quickly rise to dangerous levels since air and propane are still being supplied to the reformer. Figure 33 shows the location of the backpressure valve controls and engine starter on the control panel.

The pressure at the backpressure valve must constantly be monitored while attempting to start the engine. Multiple combustion attempts have indicated that a pressure of approximately 17 psi allows

engine combustion to take place. Once the engine is operating at the desired speed, the pressure at this valve will adjust back to atmospheric as the syngas is now traveling to (and effectively through) the engine rather than through the exhaust lines to the environment.

Similar to pure propane combustion in the engine, loading can be applied using reformed propane as a fuel source. The same procedure is taken to load the engine by applying heaters to the generator. Currently, engine combustion on reformed propane is possible for no load (aka idle), one heater, and two heaters. Of note, the exact quantities of propane and air supplied to the reformer to produce the appropriate levels of syngas for combustion in the engine are found using a numerical model as discussed in Chapter 3.

2.2.4 Operating Procedure for Glycerin Reforming and its Subsequent Combustion

The final goal of the syngas rig is glycerin reforming and its subsequent engine combustion. However, before partial combustion of glycerin is possible, the reformer must first be preheated in order to initiate the partial oxidation and steam reforming reactions of the water-glycerin mixture. Propane is used to preheat the reformer through the procedure mentioned previously. An air and propane flow rate of 7.5 g/s and 1.5 g/s, respectively, should be supplied to the reformer to reach the desired initiation temperature. At these flow rates, the mixture of air and propane is sufficiently rich (A/F ratio of 5) allowing the reformer to be heated slowly. An air to fuel ratio closer to stoichiometry would quickly increase the upper reactor temperature without allowing the catalyst temperature to stabilize. Once the acceptable reformation temperature has been achieved (800 K at the upper reactor and 600 K in the catalyst bed), glycerin can then be supplied to the reformer.

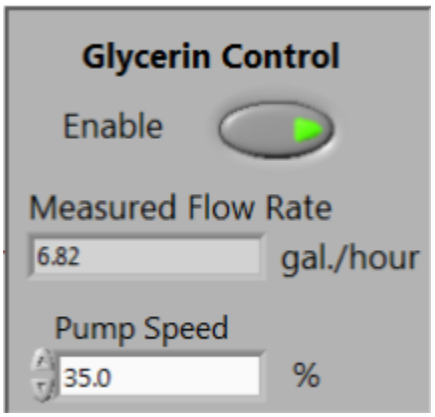

Figure 34 - Glycerin control window during no load reformed glycerin combustion

First, the butterfly valves after the glycerin tank and before the glycerin pump must be opened. Next, the glycerin pump motor controller must be engaged by pushing the "Glycerin Control Enable" button on the LabVIEW software shown in Figure 34. The initial pump speed is always initially set at 0%, but can be increased until the desired glycerin flow rate is achieved.

Once the glycerin motor controller has been enabled, the pump speed can be adjusted by increasing the pump speed percentage box. As glycerin is supplied to the reformer, the upper reactor and catalyst temperature should be monitored. Due to the high viscosity of glycerin, it takes several minutes before the pumping lines are filled and reformation begins to take place. It is evident that exothermic reforming of glycerin begins when the catalyst temperature begins to rise. Before glycerin is supplied, the catalyst bed should stabilize around 600 K.

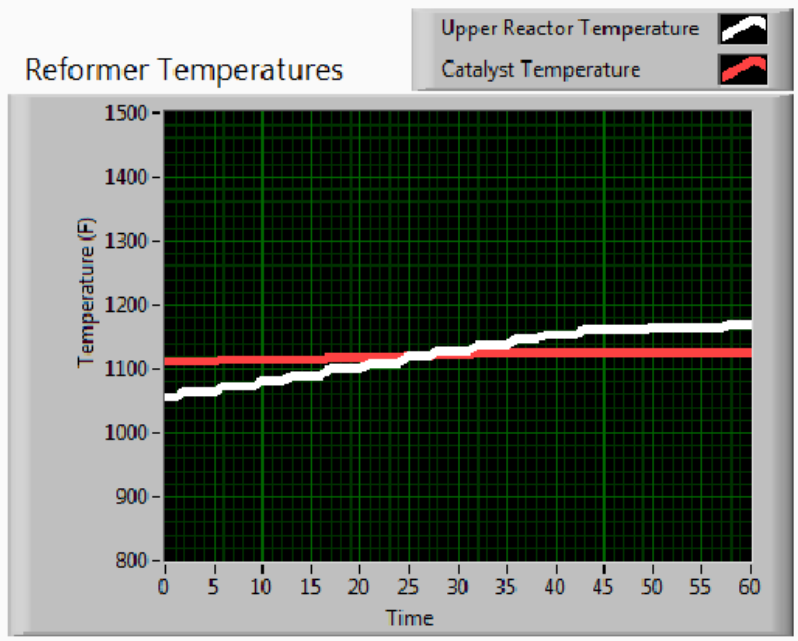

Figure 35 - Temperature of upper reactor and catalytic material during transition to exothermic glycerin reformation.

Once the glycerin is introduced, the catalyst temperature will rise and the upper reactor temperature will simultaneously begin to fall. This is because unlike propane, glycerin cannot be ignited through the spark plug and requires a catalytic process to convert the liquid into a reformed gas. Hence, propane preheats the catalyst bed that causes glycerin to vaporize. Then, upon interacting with the catalytic material, the gaseous glycerin releases energy while converting into a hydrogen rich syngas. Figure 35 indicates the change in upper reactor and catalyst temperature as glycerin is first supplied to the reformer. The X-axis in this figure indicates the amount of time that has passed and a value of zero represents current values.

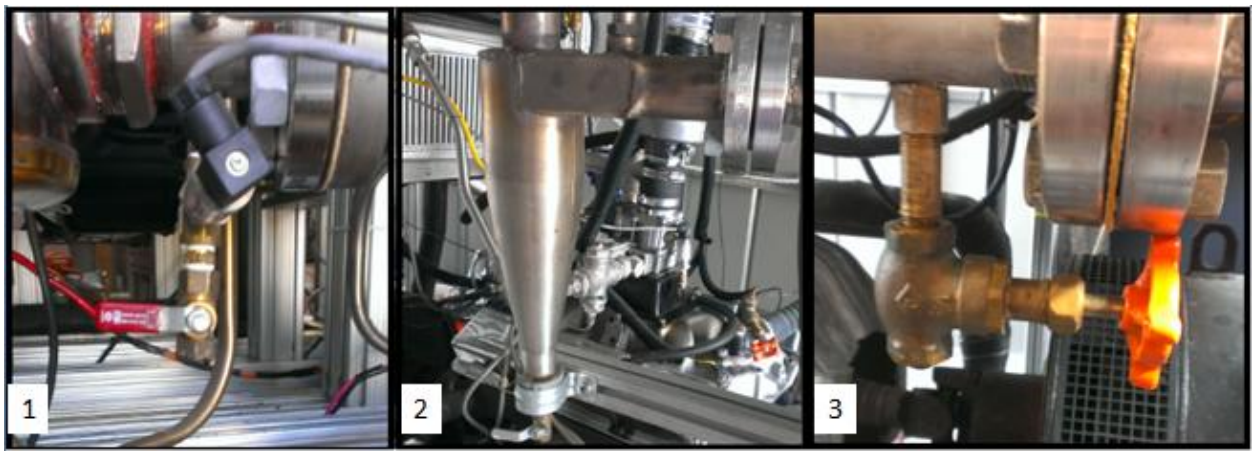

Figure 36 - Post reformer exhaust drain (1), post heat exchanger exhaust drain (2), and post back pressure valve exhaust drain (3).

While glycerin is being supplied it is important to periodically check the three drains at the low points in the reformer lines. The first drain is located between the propane heat exchanger and the reformer, the second is located after the heat exchanger in the cyclone separator, and the third is located after the backpressure valve in the exhaust line. As the syngas travels through the heat exchanger and exhaust lines, the temperature of the gas quickly drops. This drop in temperature leads to fluid condensation in the exhaust lines. These drains should be emptied regularly throughout glycerin reformation and are shown in Figure 36.

The specific values for final reformer temperatures, flow rates of glycerin, and flow rates of air will be discussed in Chapter 4 in order to achieve syngas combustion using glycerin. Once the desired values are reached, the procedure for syngas combustion in the engine is similar to that of reformed propane. The backpressure valve should be closed as the engine starter button is pushed.

It is important to note that propane is still being supplied to the reformer when reformed glycerin engine combustion begins. Since some of the constituents in the reformed glycerin syngas (such as carbon dioxide and water) reduce the likelihood for combustion to begin, adding propane helps initially stabilize engine combustion. Once the engine speed has evened out, the propane flow rate can slowly be reduced until no propane is supplied. At this point, it is possible to close the “Reformer

Propane" and "Master Propane" solenoid valves. It is also possible to turn off the igniter as exothermic reformation of glycerin has already begun. The temperature of the catalyst will remain constant as long as glycerin is supplied.

Similar to reformed propane combustion in the engine, it is also possible to load the generator to produce electricity from the reformed glycerin. Before adding a load to the generator through use of either or both of the two electric heaters, the flow rate of air and glycerin should be increased to the appropriate flow rates. Once the flow rates and temperatures have stabilized, it is possible to load the engine.

2.2.5 Data Collection Procedure

One of the most important aspects of the syngas rig is data collection for further analysis. All of the sensors can be monitored in real time, but it is also beneficial to save this data to complete calculations and compare with previous tests. Two types of data collection are available with the LabVIEW program; system processes data, and in-cylinder pressure traces.

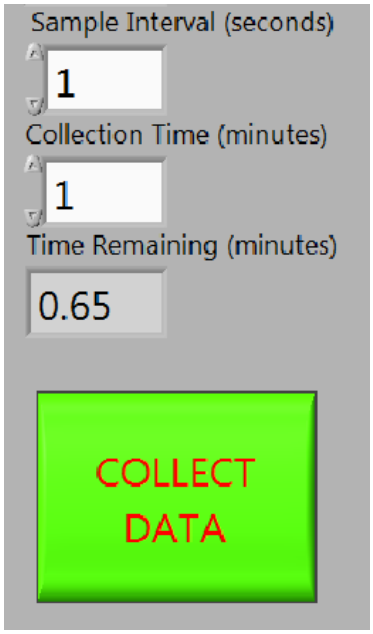

Figure 37 - Data collection window during recording procedure

Recording system process data can be accomplished in the program on the front panel screen as shown in Figure 37. This figure illustrates that the operator can adjust the sample interval and sample length. Sample interval refers to how often a data point is taken and sample length refers to the length of the entire recorded test. The values for these parameters shown in Figure 37 indicate that data will be recorded for one minute with a single data point taken every second. Once the "Collect Data" button is pressed, the time remaining in the data collection can be monitored. Upon completion, a text file is created and the user is prompted to save the file for further analysis.

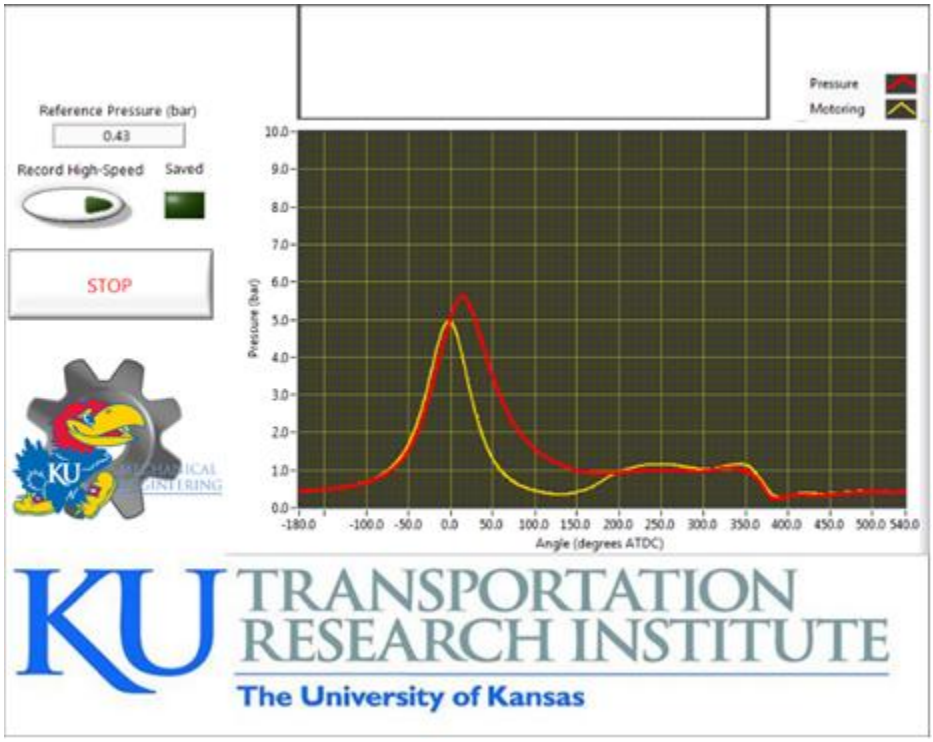

Figure 38 - In-cylinder pressure trace at no load 1800 RPM pure propane engine combustion with the red line indicating the pressure during combustion (yellow line is a motoring trace)

In addition to the data recording available for the system processes, it is also possible to capture data for in-cylinder pressure traces in a similar manner. Figure 38 shows the LabVIEW window of the in-cylinder pressure traces and pressing the "Record High-Speed" button on this screen saves the data.

Data is recorded for 20 thermodynamic engine cycles from -180 degrees BTDC to 540 degrees ATDC and is averaged before being saved. The two curves shown on the graph in Figure 38 indicate a motoring curve in yellow and the current test pressure curve in red. The motoring curve refers to the pressure in the cylinder when combustion is not taking place. The peak in the motoring curve corresponds to when the pressure is highest, near TDC. The red curve corresponds to the actual pressure in-cylinder during combustion. The peak pressure is later than TDC for this curve as expected for optimum performance [23].

2.2.6 Shutdown Procedure

After testing has been completed, implementing a proper shutdown procedure is just as essential as an appropriate startup process. The first step when shutting down the rig consists of unloading and turning off the engine. First the back pressure valve should be opened completely and the heaters can be removed and the power switch shown in Figure 33 can be turned off. Once the engine has stopped, it is often useful to turn the same switch back on in order to continue running the engine coolant fan while the other systems are still operating.

After the engine has been turned off, purging the reformer exhaust lines is necessary. Before turning off the glycerin supply, it is useful to turn on the igniter and begin supplying propane to the reformer again. Once propane is supplied, it is possible to shut off the glycerin pump and close the butterfly valves on the glycerin supply line. As mentioned previously, when reformed glycerin travels through the exhaust lines, there is a tendency for the mixture to condense. Continuing to supply propane and air to the reformer allows the reformed glycerin still in the lines to stay warm and travel to the exhaust. Similar to when running on glycerin, it is important to continue to drain the condensed fluid until no more reformed glycerin passes through the exhaust. It is evident that all of the glycerin is gone and the lines are purged when the smoke in the exhaust lines (seen outside the enclosure) changes from white to clear.

The next step in the shutdown procedure is the cooling of the reformer. In order to close down the reformer, first the igniter must be turned off. If fuel is shut off first, the air-fuel ratio becomes leaner and more towards stoichiometry (ideal combustion) resulting in a temperature rise in the reformer. Turning off the igniter causes the temperature to begin to fall as propane combustion ceases. After which, the flow of propane can be stopped. It is important to remember to close the propane valve when purging has been completed. During this time, it is still necessary to continue supplying air to the reformer because it is relatively hot and needs time to cool. The upper reactor temperature will quickly fall, but the large mass of the catalyst will retain heat for significantly longer. Complete cooling of the reformer may take between 30 minutes to an hour. Once the reformer catalyst has reached a safe temperature (usually 200-300 F), it is possible to turn off the air supply.

The final step in shutting down the syngas rig is turning off the data acquisition components. The shutdown switch can be turned off and the LabVIEW program can be closed by pressing the shutdown button in Figure 27. Finally, it is possible to turn off the charge amplifier and power supply to the in-cylinder pressure components, as well as the cRio power supply.

Chapter 3: Investigation of Propane Reforming and Syngas Combustion

Components of this chapter published as: "Combustion of Reformed Propane as Segue to Glycerin Reforming," D. Pickett and C. Depcik, ASME 2013 International Mechanical Engineering Congress & Exposition Conference, 13-21 November 2013, San Diego, CA (IMECE2013-62355).

3.1 Abstract

Biodiesel is a potential fuel that reduces dependency on petroleum products. Although its upstream fabrication results in it being a renewable resource, the downstream components are the focus of this chapter. Glycerin is a byproduct from biodiesel production and currently has few uses as a means to recover some of the energy required to produce biodiesel. One such option is to convert glycerin into a hydrogen rich mixture over a catalyst for subsequent use in an internal combustion engine. A unique reformer and engine/generator setup at the University of Kansas allows the exploration of propane reforming and its subsequent combustion as the first step into glycerin reforming. In particular, the analysis of propane reforming will lead to the specific experimental conditions (e.g., flow rates) needed prior to glycerin reforming. This chapter will document the experimental side of propane reforming along with models used in its analysis and extrapolation to glycerin.

3.2 Introduction

It is estimated that oil production will peak by 2030 necessitating widespread usage of alternative fuels [5]. In the past several years, biodiesel production has increased as a means to reduce the United States dependence on petroleum sources. Biodiesel is a viable alternative to petroleum because it can readily be used in any diesel engine with little modification while maintaining the same level of performance [9, 24]. The most common way to produce biodiesel is through transesterification. This process refers to the catalyzed chemical reaction of renewable lipid feedstock, such as vegetable oil or animal fat, and an alcohol, most commonly methanol, to yield fatty acid alkyl esters (biodiesel) and

glycerin [16]. There has been some debate on using vegetable oil as a potential feedstock because the use of fertile lands needed to produce biofuels reduces the available land area for food crops [25]. However, assessments of biodiesel production show that it is a potential economic solution to the United States dependence on petroleum [26]. It is important to note that this assessment must include the study of downstream components or byproducts of biodiesel production.

One byproduct created during the production of biodiesel is glycerin, $C_3H_5(OH)_3$, which currently yields about 0.8 pounds of glycerin per gallon of fuel [27]. Glycerin is a colorless, odorless, nontoxic, highly viscous liquid that is widely used in the food and pharmaceutical industry, as well as in the production of soaps. Glycerin is considered one of the leading sources of hydrogen production because of its naturally renewable derivation, as well being carbon dioxide (CO_2) neutral [28]. However, glycerin cannot be used directly as a fuel because it is subject to caking or settling and solidifying in the fuel lines. Researchers have attempted to use glycerin as a fuel additive, but they are unable to get the fuel mixture to atomize and burn properly at high glycerin concentrations in an engine due to its high viscosity (also causing an increased ignition delay) [17]. Fuel additive studies completed using glycerin at low concentrations have shown that increasing glycerin content causes hydrocarbon (HC), carbon monoxide (CO), and nitrogen oxide (NO_x) concentrations to increase while brake thermal efficiency decreases [15, 17-19].

As a result, for combustion purposes glycerin should first be converted into a hydrogen rich gaseous mixture (syngas) through catalytic methods, such as partial oxidation. This hydrogen rich fuel can be then burned in an engine/generator system in order to produce energy. Hydrogen is expected to play a major role in energy supply in the future because of its clean burning nature [20, 21]. A secondary reason why reforming is beneficial is to reduce emissions. Although glycerin is non-toxic, acrolein fumes that are created from directly burning the glycerin are extremely toxic [17]. A catalytic aftertreatment

system could help reduce these fumes, but the syngas produced from glycerin reforming has the potential to burn significantly cleaner.

At the University of Kansas (KU), a unique experimental setup includes a full-scale reformer and Chevy 350 in^3 V8 engine used to reform glycerin and create power from its subsequent syngas. Moreover, work is underway at understanding the chemical process of glycerin reformation across nickel catalysts using a small reactor scale. This is geared towards optimizing the catalytic materials and maximizing hydrogen production. However, since nickel sinters at 1073K [29] utilizing this material in the full-scale reformer and testing via trial and error is not a smart tactic. As a result, propane is used to find the different flow rates for running both the reformer and engine. This will minimize the effort when it comes to using glycerin while also providing a safe avenue for the catalytic material. It is important to mention that it does not make sense to reform propane prior to combustion in an engine because of the loss of available energy. However, this methodology at dialing in the right conditions for the reformer will allow easier setup of glycerin. This is similar to numerical studies that used methane for the reforming fuel (e.g., [30]); however, in this effort, both simulation and experimentation provides a more reliable transition to glycerin.

As a result, this chapter describes a simplified fuel reforming combustion model. Moreover, an explanation of the experimental setup including the reformer and engine is provided. Furthermore, experimental results are presented with respect to propane reforming and subsequent syngas combustion. Finally, a parametric study is indicated that will lead into the combustion of reformed glycerin in the following chapter.

3.3 Modeling

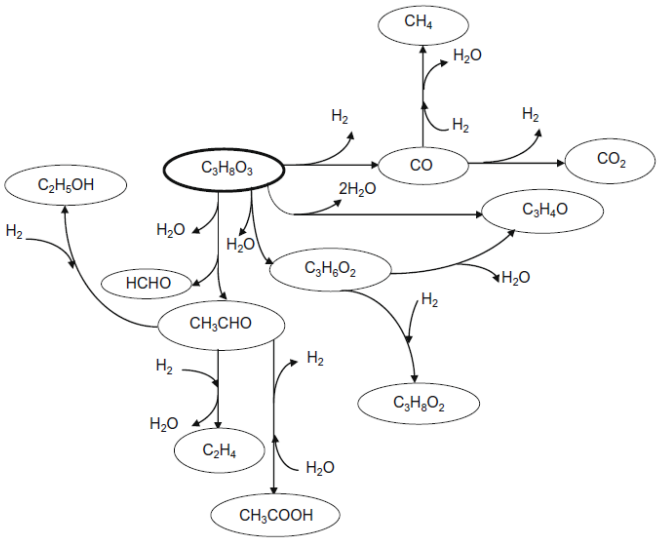

Figure 39 - Potential reaction pathways during the glycerin reforming process [31].

The following modeling efforts use an equilibrium assumption with kinetic experiments currently underway in the Chemical and Petroleum Engineering Department at KU. Glycerin can be broken down into a hydrogen rich syngas through multiple complex reactions as shown in Figure 39. The different pathways during the reforming process are determined by the amount of constituents along with the energy supplied to the reaction.

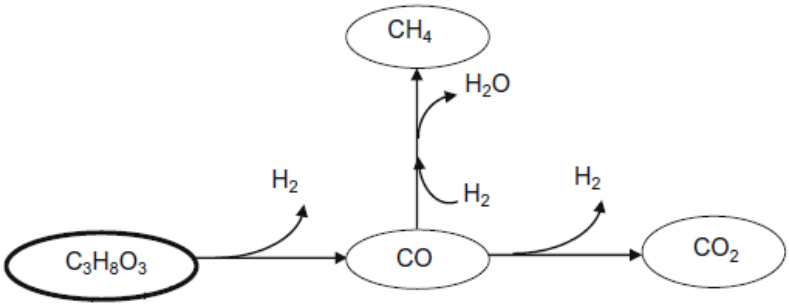

Figure 40 - Ideal reforming pathway for optimal hydrogen production from glycerin.

This typically occurs through the exothermic reaction of partial oxidation and steam reforming with the desired glycerin-reforming pathway expressed in Figure 40 [32]. This route is preferred as it

provides the highest specific energy syngas. Alternative directions may require more energy and/or the resulting product has less potential energy.

With respect to the model development, the reforming of an oxygenated hydrocarbon fuel with simplified air can be represented on a one-mole air basis as:

$$f\mathrm{C}_{\alpha}\mathrm{H}_{\beta}\mathrm{O}_{\gamma} + \left(0.2101\mathrm{O}_2 + 0.7899\mathrm{N}_2\right) \rightarrow a\mathrm{CO}_2 + b\mathrm{H}_2 + c\mathrm{CO} + d\mathrm{H}_2\mathrm{O} + e\mathrm{N}_2 + g\mathrm{CH}_4 \quad (2)$$

where carbon monoxide (CO), hydrogen (H_2), and methane (CH_4) in the products represent the syngas produced. Using the atom balance, four equations result:

$$\mathrm{C}: \; f\alpha = a + c + g \quad (3)$$

$$\mathrm{H}: \; f\beta = 2b + 2d + 4g \quad (4)$$

$$\mathrm{O}: \; f\gamma + 2(0.2101) = 2a + c + d \quad (5)$$

$$\mathrm{N}: 0.7899 = e \quad (6)$$

However, six equations are necessary to calculate the molar quantities of products (*a*, *b*, *c*, *d*, *e,* and *g*) in Equation 2. In order to find the other two required equations, it is necessary to have a better understanding of the chemical reactions occurring in Figure 40. In particular, there is one primary reaction and two secondary reactions. The preferred reaction is the breakdown of glycerin and water into H_2 and CO through partial oxidation. The two secondary reactions that occur are the water gas shift (WGS) and steam methanation (SM) reactions via Equations 7 and 8, respectively [33]:

$$\mathrm{CO} + \mathrm{H_2O} \Leftrightarrow \mathrm{CO_2} + \mathrm{H_2} \quad (7)$$

$$\mathrm{CO} + 3\mathrm{H_2} \Leftrightarrow \mathrm{CH_4} + \mathrm{H_2O} \quad (8)$$

These reactions occur because of the influence of water at the temperatures encountered during reforming. In particular, including water helps shift the WGS reaction more towards the production of hydrogen [20]. Moreover, adding water to the glycerin reduces the viscosity of the

mixture and makes pumping easier. Analysis of both of these secondary reactions is necessary to calculate the final constituents.

An energy balance of the partial oxidation and WGS reactions result in 251.2 and 41.2 kJ/mol energy released, respectively; whereas, the SM reaction results in 206.3 kJ/mol energy released [27]. As a result, the overall reaction of glycerin into syngas is exothermic. Therefore, the energy given off by the reactions will allow for a continuous syngas production without requiring additional heat (proven and discussed in Chapter 4). Although methane does have thermodynamic potential, this reaction is somewhat undesirable since the energy potential contained in CO and H_2 is greater (i.e., energy is lost in the exothermic SM reaction). These reactions create a nonlinear set of equations for solution and, as a result, require an equilibrium analysis in order to evaluate the overall process. Making this assumption, computational efforts are reduced by removing the specific time rate of change within the reformer (kinetics). However, this simplified analysis now provides more of a global understanding of the process. This is sufficient for this effort since the reformer is run under steady-state conditions. With this assumption, it is now possible to formulate a method to solve for the constituents in the overall reformation reaction of Equation 2 [30].

Each of the two reactions has a specific equilibrium constant that is a function of the quantities of constituents in the reaction. These equilibrium reactions for the WGS and SM reaction can be found in Equations 9 and 10, respectively:

$$K_{\mathrm{WGS}} = \frac{X_{\mathrm{CO_2}} X_{\mathrm{H_2}}}{X_{\mathrm{CO}} X_{\mathrm{H_2O}}} \tag{9}$$

$$K_{\mathrm{SM}} = \frac{X_{\mathrm{CH_4}} X_{\mathrm{H_2O}}}{X_{\mathrm{CO}} X_{\mathrm{H_2}}^3} \left(\frac{p}{p^0} \right)^{-2} \tag{10}$$

where *X* is the molar ratio of each specific molecule and p is the pressure at which the reaction takes place. It is important to note that there is pressure dependence in the SM equilibrium equation and not

in the WGS version. This dependence is a result of the fundamental formulation of the equilibrium analysis. In particular, the number of moles of products and reactants are the same for the WGS reaction canceling any pressure dependence. However, for the SM reaction there are four moles of reactants and only two moles of products that causes squared pressure dependence.

Adding Equations 9 and 10 to Equations 3 through 6 provide for the six necessary equations to solve for the unknown quantities of product constituents. These equations require the calculation of the equilibrium constants (K_{WGS} and K_{SM}) using a Gibbs free energy (ΔG) analysis. The equation used to solve for the equilibrium constants is found in Equation 11 where ΔS is the molar entropy, R_u is the universal gas constant, ΔH is the molar enthalpy and T is the reaction temperature [30]:

$$K^o = \exp\left(-\frac{\Delta \bar{G}^o}{R_u T}\right) = \exp\left(\frac{\Delta \bar{S}^o}{R_u} - \frac{\Delta \bar{H}^o}{R_u T}\right) \tag{11}$$

with the values of entropy and enthalpy tabulated for all of the constituents in both the WGS shift and SM reaction.

Initially, the author attempted to solve these six equations simultaneously using the *fsolve* routine in Matlab. However, convergence was unsuccessful due to the highly non-linear nature of the equations, specifically the third order dependency in the denominator of Equation 10 for hydrogen. As a result, the NASA Chemical Equilibrium with Applications (CEA) program was utilized to handle the equilibrium calculation [34]. This program was linked to MATLAB in order to provide for a quick methodology of finding the flow rates of syngas components as a function of temperature. In specific, MATLAB uses the experimental flow rates of fuel and air to the reformer and writes a CEA input file. Then, MATLAB calls the CEA executable file and reads the output equilibrium values.

```
25
26      %The following is: [mdot_propane,mdot_air,and temp]
27 -    file_data = [0.645046571 3.741869778 458.1761472
28          0.645046571 4.933616556 634.3963841
29          0.645046571 6.125363333 893.9564349
30          0.645046571 7.317110111 1031.226838
31          0.645046571 8.508856889 1117.367184
32          0.883048143 3.741869778 474.9727461
33          0.883048143 4.933616556 630.5074478
34          0.883048143 6.125363333 923.5685953
35          0.883048143 7.317110111 1025.648562
36          0.883048143 8.508856889 1100.978002
37          0.883048143 9.700603667 1193.11604
38          1.121049714 3.741869778 487.65326
39          1.121049714 4.933616556 626.6185114
40          1.121049714 6.125363333 953.1807557
    :           :           :           :
100         3.263063857 8.50885688  617.0828008
101         3.263063857 9.700603667 710.5922796
102         3.263063857 10.89235044 792.4668738
103         3.263063857 12.08409722 1055.41271
104         3.263063857 13.27580000 1318.36
105         3.501065429 8.50885688  479.077073
106         3.501065429 9.700603667 584.6286041
107         3.501065429 10.89235044 721.018031
108         3.501065429 12.08409722 1020.156752
109         3.501065429 13.27580000 1319.3
110         3.739070000 9.700603667 458.665
111         3.739070000 10.89235044 649.596
112         3.739070000 12.08409722 984.901
113         3.739070000 13.27580000 1320.2];
```

Figure 41 - Raw data taken from the reformer temperature map.

In order for the numerical model to function, all of the data for the reforming map was first inputted into the program. Experimental methods regarding the reformer map will be discussed in detail in the next section. Figure 41 shows a screenshot of the program window indicating the file data from the map. The first column of data is propane flow rate with units of g/s, followed by air flow rate also in g/s, and finally the temperature of the reformer in Kelvin.

```
119        %The following writes an input file for the NASA CEA code using a specified
120        %value for Temperature, Pressure, and moles of input fuel and air.
121 -      line1 = 'problem   ';
122 -      formatSpec = '    tp   t,k=%f,  p,bar=%f,';
123 -      Pressure = 0.98049;
124 -      line2 = sprintf(formatSpec,Temperature,Pressure);
125 -      line3 = 'react  ';
126 -      formatSpec = '  fuel= C3H8 moles=%f';
127 -      Moles_Reactants = mdot_pro/W_C3H8;
128 -      line4 = sprintf(formatSpec,Moles_Reactants);
129 -      formatSpec = '  oxid= O2   moles=%f';
130 -      Moles_Oxygen = mdot_air/W_Air*.2101;
131 -      line5 = sprintf(formatSpec,Moles_Oxygen);
132 -      formatSpec = '  oxid= N2   moles=%f';
133 -      Moles_Nitrogen = mdot_air/W_Air*.7899;
134 -      line6 = sprintf(formatSpec,Moles_Nitrogen);
135 -      line7 = 'outp trace=1e-10';
136 -      line8 = 'only CO CO2 H2 H2O N2 O2 CH4';
137 -      line9 = 'end';
138 -      fid = fopen('problem.inp','wt');
139 -      fprintf(fid,'%3.50s\n',line1,line2,line3,line4,line5,line6,line7,line8,line9);
140 -      fclose(fid);
141        %The following calls the NASA CEA code and passes in the previously written
142        %data input file
143 -      fname = 'problem.inp';
144 -      system(['FCEA2.exe <', fname]);
```

Figure 42 - Matlab screenshot indicating the NASA text file production and execution.

Once the data is ready to be called, a loop is created so that all of the 86 data points can be used within the program. Next, a text file is written line by line in the proper format of NASA CEA coding format. The program dynamically changes the input text file at each iteration depending on the flow rates of propane and air, as well as the reforming temperature. Finally, the program sends the previously created input file to the CEA program. Figure 42 is a screenshot of the section of the program that completes these actions. Lines 121 through 140 create the input file and lines 143 and 144 execute the CEA program.

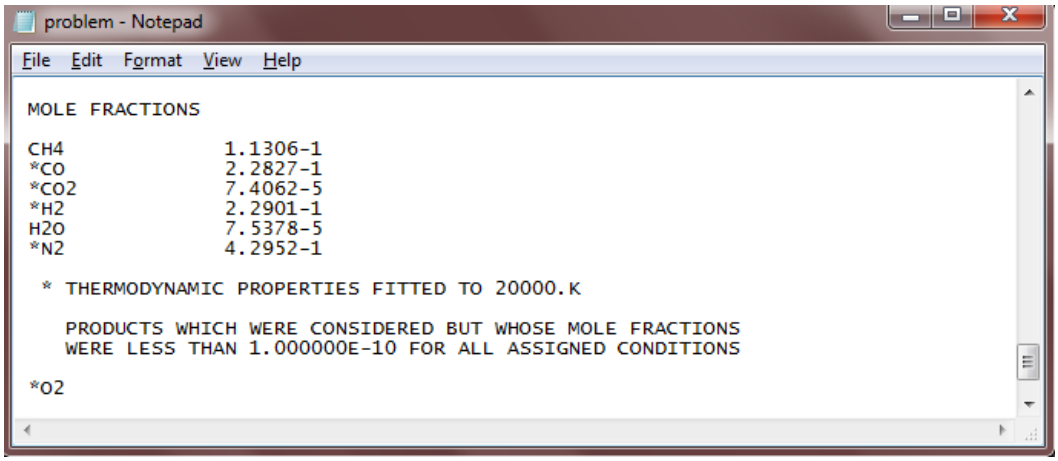

Figure 43 - Text file result from the NASA CEA program.

Next, the program must read in the output CEA text file for further analysis. The primary goal of the CEA program is to find the molar ratio of output species (i.e., mole fractions), but these values are saved as characters rather than numbers in the output file with an example output file shown in Figure 43.

```
145        %The following reads the ouput file from the NASA CEA code and converts the
146        %values for mole fractions of all products from strings into numbers
147 -      fid = fopen('problem.out');
148 -      A = fscanf(fid, '%c', [1 inf]);
149 -      fclose(fid);
150 -      if Temperature >= 1000
151 -          X_CH4 = str2double(A(3387:3392))*10^(str2double(A(3393:3394)));
152 -          X_CO = str2double(A(3414:3419))*10^(str2double(A(3420:3421)));
153 -          X_CO2 = str2double(A(3441:3446))*10^(str2double(A(3447:3448)));
154 -          X_H2 = str2double(A(3468:3473))*10^(str2double(A(3474:3476)));
155 -          X_H2O = str2double(A(3495:3500))*10^(str2double(A(3501:3502)));
156 -          X_N2 = str2double(A(3522:3527))*10^(str2double(A(3528:3530)));
157 -      end
158 -      if Temperature < 1000
159 -          X_CH4 = str2double(A(3386:3391))*10^(str2double(A(3392:3393)));
160 -          X_CO = str2double(A(3413:3418))*10^(str2double(A(3419:3420)));
161 -          X_CO2 = str2double(A(3440:3445))*10^(str2double(A(3446:3447)));
162 -          X_H2 = str2double(A(3467:3472))*10^(str2double(A(3473:3475)));
163 -          X_H2O = str2double(A(3494:3499))*10^(str2double(A(3500:3501)));
164 -          X_N2 = str2double(A(3521:3526))*10^(str2double(A(3527:3529)));
165 -      end
```

Figure 44 - Matlab screenshot that reads the molar ratio of each species in the NASA CEA text file.

Therefore, this output file is saved to a temporary variable in Matlab: “A”. Each of the molar ratio values are then converted from string values to number values. However, depending on the

reforming temperature, the location of the molar ratios are different for each iteration. Lines 147 to 149 in Figure 44 show how the output file is read and saved to the temporary variable and then closed. Lines 150 to 165 show the conversion of each molar ratio from a string to number value. The output file of the NASA CEA program originally writes the values of molar ratios in scientific notation and depending on the character location of each of these strings, a different portion of the temporary variable must be called and converted to a number. For example, "A(3387:3392)" in Figure 44 refers to the value of "1.1306" in Figure 43. Similarly the value of "A(3393:3394)" refers to the exponent value of "-1" in Figures 44 and 43, respectively.

After reading the output, conservation of mass can be applied to calculate the mass flow rate of the resulting syngas.

$$\dot{m}_{air} + \dot{m}_{C_3H_8} = \dot{m}_{syn} \tag{12}$$

The molecular weight of the syngas can be found by summing the multiplication of each species' molecular weight by their corresponding molar ratio (i.e., mole fraction). Dividing the syngas mass flow rate by the molecular weight of the mixture calculates the molar flow rate produced by the reforming process. Now, the molar flow rate of each product can be found by using each species mole fraction. The molar flow rate of each species is essential in the calculation of the heat release of the reaction from the first law of thermodynamics:

$$\dot{n}_{air}\overline{h}_{air} + \dot{n}_{C_3H_8}\overline{h}_{C_3H_8} = \sum \dot{n}_{syn}\overline{h}_{syn} + \dot{Q} \tag{13}$$

where $\dot{n}$ is the molar flow rate, $\overline{h}$ is the molar enthalpy and $\dot{Q}$ is the heat transfer from the reactor.

The heat transfer to the ambient involves convection and is modeled as:

$$\dot{Q} = h_c A_s \left(T_{ref} - T_{amb} \right) \tag{14}$$

In this equation, the temperature leaving the reformer (T_{ref}), ambient temperature (T_{amb}), and surface area (A_s) are measured. As a result, the convective heat transfer coefficient can be calculated using the

heat release of the reaction via Equation 13 and this equation. The calculation of the convective heat transfer coefficient is important as it will be used in the glycerin reforming efforts in order to more accurately predict the temperature leaving the reformer and, subsequently, the species through equilibrium.

3.4 Experimental Setup

The experimental setup of this project involves three main pathways. The engine/generator system is capable of running using pure propane (PP), reformed propane (RP), and reformed glycerin (RG) as a fuel source. Using PP accomplishes two goals that include (1) preheating the reformer and (2) calculating energy requirements for running the engine. It is necessary that the reformer be preheated in order to initiate the exothermic (and self-sustaining) reactions for propane and glycerin reforming. Another important use of PP is to calculate the energy requirements to run the engine at different loads (i.e., power). In specific, matching the energy content of PP with the energy content of RP and RG will ensure that the engine runs at the specific load levels required. This occurs by using the numerical model described prior to find the syngas flow rates required to match the energy content. The lower heating value of the syngas is calculated using Equation 15:

$$Q_{LHV_{syn}} = Y_{\mathrm{H_2}} Q_{LHV_{\mathrm{H_2}}} + Y_{\mathrm{CO}} Q_{LHV_{\mathrm{CO}}} + Y_{\mathrm{CH_4}} Q_{LHV_{\mathrm{CH_4}}} \quad (15)$$

where Y and Q_{LHV} are the mass fraction and mass-based lower heating value of each syngas species with available energy, respectively. The energy content of the resulting syngas can be calculated and matched to the required energy content to run the engine using Equation 16:

$$\dot{m}_{\mathrm{C_3H_8}} Q_{LHV_{\mathrm{C_3H_8}}} = \dot{m}_{syn} Q_{LHV_{syn}} \quad (16)$$

This equation will serve as the initial calibration tool for using RG as a fuel source. The procedure for using RG as a fuel source will be similar to that of RP. First, the reformer will be preheated using

propane until the desired temperature is reached. At this time, a mixture of glycerin and water will be added to the reformer to produce syngas that is sent to the engine.

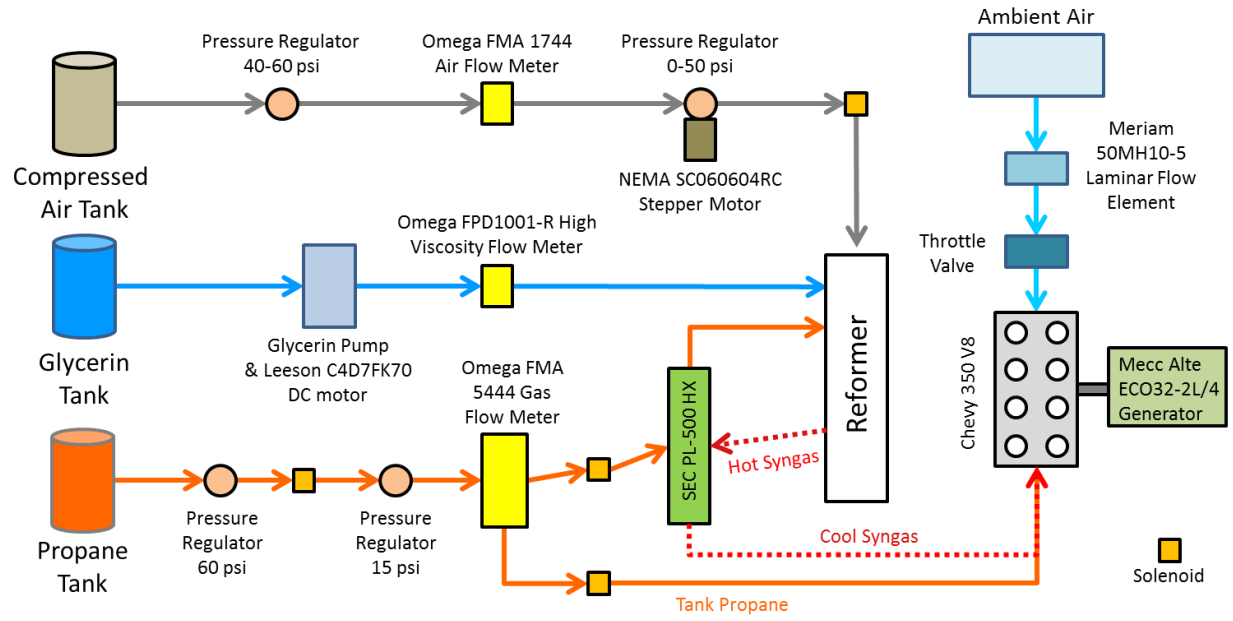

Figure 45 - Complete flow structure of the reformer, engine, and generator setup.

Figure 45 shows the complete flow structure of the reformer, engine, and generator setup. The orange lines in the lower part of the figure indicate how propane is supplied to the reformer or to the engine for baseline tests. Propane is sent at approximately 15 psi and is controlled by an Omega FMA 5444 gas flow controller. Dashed red lines indicate the flow of syngas, cooled in a heat exchanger before sending to the engine. This SEC PL-500 heat exchanger helps prevent engine knock and increase the density of the mixture. Glycerin (dark blue lines) is pumped to the reformer by a Leeson C4D7FK70 DC motor and its subsequent syngas is also cooled in the same heat exchanger before sending to the engine. Glycerin flow is measured using an Omega FPD 1001-R high viscosity flow meter. Compressed air (gray lines) is constantly supplied while reforming takes place and is monitored by an Omega FMA 1744 air flow meter. Control of the air-fuel ratio in the reformer is accomplished with a custom-built air flow controller made using a NEMA SC060604RC stepper motor and Parallax BS-2 microprocessor.

The reformer was filled with 22 mm aluminum oxide spheres. These spheres were not coated with catalytic material but are the same size as the nickel-coated spheres to be used in future glycerin tests. This ensures the same flow patterns inside the reformer. The generator is a Mecc Alte ECO32-2L/4 model and power draw from the generator is measured using a Woodward GCP-20 generator set controller. A Meriam 50MH10-5 laminar flow element (LFE) is used along with an Omega PX277-30D5V to measure volumetric air flow to the engine when running. Spark timing adjustments are completed using an aftermarket Dynamic EFI EBL Flash system ECU. An aftermarket Woodward 8404-3002 air-fuel valve and Woodward 8404-4009 throttle valve maintain the air-to-fuel ratio for all tests. This provides a way to ensure repeatability even when intake temperatures vary. Environmental conditions are monitored using an Omega EWS-RH humidity and temperature sensor and Omega EWS-BP-A barometric pressure sensor. A Kistler 6118B pressure transducer and 2614B1 encoder allow engine pressure traces to be recorded during combustion. In addition to the components shown in Figure 45, Omega K-type thermocouples and Omega PX-319 pressure transducers are used throughout the setup. These sensors are placed between all of the major components to monitor changes in pressure and temperature. Data acquisition is accomplished using an NI cRIO-9073 chassis with all of the information monitored in a LabVIEW program created by the authors.

3.5 Results and Discussion

The experimental data presented is broken down into three different subsections: the reformer map, engine map, and propane syngas production. These subsections illustrate the methodology used in order to calculate the required flow rates for air and propane in order to produce a useful reformed propane syngas. This leads into the analysis of reformed glycerin and map creation prior to testing.

3.5.1 Reformer Map

The first experimental map that was completed was a temperature map of the propane reforming process over the possible ranges of flow rates for propane and compressed air. This indicates

the operating envelope of the reformer for preheating the reformer and providing RP for running the engine. The propane flow rate can be consistently measured from a maximum of 3.7 g/s until a minimum of 0.4 g/s while air can be supplied up to 13.3 g/s. With these flow rates determined, three intermediate propane flow rates were additionally tested, at 1.2, 2.0, and 2.85 g/s.

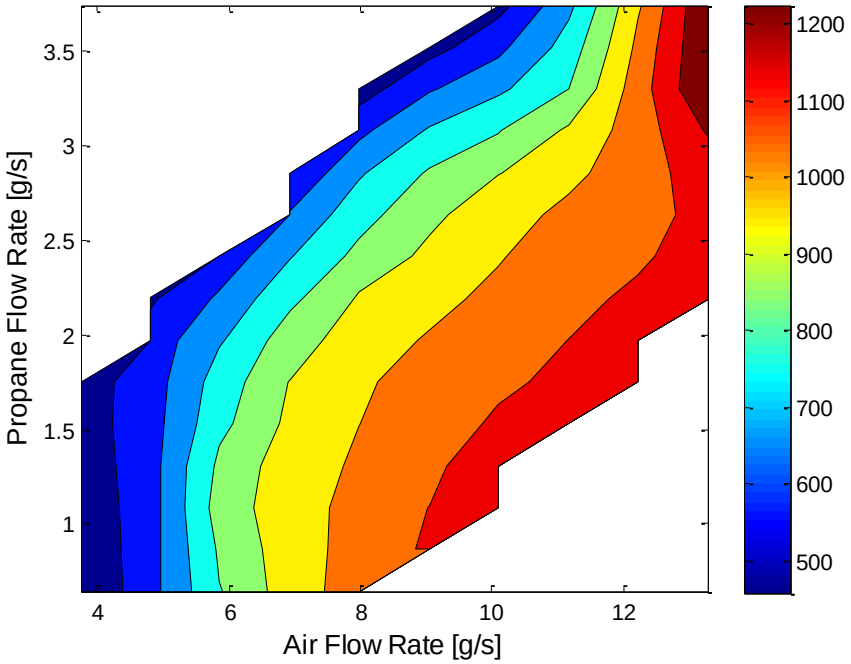

Figure 46 - Map of reformer temperature in K as a function of reformer air and propane mass flow rates.

At each propane flow rate, the air flow rate was first reduced in order to find the minimum value where combustion would still occur (usually near an air-to-fuel ratio of 2-2.5). A significant and continuing temperature drop as measured by thermocouples in the reformer indicates when combustion no longer takes place. While at the same propane flow rate, the air flow rate was gradually increased in order to start leaning out the mixture and increase the temperature in the reformer. A temperature of 1200 K was used as the limit in order to prevent the metal from melting and the resulting temperature map is shown in Figure 46. Steady state for these tests was specified as the maintaining of the reformer temperature for five minutes with fluctuations less than 20 K. It is

important to note that this system is housed in a shed exposed to the ambient; hence, rigorous control of external temperatures was not possible.

The results illustrate that the contours in Figure 46 fall primarily on isotherms according to constant air-to-fuel ratios as to be expected. The temperatures rise as combustion becomes less rich (more like stoichiometric) moving from upper left to lower right.

From this information, heat release calculations were completed in order to calculate the heat transfer from the reformer via Equation 13. The convective heat transfer coefficient could then be calculated via Equation 14 using the known surface area of the reformer and ambient temperature. The average convective heat transfer coefficient was found to be 26.55 $Wm^{-2}K^{-1}$ with a standard deviation of 3.85 $Wm^{-2}K^{-1}$. This coefficient will be used during glycerin reforming tests in order to more accurately predict the resulting syngas constituents.

3.5.2 Engine Map

Prior to running the engine on RP, it was important to find the flow rates required for running on PP using the Omega flow meter. Three different generator loads were possible using two Dayton 3VU34A heavy-duty electric heaters drawing power from the generator. The power drawn from the generator using one and two heaters is 3.6 and 6.5 kW, respectively. The flow rate of propane for no load at 1200 revolutions per minute (RPM) was 1.46 g/s. The energy content of the fuel at this load can be calculated by multiplying the flow rate by the Lower Heating Value of propane (46.35 MJ/kg) resulting in an energy content of 67.7 kW. As mentioned prior, this energy content must be (at least) matched by the reformed fuel via Equation 16 in order to achieve the same engine performance. Similar to the baseline test at 1200 RPM, additional data points were taken for 1800 RPM, required by the generator to produce power, and over three different loads corresponding to zero, one, or two heaters. Table 4 provides the engine requirements for all tested engine speeds and generator loads.

Table 4 - PP flow requirements in order to run the engine and generator at different speeds and loads.

Engine Setup	Propane Flow Rate [g/s]	Air Flow Rate [g/s]	Energy Content [kW]
1200 RPM / No Load	1.46 (+/- .022)	22.3 (+/- .061)	67.7
1800 RPM / No Load	2.55 (+/- .039)	38.3 (+/- .149)	118.2
1800 RPM / 3.6 kW	3.19 (+/- .014)	47.9 (+/- .141)	147.9
1800 RPM / 6.5 kW	3.65 (+/- .016)	54.8 (+/- .153)	169.2

The air-to-fuel ratios for all of the different load and speed settings fall between 15.0 and 15.2. These values are less than the stoichiometric air-to-fuel ratio of propane (15.6) meaning the engine is constantly operating in a slightly rich environment. As Heywood elucidates, maximum power production is in a slightly rich air-to-fuel environment [23]. This, again, validates similar to Figure 46 that the experimental setup is running properly and the data collected follows the proper trends.

3.5.3 Engine Running on Reformed Propane Syngas

The second step prior to reforming glycerin is to run the engine using RP. Prior to doing so, the numerical model is used to calculate the species produced when propane is reformed. The reforming temperature map of Figure 46 was used to provide the inputs for the numerical model; air flow rate, propane flow rate, and the reforming temperature.

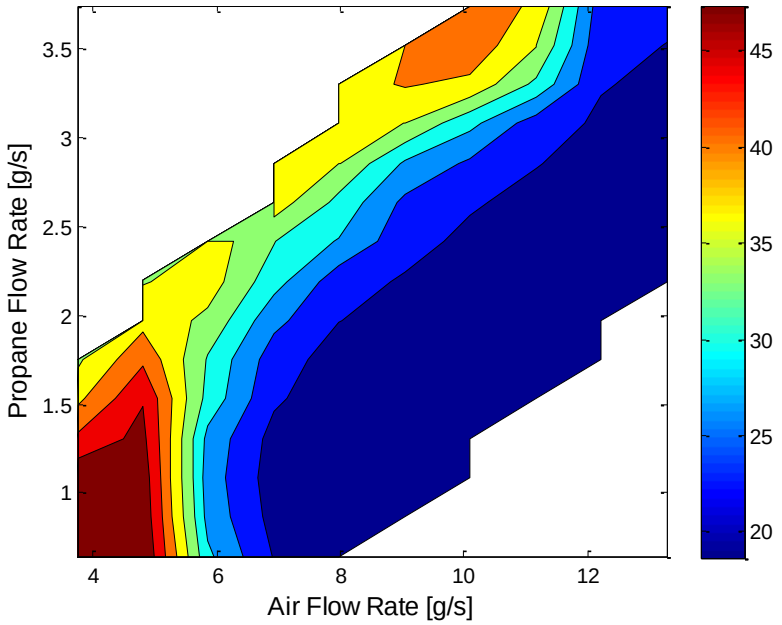

Figure 47 - Effective syngas LHV map in MJ/kg of RP using the conditions found experimentally in Figure 46.

The program then calculates the species produced using equilibrium (using the *tp* option in CEA) and subsequently the LHV of the resulting RP syngas from Equation 15 minus the non-fuel species (CO_2, H_2O, N_2) that will act like Exhaust Gas Recirculation (EGR) in the setup. Note that the stock engine EGR system was disabled prior to testing. The RP LHV map correlating to the reformer temperature map is shown in Figure 47.

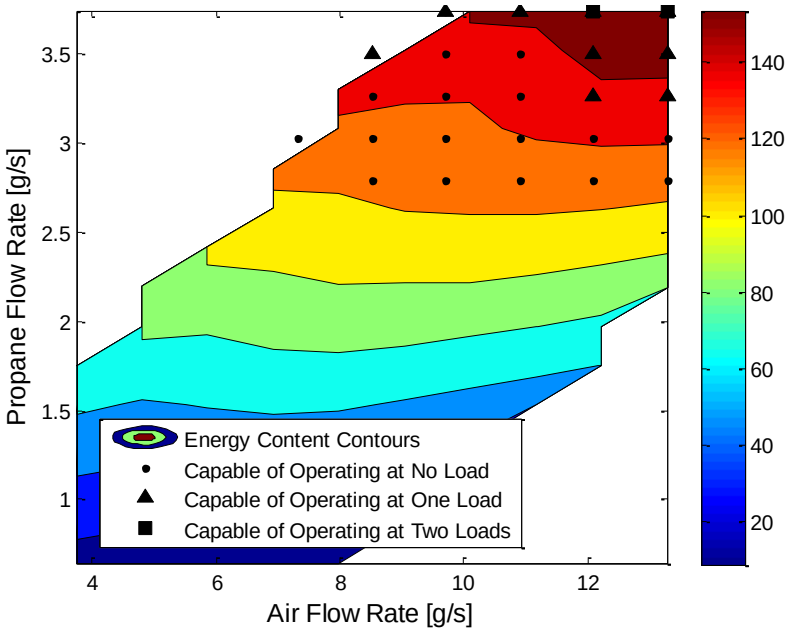

Figure 48 - RP syngas energy content in kW as a function of air and propane flow rates.

Using this information and multiplying it by the syngas mass flow rate of Equation 12, the theoretical energy content can be calculated. Figure 48 shows the plot of theoretical RP syngas energy content as a function of air and propane flow rates. In this figure, the conditions under which the engine can be operated by RP are indicated as a function of loading at 1800 RPM.

Using this information, the engine was successfully operated using reformed propane. When the engine operates at 1200 RPM and no load, the required flow rate of PP is 1.46 g/s. However, the required flow rate of RP was found to be 1.87 g/s. Additional tests were completed at 1800 RPM to show that the syngas can produce sufficient energy to produce electricity with the generator. In particular, at no load successful combustion of reformed propane did not take place until 3.04 (+/- .012) g/s of propane was supplied to the reformer along with 12.07 (+/- .052) g/s of air. This flow rate of propane and air produces syngas with an energy content of 126.5 kW, 7.0% more than required with PP. With one heater, the flow rates of propane and air were 3.43 (+/- .011) g/s and 12.94 (+/- .027) g/s, respectively. Finally, with two heaters, the propane and air flow rates were increased to 4.02 (+/- .013)

g/s and 13.46 (+/- .031) g/s, respectively. The comparative results between PP and RP energy needed are provided in Table 5.

Table 5 - Comparison of RP theoretical requirements and actual energy needed.

Engine Setup	PP [kW]	RP [kW]	Change [%]
1200 RPM / No Load	67.7	73.7	8.8
1800 RPM / No Load	118.2	126.5	7.0
1800 RPM / 3.6 kW	147.9	156.9	6.1
1800 RPM / 6.5 kW	169.2	179.2	5.9

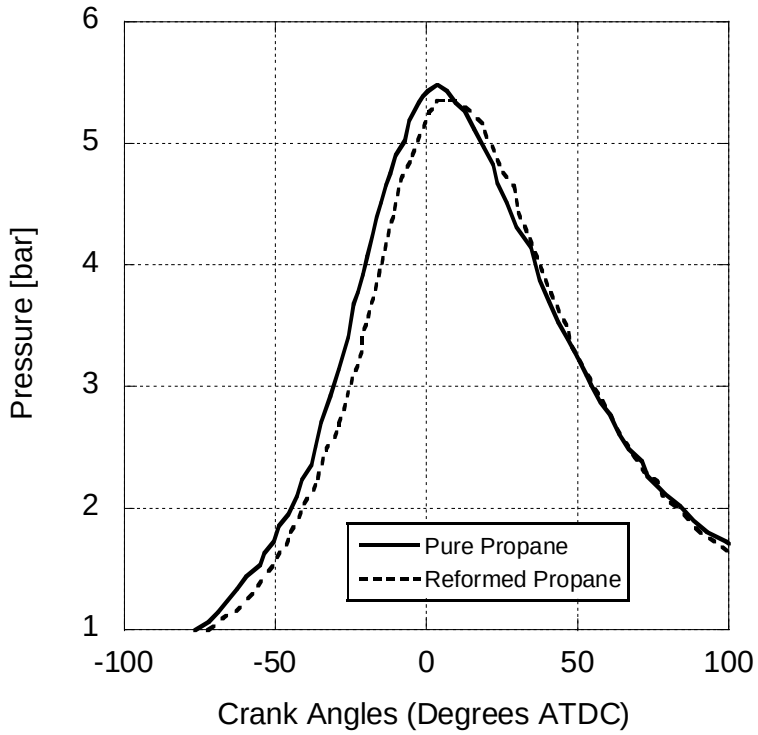

Figure 49 - In-cylinder pressure data at no load and 1800 rpm for both PP and RP.

It is important to note that the syngas mixture has a smaller LHV than pure propane (46.35 MJ/kg). This is anticipated because energy availability is being lost during the conversion process. Furthermore, additional species are present, like water and carbon dioxide, which effectively act as EGR

reducing the power output and combustion speed slightly. This is indicated via Figure 49 via a lower maximum pressure in the cylinder when running on RP. Overall, the graphs are similar (and should be) because the same total amount of energy is added in order to achieve the power needed by the engine. Differences in the curves can be related to the higher temperature of RP in comparison to PP and dissimilar intake pressures stemming from the flow pathways according to Figure 45. As a result, a higher mass flow rate of syngas is required to balance Equation 16 and achieve the same engine performance as PP. This is indicated via the required propane flow rates when running on PP and RP (Table 5) and the change in percentage energy needed. As a result, operating on RP is less efficient; however, this methodology proves the validity of using syngas to run the engine and illustrates how to calibrate the model for glycerin use in the future.

3.6 Conclusion

As oil production begins to peak in the upcoming years, alternative fuels will become a necessity to keep up with energy demands. Glycerin is a viable alternative fuel because it contains a significant hydrogen component. Direct combustion of glycerin in an engine, however, is not possible due to its high viscosity and poor atomization. Therefore, glycerin must first be reformed into a hydrogen rich syngas. A unique experimental setup at KU reforms glycerin into syngas for its subsequent combustion in an internal combustion engine.

Before glycerin testing is possible, propane was used to find the operating temperatures of the reformer and calculate the flow rates and energy requirements needed to run the engine. Literature research was completed to better understand the reactions taking place and to help generate a numerical model based on chemical equilibrium. This model was used to estimate the species produced by reforming propane and calculate the energy content of the resulting syngas. It was then possible to achieve combustion of the reformed propane in the engine at three different generator loads. This combustion of reformed propane along with a calculation of heat transfer from the reformer provided

the methodology to calibrate the model for upcoming glycerin tests. In particular, this model predicts the flow rates needed for the glycerin/water mixture and air that can operate the engine.

Chapter 4: Investigation of Glycerin Reforming and Syngas Combustion

The primary goal of the syngas generator rig is to achieve reformed glycerin combustion in the engine. This chapter describes the efforts completed in order to accomplish this outcome. The first section indicates the adjustments made to the numerical model (described in Chapter 3) for glycerin reformation. The model uses the same fundamental equations as the previous version, but now utilizes a mixture of glycerin and water instead of propane. A theoretical temperature map is produced that is used to calculate the lower heating value (LHV) of the reformed glycerin. This is applied to find the theoretical energy content of the syngas over the operating range of the reformer. The second section of this chapter describes the efforts involved in creating the nickel catalyst used in the reformer. Literature research was completed in order to find the best catalyst precursor and material content. Also described in this section is the procedure of applying the nickel to the support media. Finally, this chapter ends by demonstrating the successful combustion of reformed glycerin in the engine including a discussion of the results.

4.1 Glycerin/Water Modeling

The next step in the methodology is to understand the glycerin reforming process. A nickel-based catalyst will be introduced into the reformer in order to aid in the glycerin reformation process. Literature research describes the optimal temperatures at which this process should be achieved. If the temperature is too low, there will be carbon poisoning on the catalyst [35]. At temperatures that are too high, the catalytic material in the reformer can sinter [28]. Both of these negative results would cause a loss of surface area of the catalyst and reduce the rate at which glycerin could be reformed. It was found that the ideal temperature for hydrogen production of a glycerin/water mixture is approximately 800 K [36-38].

It has been shown experimentally that a glycerin water mixture of 80/20% by volume results in the highest hydrogen production while still minimizing carbon dioxide [39]. Based on the findings in the

literature, adjustments were made to the numerical model described in the previous chapter in order to simulate a mixture of glycerin and water. An iterative procedure is required to estimate the energy potential of the resulting syngas starting with an approximation of the final reformer temperature. This predicted value, along with the ambient temperature entering the reformer, is used as an input to the NASA CEA program. Furthermore, this guessed final reformer temperature is employed to calculate the theoretical heat transfer to ambient using Equation 14 with the heat transfer coefficient, surface area of the reformer, and ambient temperature known. The next step requires the calculation of molar enthalpy of the exhaust species via Equation 13. From the molar enthalpy of the mixture and heat transfer, the right hand side of Equation 13 is computed. This is compared to the summation of enthalpies of the inlet mixture, air, glycerin, and water at 298 K (i.e., estimated ambient temperature entering the reformer). The final reformer temperature can then be updated using linear interpolation with a second estimated temperature until the values converge. This technique is completed over the entire operating range of the air and glycerin/water supply. Of note, future students can use the model developed in order to perform their own parametric studies with respect to water percentage and hydrogen production.

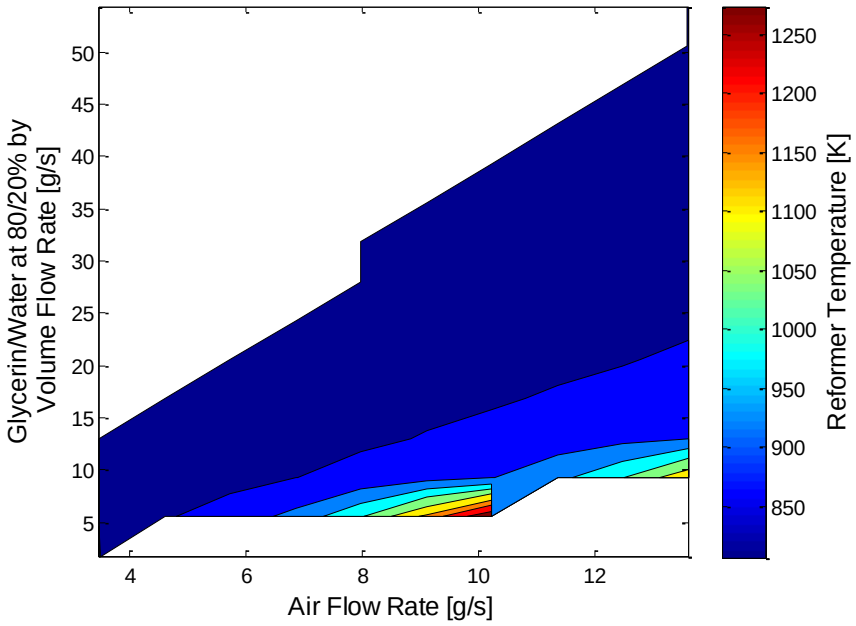

Figure 50 - Syngas temperature as a function of glycerin/water and air flow rates to the reformer.

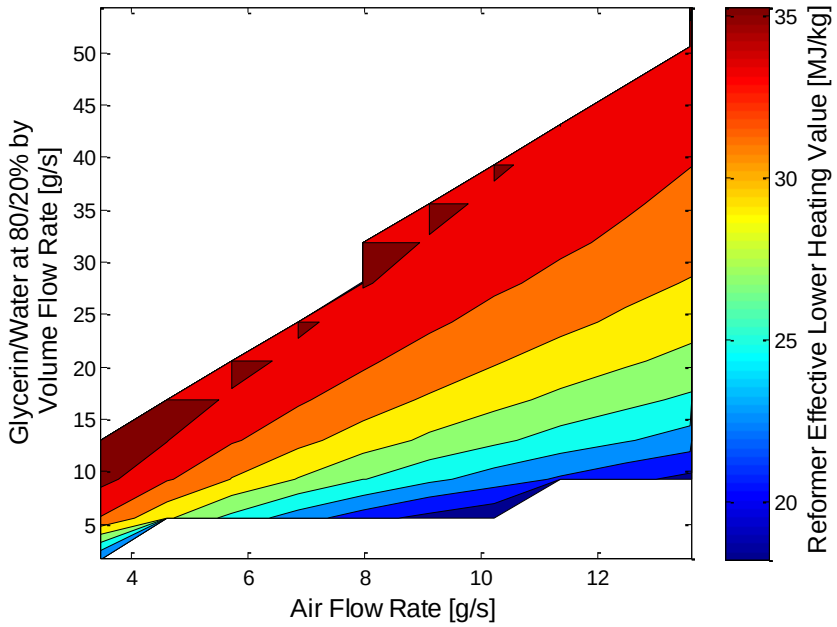

Figure 51 - Effective lower heating value of syngas exiting the reformer as a function of glycerin/water and air flow rates

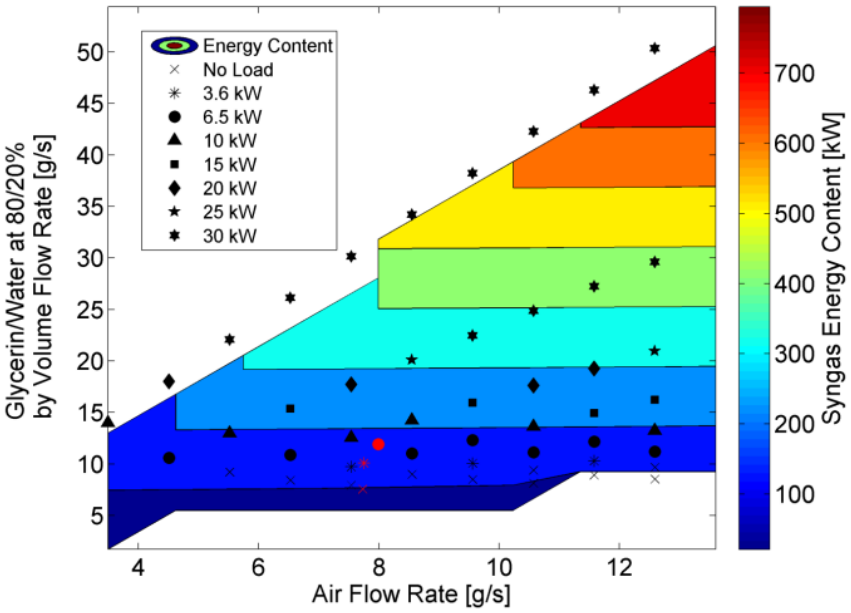

Figure 52 - Prediction of generator power output based on glycerin/water and air flow rates to the reformer

The converged temperature values from the numerical model are shown in Figure 50. This figure indicates a nearly constant temperature over the operating range of the reformer with glycerin until the air to fuel ratio reaches the stoichiometric limit. This data is then used to calculate the LHV of the reformed glycerin (aka syngas) using the same procedure as indicated in Chapter 3. The LHV map produced by the model is shown in Figure 51. In addition, the theoretical energy content of the syngas is shown in Figure 52 with the potential power created by the generator indicated.

It is important to note from Figure 52 that the power generated is primarily a function of the glycerin/water flow rate. Compared to propane partial combustion where air flow controls the species produced, glycerin reformation is a catalytic reaction. This is beneficial in that the air flow rate can be adjusted simply to reduce the temperature of the reformer in order to prevent sintering from occurring. Moreover, regulating the air flow rate will help lower the temperature of intake syngas stream to the engine lessening the likelihood of engine knock [23]. As long as the temperature of the reformer stays above the vaporization point of glycerin (563.15 K), exothermic reformation should continue because of the significant energy released due to partial oxidation and steam reforming.

4.2 Reformer Catalytic Material Preparation

This section details the production of the catalytic material used in the reformer in order to improve the conversion of a glycerin and water mixture. First, a catalytic material was chosen based on a literature review. Common catalysts used in glycerin/water reformation for hydrogen production include nickel, cobalt, cobalt-nickel, platinum, and rhodium [40-43]. Coke deposition (aka carbon poisoning) is one of the leading causes for catalytic deactivation over time and was a leading factor in catalyst selection. Cobalt and cobalt-nickel catalysts exhibit greater carbon poisoning than nickel catalysts. Temperature programmed removal of carbon deposits were required for cobalt catalysts, which is not feasible for glycerin reformation when continuous and uninterrupted power generation from the syngas is the ultimate goal. Platinum has been successfully used to produce a hydrogen rich

syngas from glycerin at temperatures below 450°C with similar conversion efficiency to that of nickel catalysts at higher temperatures. The cost of platinum, however, greatly outweighs the need for lower reformation temperatures since the current setup can easily reach high temperatures. Analysis of rhodium catalysts indicates a slightly higher conversion rate of glycerin to hydrogen with decreased coke formation. Similar to platinum, the price of rhodium also greatly outweighs the benefits when compared to nickel catalysts.

A literature review was also completed to find the best support media for the catalyst. Aluminum oxide, ceria, ceria promoted alumina, and magnesium oxide are common support media used in glycerin reforming [43, 44]. Studies comparing nickel catalysts applied to magnesium oxide, ceria, and aluminum oxide found significantly higher hydrogen conversion with aluminum oxide [43]. This is because nickel is able to disperse more readily across aluminum oxide than the other catalysts resulting in a greater hydrogen generation rate. Moreover, investigating support media found that many of the options presented are not available at the size needed for the reformer; i.e., most are for bench-scale packed beds. Because of this research, aluminum oxide spheres at 99% purity were chosen as the support media due to their relatively good absorption factor. The author was able to find aluminum oxide spheres at approximately the same size as the initial uncoated spheres used in propane reforming tests (3/4 inch). As a result, the flow patterns in the reformer remained relatively the same and the model created is still applicable. Finally, the cost of the spheres was reasonable since this is a widely used media (est. cost = $210.00).

The incipient wetness technique was used in order to impregnate the nickel catalyst into the support media spheres. This is accomplished by dissolving a nickel salt precursor in water and immersing the spheres in the solution. The coated spheres are then dried in a box furnace and then calcined. The choice of precursor affects how the final catalyst will behave. Literature research was completed to find the best salt precursor for this technique [45, 46]. Nickel nitrate hexahydrate, nickel chloride, and nickel

acetylacetonate were considered as possible precursors to be used to produce the catalyst. It was found that nickel nitrate hexahydrate at a weight percent between seven and eight percent produces the best catalyst [45]. This precursor provides the highest dispersion across the support media while reducing the likelihood of carbon poisoning and deactivation over time.

Figure 53 - Catalytic support media before catalyst was introduced

Figure 54 - Catalytic support media immersed in nickel salt bath

Production of the final supported catalyst involved multiple steps, first of which was creating a container to hold the support media. Figure 53 shows the aluminum oxide support media in a stainless steel container. Next, the catalytic support media was immersed into a water bath with the nickel salt precursor dissolved. The goal of the impregnation was to achieve between 7% and 8% nickel by weight and the catalytic support media was weighed before immersion into the bath (11.3 kg). Figure 54 shows the support media immersed in the water and nickel salt precursor solution.

After immersion in the bath, the catalyst was dried in a high temperature box furnace at 125°C for 24 hours. A Carbolite ELF 11/6/301 box furnace was purchased for the drying and calcination process. This furnace was chosen because of the operating temperatures that can be achieved, as well as the large internal furnace volume. After the drying procedure was completed, the catalyst was weighed again to check the weight percent of nickel applied to the support media. The procedure of immersion and drying was repeated until the appropriate weight percent was achieved. Upon measuring the weight after the third iteration, it was found that the catalyst and support weighed 12.2 kg. This indicates that 0.9 kg of nickel was impregnated into the alumina for a final weight percent of 7.4%.

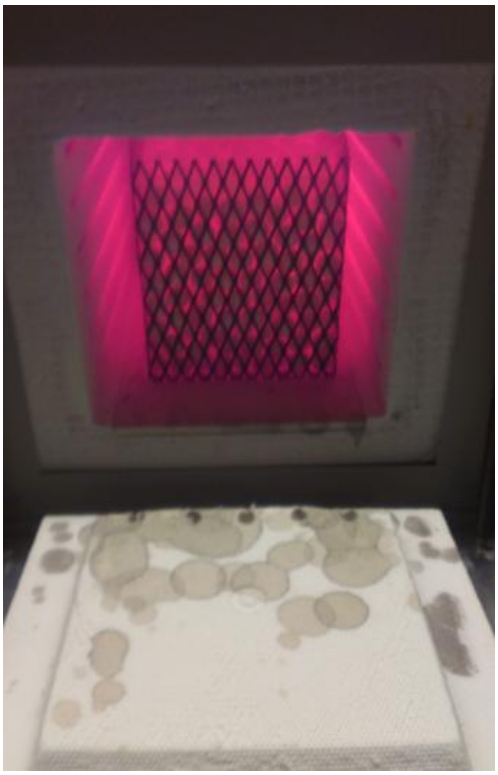

Figure 55 - Catalytic material after six hours at 800°C

The final step in the production of the catalyst is the calcination process that includes superheating the catalyst in the box furnace at 800°C for six hours. Figure 55 shows the catalyst after the calcination process. Although a weigh percent of nickel added to the support media was measured to be 7.4%, it is possible that this value could be lower due to the calcination process. After drying in the furnace the nitrates from the salt precursor are still on the support media. After calcining, these nitrates are removed which could potentially lower the measured weight percent of nickel. Future development of the catalyst should include additional weight measurements after calcinations.

4.3 Glycerin/Water Reformation

In order to convert the glycerin and water mixture into a useful fuel for the engine, it must first be converted in a self-sustaining manner in the reformer. Tests were completed to ensure that this mixture reformation does occur exothermally. If not exothermic, additional heat must constantly be supplied to the reformer (e.g., adding propane and leaving the igniter on) resulting in a loss of available

energy. Furthermore, testing the reformation process before employing the engine/generator also provides an avenue to validate the numerical model as discussed in Section 4.1. Initial reformation tests with the new catalytic material indicated that the reaction occurred in a highly exothermic manner. The temperature of the reformer quickly rose above the desired operational threshold of the reformer and needed to be shut down. Half of the catalytic beads were then removed to better control the reaction and keep the temperature in a safe range.

These tests were carried out using 99% pure food grade glycerin with specifications shown in Table 6. Lower quality glycerin contains impurities left over from the biodiesel production process that could hinder or help the conversion to a hydrogen rich fuel. Hence, this effort wanted to remove this potential influence and provide results based purely on glycerin reformation. Once successful operation occurred at a safe temperature threshold, an analysis of the effluent from the reformer was completed in order to compare to numerical predictions.

Table 6 - Purified glycerin technical specifications.

Test Parameter	Result	Limits	Units
Glycerin Content	99.9	99.5, min	% Mass
Specific Gravity	1.262	1.249, min	N/A
Chlorides	<10	10, max	ppm
Sulfates	<20	20, max	ppm
Heavy Metals	<1	5, max	ppm
Chlorinated Compounds	<30	30, max	ppm
Fatty Acid/Esters	0.3	1, max	ppm
Water	<0.5	0.5, max	% Mass

An SRI 8610 gas chromatograph (GC) was used to calculate the species produced from this reformation process. A gas chromatograph is capable of separating and analyzing components in a mixture of a gas sample. During testing, a carrier gas of nitrogen or argon forces the sample through the GC column. The sample being analyzed interacts with the walls of the GC column causing each compound to extract from the mixture at a different time, known as elucidation time. The elucidation

time of the species in the gas is detected and analyzed electronically by a flame ionization detector (FID) and thermal conductivity detector (TCD). The FID operates by detecting ions formed during combustion of organic compounds in a hydrogen flame. The generation of ions is directly proportional to the concentration of organic species in the sample gas stream. Compounds such as carbon monoxide and carbon dioxide cannot, however, be detected by an FID alone. Instead, a methanizer is used to convert CO and CO_2 to methane that in turn can be detected with the FID. The TCD operates by detecting the change in thermal conductivity of an electronically heated filament in a temperature controlled cell. When a species moves through the column, the filament temperature increases and changes its resistance. This change in resistance is proportional to the concentration of the compound in the sample stream. The comparison of elucidation times for different compounds provides an analytical usefulness.

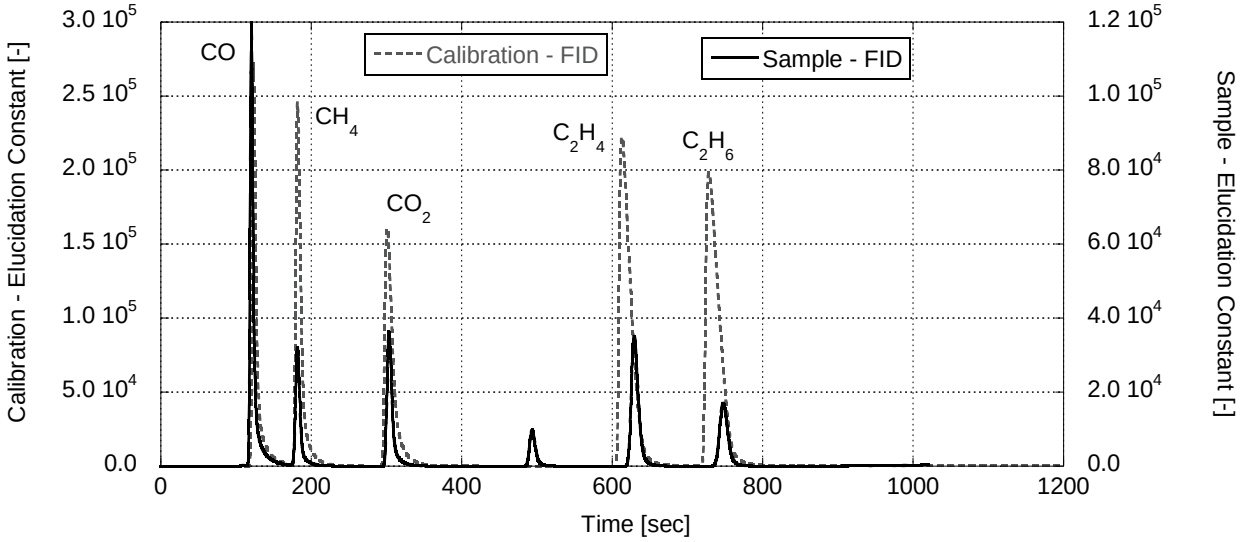

Figure 56 - No load, FID calibration and sampled data

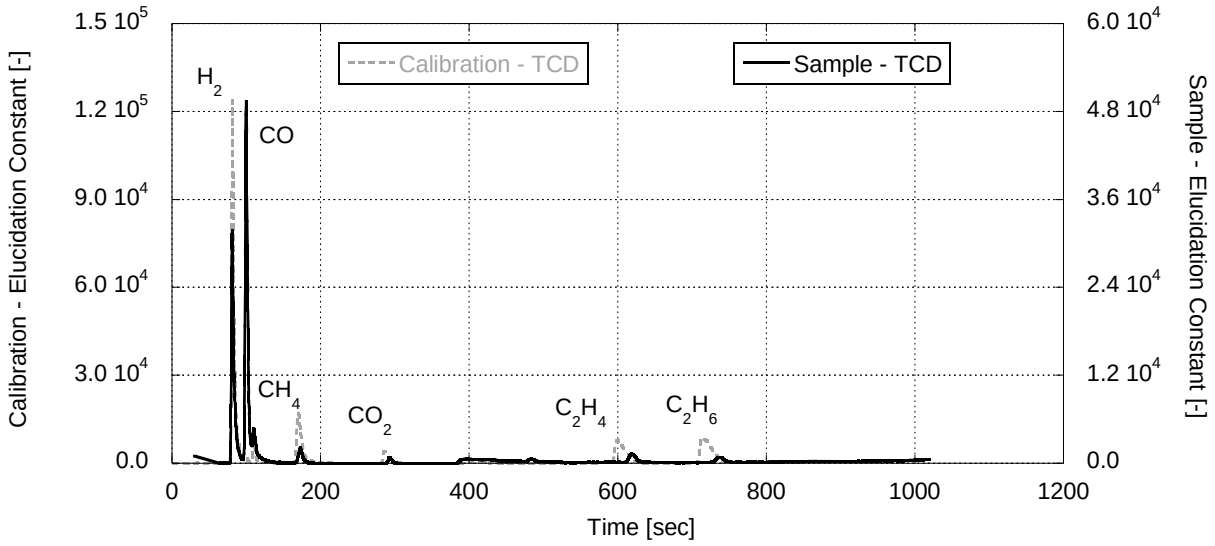

Figure 57 - No load, TCD calibration and sampled data

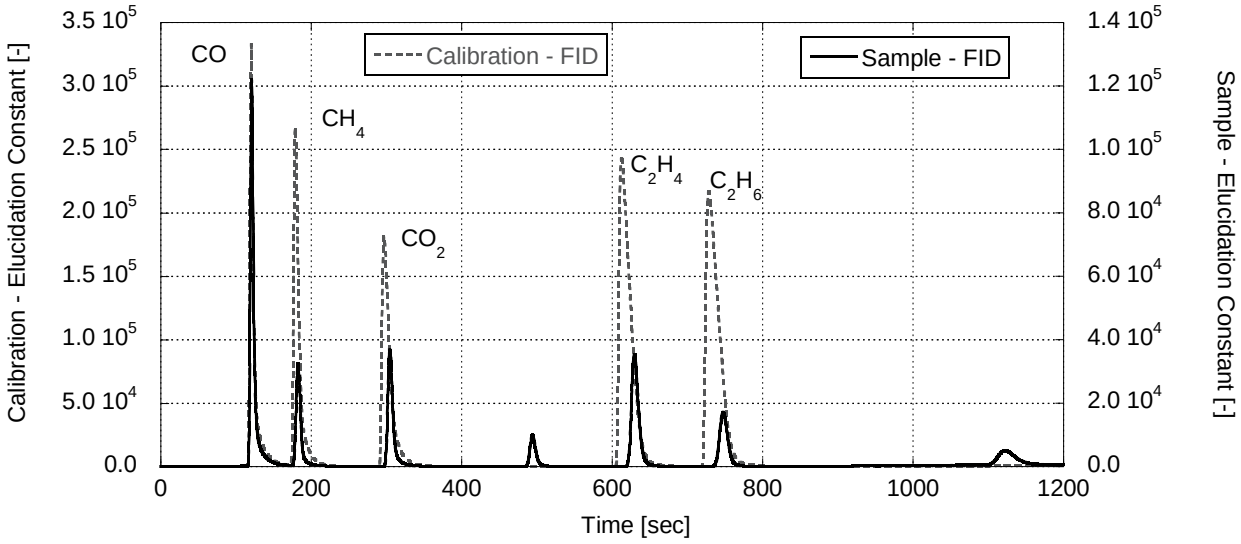

Figure 58 - One load, FID calibration and sampled data

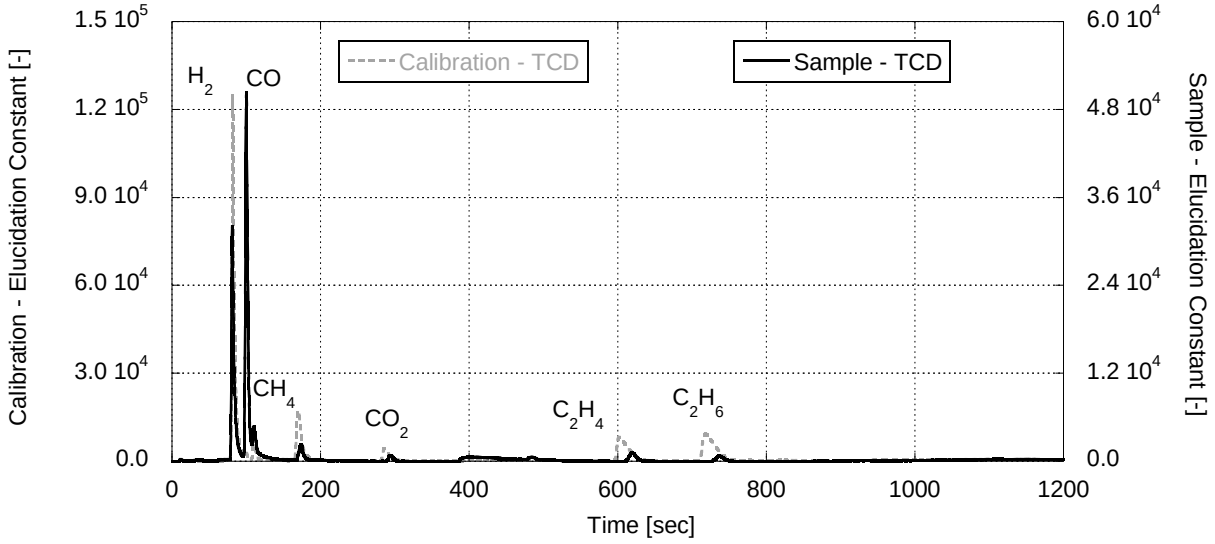

Figure 59 - One load, TCD calibration and sampled data

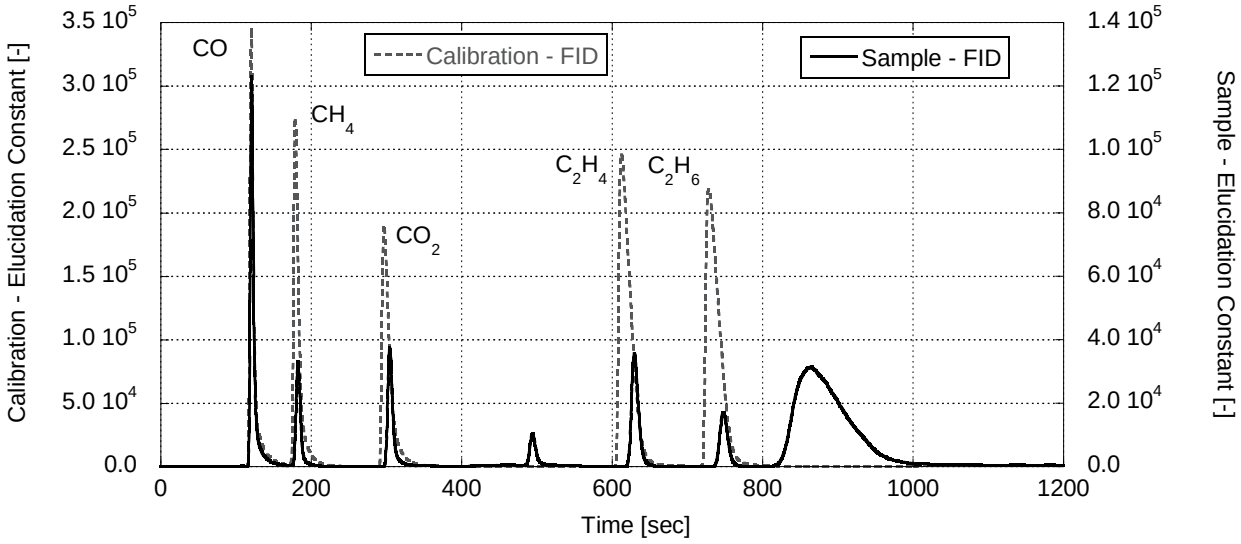

Figure 60 - Two loads, FID calibration and sampled data

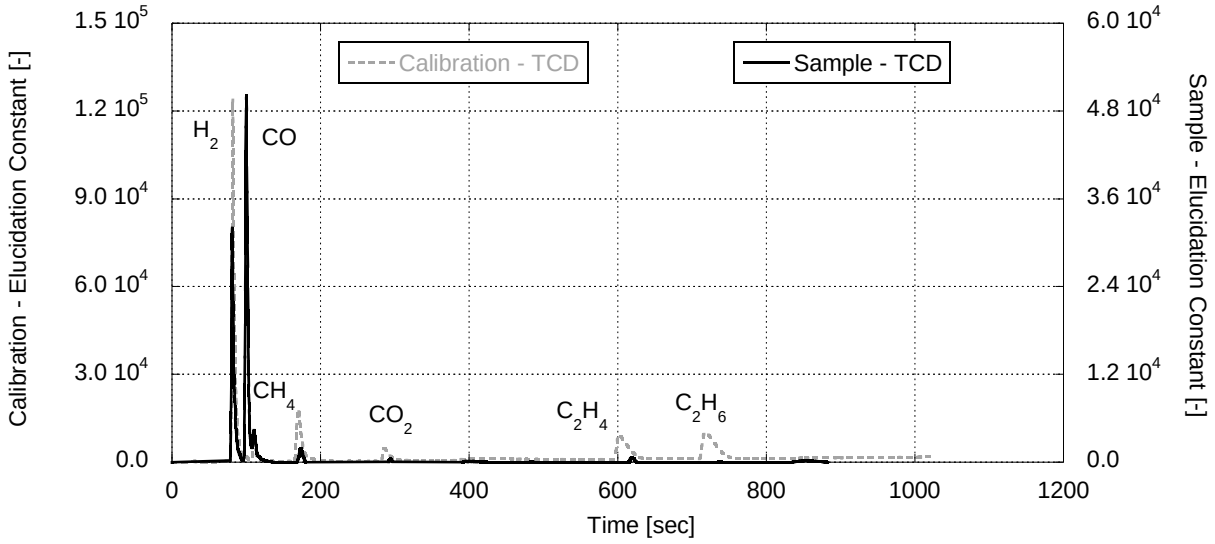

Figure 61 - Two loads, TCD calibration and sampled data

In order for useful calculations to be completed, a calibration gas must first be used to find the baseline elucidation times for gas species being analyzed. Reformed glycerin sample tests were completed using a calibration tank with equal parts hydrogen, carbon monoxide, methane, carbon dioxide, ethane, and ethylene. A septum was placed on the calibration tank valve allowing for samples to be taken using a 250 micro liter syringe. Since the calibration tank contains equal parts by volume, it is known that 41.66 micro liters of each species is injected. Elucidation times were recorded for each of the six species in the calibration tank for both the FID and TCD channels. Figures 56-61 show the plots of elucidation times for three different calibration tests on each channel and three different sample tests on each channel.

The calibration plots for FID and TCD have different peaks which correspond to each of the different gases in the calibration tank. FID plots do not show hydrogen since it is burned while converting all other species to methane for detection. The peaks in the FID plot correspond to carbon monoxide, methane, carbon dioxide, ethylene, and ethane from left to right. The peaks in the TCD plot correspond to hydrogen, carbon monoxide, methane, carbon dioxide, ethylene, and ethane from left to

right. TCD plots are much more sensitive to hydrogen content than any other compound explaining why the first peak (hydrogen) is significantly higher than any other.

A comparison between elucidation times of each species between the sample and calibration plots show additional peaks in the sample tests that correspond to hydrocarbon mixtures that were not present in the calibration tank. Since these specific hydrocarbons are unknown, it is not possible to calculate the quantities of these species in the mixture. The only useful data that can be taken from the sample tests are the volumes of hydrogen, carbon monoxide, methane, carbon dioxide, ethylene, and ethane. The FID plots for all three load settings indicate a peak between carbon dioxide and ethylene that was not present in the calibration tank. It is estimated that this peak corresponds to acetylene, a common hydrocarbon that elucidates after carbon dioxide and before ethylene.

In order to calculate the volume of each of these species in the mixture, numerical integration was completed using the trapezoidal rule for each of the peaks in the calibration and sample plots. The volume of each species could be calculated by multiplying the known volume of each species in the calibration sample (41.66 micro liters) by the ratio of sample area to calibration area for each species. Table 7 presents the results of this calculation.

Table 7 - Gas chromatography results for calibration area, sample area, and volume of each species at all three generator loads.

	Species	Calibration Area	Sample Area	Volume (micro liter)
No Load	Hydrogen	25989.42	11238.18	18.017
	Methane	115219.80	1319.08	0.477
	Carbon Monoxide	99087.90	43831.22	18.431
	Carbon Dioxide	105794.86	22040.42	8.680
	Ethylene	201507.24	19852.12	4.105
	Ethane	204153.68	11191.18	2.284
One Load	Hydrogen	24759.80	12258.62	20.629
	Methane	106776.20	1535.64	0.599

	Carbon Monoxide	107887.44	38672.00	14.935
	Carbon Dioxide	132798.60	19073.40	5.984
	Ethylene	217941.56	19816.62	3.789
	Ethane	220320.00	11117.38	2.103
Two Loads	Hydrogen	26525.22	16900.74	26.548
	Methane	118265.90	12268.08	4.322
	Carbon Monoxide	110893.32	36219.52	13.608
	Carbon Dioxide	117712.50	15223.90	5.388
	Ethylene	225313.04	19615.80	3.628
	Ethane	228571.68	10754.32	1.960

Initial analysis of the results from the GC tests indicates that the volume fraction of the species was lower than expected. For example, the hydrogen result at two loads is only 26.548 micro liters that corresponds to a volume fraction of 0.106 (26.548 micro liter species/250 micro liter injection). These low volume fractions are a result of air in the sample that is not detected by the GC. As a result, the volume of each species must be adjusted to compensate for the air content in the mixture by considering the total area under the curve for both FID and TCD plots. The entire area under the curve for the calibration tests of the FID and TCD plots correspond to 250 micro liters of sample injected. The entire area under the curve for sample tests for FID and TCD plots only account for the species that can be analyzed by the GC (not air). By multiplying the volume of each species by the correlating ratio of entire area of calibration and sample plots, the volume can be adjusted to compensate for air content. For example, the entire area of the TCD calibration plot is 101313 and the area of the corresponding TCD sample plot is 33185.78 for two loads. Hence, multiplying the volume of hydrogen at two loads by this area ratio (101313/33185.78) results in 81.048 micro liters of hydrogen in the sample. This analysis was completed at all loads for each species and the results are shown in Table 8.

Table 8 - Gas chromatography results for species volume, adjusted species volume, and volume fraction at all three generator loads after adjusting for air in the sample.

Species	Volume (micro liter)	Adjusted Volume (micro liter)	Volume Fraction

No Load	Hydrogen	18.017	55.004	0.220
	Methane	0.477	1.588	0.006
	Carbon Monoxide	18.431	61.348	0.245
	Carbon Dioxide	8.680	28.892	0.116
	Ethylene	4.105	13.663	0.055
	Ethane	2.284	7.603	0.030
One Load	Hydrogen	20.629	62.978	0.252
	Methane	0.599	1.994	0.008
	Carbon Monoxide	14.935	49.712	0.199
	Carbon Dioxide	5.984	19.918	0.080
	Ethylene	3.789	12.610	0.050
	Ethane	2.103	6.998	0.028
Two Loads	Hydrogen	26.548	81.048	0.324
	Methane	4.322	14.386	0.058
	Carbon Monoxide	13.608	45.295	0.181
	Carbon Dioxide	5.388	17.934	0.072
	Ethylene	3.628	12.074	0.048
	Ethane	1.960	6.525	0.026

In addition to adjustments made to air content, it is also necessary to compensate for water in the sample. The effluent of the reformer should contain water since carbon dioxide is being produced; i.e., a hydrocarbon-based fuel is being converted, therefore if CO_2 is being produced, H_2O should also be generated. However, it took nearly an hour to transport the sample from the syngas rig to the GC testing lab and perform the sample injections. In this time, the sample cooled to room temperature and the water content condensed in the gas sampling bag (this liquid was noticed by the author). Therefore, the results of Table 8 are presented on a dry basis (no H_2O) and need to be converted to a wet basis (with H_2O) in order to generate proper volume fractions.

The rich combustion reaction of glycerin on a wet basis is written as:

$$(0.8\mathrm{C_3H_8O_3} + 0.2\mathrm{H_2O}) + a(\mathrm{O_2} + 3.76\mathrm{N_2}) \rightarrow b\mathrm{CO_2} + c\mathrm{CO} + d\mathrm{H_2O} + e\mathrm{H_2} + f\mathrm{CH_4} + g\mathrm{N_2} + h\mathrm{C_2H_4} + i\mathrm{C_2H_6} \quad (17)$$

Converting to a wet basis from a dry basis requires the calculation of b, c, d, e, f, g, h, and i. Solving for these variables requires eight equations; the first seven equations that follow are derived from the

initial carbon balance of Equation 17 and the volume fractions as indicated in Table 7 with the two load results provided as an example:

$$\mathrm{C}: (0.8)(3) = b + c + f + h + i \tag{18}$$

$$\mathrm{CO_2}: \frac{b}{b + c + e + f + g + h + i} = .072 \tag{19}$$

$$\mathrm{CO}: \frac{c}{b + c + e + f + g + h + i} = .181 \tag{20}$$

$$\mathrm{H_2}: \frac{e}{b + c + e + f + g + h + i} = .324 \tag{21}$$

$$\mathrm{CH_4}: \frac{f}{b + c + e + f + g + h + i} = .058 \tag{22}$$

$$\mathrm{C_2H_4}: \frac{h}{b + c + e + f + g + h + i} = .048 \tag{23}$$

$$\mathrm{C_2H_6}: \frac{i}{b + c + e + f + g + h + i} = .026 \tag{24}$$

The eighth equation requires a correlation between wet basis combustion products and dry basis. Literature review indicated that this can be accomplished by assuming the H_2O:CO_2 ratio is equal to the H_2:CO ratio [21]:

$$\frac{d}{b} = \frac{e}{c} \tag{25}$$

The solution to these eight equations was found using the Interactive Thermodynamics 3.1 simultaneous equation solver and the wet basis volume fractions are shown in Table 9.

Table 9 – Gas chromatography results for volume fraction on dry and wet basis at all three generator loads and model volume fraction comparisons.

	Species	GC Volume Fraction (Dry)	GC Volume Fraction (Wet)	Model Volume Fraction
No Load	Hydrogen	0.220	0.199	0.293
	Methane	0.006	0.005	0.036
	Carbon Monoxide	0.245	0.222	0.165

	Carbon Dioxide	0.116	0.105	0.123
	Water	-	0.094	0.094
	Ethylene	0.055	0.050	-
	Ethane	0.030	0.027	-
One Load	Hydrogen	0.252	0.229	0.283
	Methane	0.008	0.007	0.074
	Carbon Monoxide	0.199	0.181	0.155
	Carbon Dioxide	0.080	0.073	0.142
	Water	-	0.092	0.096
	Ethylene	0.050	0.045	-
	Ethane	0.028	0.025	-
Two Loads	Hydrogen	0.324	0.287	0.277
	Methane	0.058	0.051	0.092
	Carbon Monoxide	0.181	0.160	0.151
	Carbon Dioxide	0.072	0.063	0.151
	Water	-	0.114	0.097
	Ethylene	0.048	0.043	-
	Ethane	0.026	0.023	-

In addition to water content that condensed in the sample bag, it is possible that some carbon dioxide was also present in the condensation that was not included in the GC analysis. The solubility of carbon dioxide in water at room temperature is 1.45 grams gas per kg liquid water. After considering the small amount of condensation found in the bag it was assumed that the carbon dioxide content present in the water was negligible.

Comparisons between the GC volume fractions of species produced from glycerin reforming and theoretical values from the numerical model are also shown in Table 8. Possible causes for variation between numerical estimates and the GC analysis are: 1) chemical kinetic effects in the reformer are not considered in the equilibrium simulation; 2) a simplistic ambient heat transfer model is used; 3) the conversion of glycerin is a three-phase phenomenon (liquid, gas, and solid interactions); and 4) there is a loss of species due to diffusion from the gas bags to the environment during the sample transport process. Future work can include increasing the accuracy of the model; however, the simplistic model is sufficient for determining approximate values for both the glycerin/water and air flow rates.

4.4 Reformed Glycerin Combustion

Once successful and self-sustaining reformation of the glycerin and water mixture was achieved, the final outcome of this effort was to generate power from the syngas. Recall that successful reformed propane combustion was achieved at no load, one load, and two loads (see Section 3.5.3). Similar to the procedure for using reformed propane as a fuel source, the numerical model was used to estimate the required flow rates of air and glycerin/water to the reformer (Figure 52). In particular, the numerical model predicted that a glycerin/water flow rate between 7 g/s and 10 g/s would achieve the appropriate energy content for nearly any air flow rate at no generator load (aka idle). For one load, the glycerin/water flow rate is estimated to be between 10 g/s and 11 g/s, and for two loads the values are 11.0 g/s and 12.5 g/s. The required energy content found using the engine map was 118.2, 147.9, and 169.2 kW for no load, one load, and two loads, respectively. All of these tests were completed at an engine speed of 1800 RPM with 3.6 kW and 6.5 kW drawn from the generator when one and two heaters (i.e., one load and two loads) were applied, respectively.

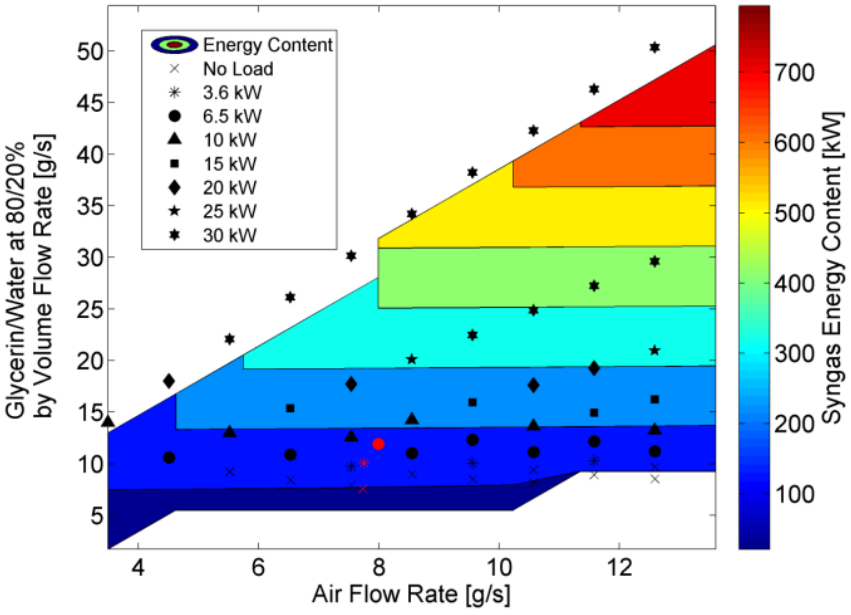

Figure 62 - Syngas energy content and predicted combustion points with successful combustion points indicated in red.

Combustion of reformed glycerin was achieved at idle with a flow rate of glycerin/water and air equal to 7.56 (+/- .97) g/s and 7.73 (+/- .01) g/s, respectively. Of importance, the air flow rate chosen for each test maintained exothermic reformation of the glycerin and water mixture while staying below the sintering temperature of the catalyst. These flow rates correspond to an energy content of 130.0 kW, which was 9.9 % more than theoretically estimated. This deviation is to be expected because of the assumptions employed by the model. Under these conditions, the syngas temperature exiting the reformer was 653.86 +/- 1.53°C.

Following the same methodology as the no load case, at one load and 1800 RPM, engine combustion was achieved at a glycerin/water and air flow rate to the reformer of 10.08 (+/- .98) g/s and 7.75 (+/- .01) g/s, respectively. These flow rates correspond to an energy content of 158.2 kW, 7.0% greater than theoretically predicted with the syngas temperature exiting the reformer at 497.51 +/- 4.29°C. Finally, at a flow rate of 11.91 (+/- 1.03) g/s and 7.99 (+/- .01) g/s for glycerin/water and air, respectively, power generation was achieved with two heaters. The energy content of the syngas when combustion took place with two heaters was 172.1 kW, 1.7% greater than estimated by the model and the syngas temperature exiting the reformer was 376.82 +/- 5.26°C. Figure 62 indicates the reformed glycerin energy content with successful combustion points indicated in red for no load, one load, and two loads.

Table 10 - Technical specifications for REG glycerin used in purified glycerin comparison tests.

Test Parameter	Result	Limits	Units	Test Method
Glycerin Content	97.07	95, min	% Mass	AOCS Ca 14-56/ USP
Methanol Content	0.01	0.1, max	% Mass	AOCS BA 13-87 modified
Water Content	0.54	2.0, max	% Mass	AOCS CA 2e-84
Matter Organic Not Glycerin	2.37	5.0, max	% Mass	Subtracted from 100%
Ash	<0.01	0.3, max	% Mass	AOCS Ca 11-55

pH	4.3	Report	N/A	pH meter
Gardner Color	2	Report	N/A	AOCS Td 1a-64

Table 11 – REG glycerin flow, 99% pure glycerin flow, and percent glycerin flow rate increase for combustion at all three generator loads.

	REG Glycerin / Water Flow (g/s)	Air Flow with REG Glycerin Flow (g/s)	Effluent Temperature with REG (C)	99% Pure Glycerin / Water Flow (g/s)	Air Flow with 99% Glycerin Flow (g/s)	Effluent Temperature with 99% (C)	Glycerin / Water Change (%)
No Load	8.54 (+/- .584)	10.49 (+/- .035)	598.27 (+/- 10.39)	7.56 (+/- .971)	7.73 (+/- .008)	653.86 (+/- 1.53)	11.5
One Load	10.98 (+/- .786)	10.51 (+/- .011)	438.99 (+/- 9.48)	10.08 (+/- .979)	7.75 (+/- .008)	497.51 (+/- 4.29)	8.2
Two Loads	12.49 (+/- 1.15)	10.57 (+/- .023)	335.95 (+/- 2.14)	11.91 (+/- 1.031)	7.99 (+/- .010)	376.82 (+/- 5.26)	4.64

Additional testing was completed using a lower grade glycerin (technical specifications in Table 10) acquired directly from Renewable Energy Group (REG), a biodiesel manufacturer. The purpose of these tests was to validate the methodology of using a glycerin feedstock source that comes directly from a biodiesel plant. The glycerin supplied by REG has been refined in the plant in order to remove some of the impurities (e.g., left over potassium hydroxide) and methanol in crude glycerin. However, they have not taken the distillation process all the way to a food-grade product since this can be energy intensive. Data points were taken at all three generator loads (no load, 3.6 kW, and 6.5 kW) with the flow rates to the reformer found in Table 11 along with the percent change of required glycerin from the initial food-grade tests. Similar to before, an 80/20% glycerin/water mixture by volume was used with the REG glycerin.

It was found that in order for engine combustion to take place, the glycerin/water and air flow rates needed to be increased for the lower grade glycerin. This is partly because the impurities in the REG glycerin (e.g., methanol) influence the conversion process to hydrogen. In addition, extra air was supplied to the reformer while testing REG glycerin in order to attempt to compensate for different ambient conditions. In specific, the ambient air was 21°C cooler while testing REG glycerin. Therefore,

the author attempted to increase the reformer temperature in order to try and maintain consistency between the tests. However, there was still a significant difference as the temperature exiting the reformer for the 99% pure glycerin tests and REG glycerin tests were 653.86 +/- 1.53°C and 598.27 +/- 10.39°C, respectively at no load. Therefore, future work should target testing food grade and the lower grade glycerin on the same day.

4.5 In-cylinder Pressure and Emissions Analysis

In order to further analyze the food-grade reformed glycerin/water power generation tests, in-cylinder pressure traces were taken along with exhaust emission species and compared to that of pure propane combustion. The in-cylinder pressure traces serve as a methodology to compare combustion timing and flame propagation speed between syngas and propane. Whereas, measurement of emissions species provides insight into complete combustion and fuel consumption.

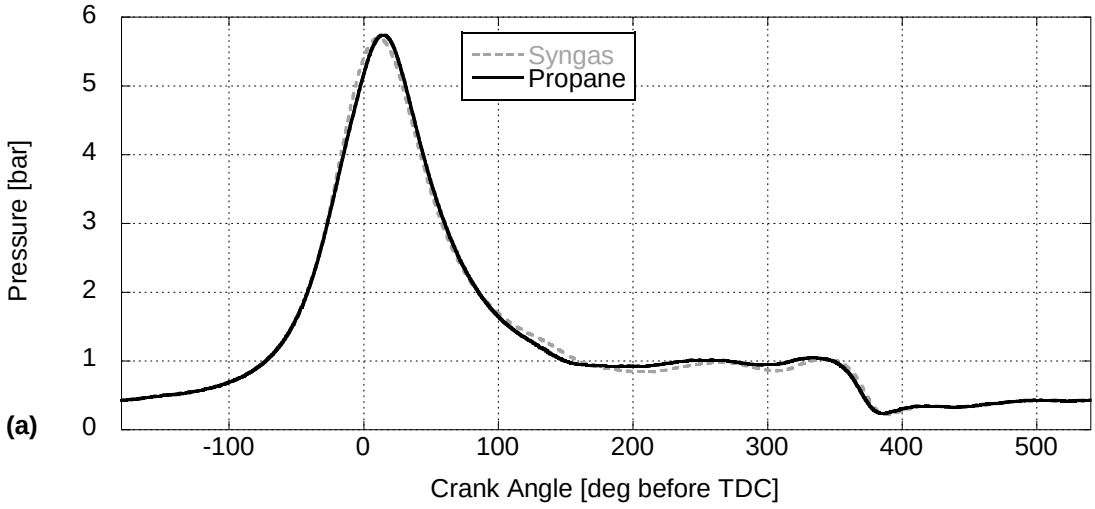

(a)

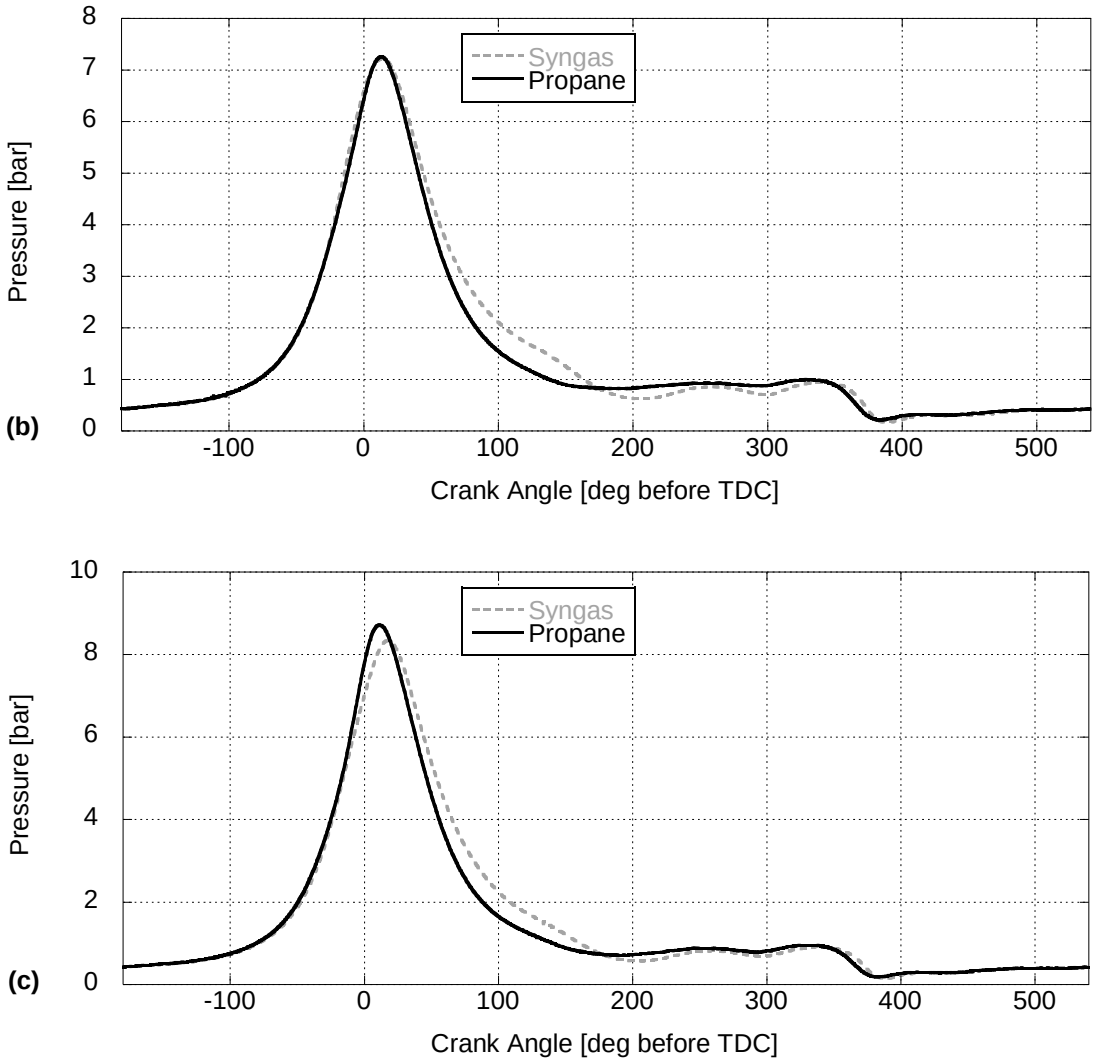

Figure 63 - In cylinder pressure comparison at (a) no load, (b) one load, and (c) two loads.

Figure 63 indicates that the pressure traces between pure propane and reformed glycerin combustion look relatively similar with R^2 values of 0.998, 0.993 and 0.988 at no load, one load, and two loads, respectively. In regards to the peak pressure and combustion speed, syngas follows propane closely even though a portion of the syngas (e.g., CO_2 and H_2O) acts as Exhaust Gas Recirculation (EGR). This EGR slows the combustion process by acting as a diluent in the mixture [23] (recall from Chapter 3 that the external EGR system on the engine was disengaged). However, the high hydrogen concentration in the syngas promotes a greater mixture laminar flame speed and faster flame propagation [21]. There is some noticeable difference at the highest power loading case. This is believed

to be due to syngas having a lower overall Lower Heating Value than propane (e.g., 29.20 vs. 46.35 MJ/kg at this load), requiring more fuel in order to make up the energy difference. Hence, the combination of added EGR and the need to burn more fuel results in a longer combustion process. Of note, spark timing was not changed between the two different fuels in order to provide a direct comparison without the influence of combustion timing.

A Semtech DS gaseous portable emission analyzer was used to monitor multiple different emissions produced during combustion. The Semtech system is capable of measuring five different emissions: carbon monoxide (CO), carbon dioxide (CO_2), total hydrocarbons (HC), nitrogen monoxide (NO), and nitrogen dioxide (NO_2). The combination of NO and NO_2 emissions are used to calculate the overall nitrogen oxides produced (NO_x). Since the NO_2 emissions found are significantly lower than the NO emissions (ratio of 0.005:1, respectively), the NO_x results presented later are largely only a function of NO emissions. This is to be expected for spark ignition engines [23]. A heated emissions line was placed in the engine exhaust and the analysis of emissions was completed for pure propane and reformed glycerin/water combustion under all loads tested.

At the beginning of each test, after starting the Semtech system a species calibration was completed using six bottled gas tanks. After calibration, experimental data was recorded at each load setting for five minutes with a data point taken every second. After testing was finished, the calibration process was repeated using the same bottled gas tanks in order to ensure that all recorded values of emissions were still within the initial calibration range. Every emission species passed the final calibration test except for carbon monoxide which required a calibration to ambient air. During the final calibration process, the reformer was purging excess reformed glycerin/water to the environment through the exhaust while cooling down. It is assumed that the relatively high levels of carbon monoxide content from the reformed glycerin/water caused the final calibration test to fail.

After completing all of the tests, data files were created for post-processing and further analysis. The Semtech system stores all of the results in a text file with each species concentration recorded. Semtech post-processing software is capable of calculating the fuel specific emissions for each species depending on the fuel used for combustion. The software requires the molecular formula, as well as its specific gravity of the combustion fuel for automatic fuel specific emission calculations. The molecular formula and specific gravity of propane (C_3H_8 and 1.522, respectively) are readily available. However, these values are unknown for the syngas necessitating the requirement of manual calculations by the author. Accompanying manual calculations for propane combustion emissions provide a methodology to verify the accuracy of the author's results.

In order to express the fuel specific emissions in grams of pollutant (g_{Sample}) per grams of fuel (g_{fuel}), the mole fraction of the pollutant to the fuel burned is computed. This is simply the ratio of the measured concentration of pollutant to the sum of the CO, HC, and CO_2 concentrations in the exhaust, which reflect the number of moles of fuel that is consumed per mole of exhaust. Then, the mass fraction of each pollutant to fuel burned is computed by multiplying the mole fraction by the ratio of the molecular weights of the pollutant to that of the fuel. This results in the following equation that was used to calculate the fuel specific emission values for propane and reformed glycerin/water engine exhaust:

$$Sample_{fs}\left(\frac{g_{Sample}}{g_{fuel}}\right)=\left(\frac{[Sample]}{[\mathrm{CO}]+[\mathrm{THC}]+[\mathrm{CO_2}]}\right)\left(\frac{MW_{Sample}}{MW_{fuel}}\right) \tag{26}$$

In this equation, $[Sample]$ refers to the concentration of the specific species being analyzed, $[\mathrm{CO}]$, $[\mathrm{THC}]$, and $[\mathrm{CO_2}]$ refer to the concentration of carbon monoxide, hydrocarbons, and carbon dioxide respectively, and MW refers to the molecular weight of the sample species and the fuel being used.

Equation 26 was first used to verify the accuracy of the Semtech post processing software for carbon dioxide during pure propane combustion. The values for propane's chemical formula and specific

gravity were entered into the software and the fuel specific value of carbon dioxide was found to be 1000.2 g CO_2/kg fuel. This was compared to the manually calculated value of 996.6 g CO_2/kg fuel indicating a 0.3% variation. In order to apply Equation 26 to reformed glycerin combustion emissions, the molecular weight of the fuel must be known. The flow rates of air and glycerin/water to the reformer were recorded during the Semtech testing and used with the numerical model described in Section 4.1. The model estimated that the molecular weight of the syngas at no load, one load, and two loads were 20.99, 21.08, and 21.13 g/mol, respectively. Results of the fuel specific emissions are shown in Table 12.

Table 12 - Emissions on a g/g_{fuel} basis with standard deviation indicated in parenthesis.

	Propane				Glycerin/Water			
	CO_2	CO	HC	NO_x	CO_2	CO	HC	NO_x
No Load	1000.177 (.246)	0.411 (.043)	0.833 (.227)	0.934 (.017)	863.017 (28.388)	81.976 (18.009)	9.265 (.320)	0.008 (.004)
One Load	1000.083 (.048)	0.434 (.032)	0.848 (.011)	2.021 (.029)	628.650 (13.276)	231.265 (8.445)	8.854 (.033)	0.098 (.016)
Two Loads	998.916 (.158)	0.573 (.040)	1.683 (.115)	3.687 (.053)	592.950 (12.697)	253.948 (8.078)	8.935 (.027)	0.143 (.013)

Comparing the results of the Semtech emissions analysis first requires calculating the A/F ratio of propane and glycerin/water for the recorded tests. The stoichiometric A/F ratio of propane was calculated as 15.6 in Section 2.2.2. A similar calculation can be completed to find the stoichiometric A/F ratio for the glycerin/water mixture. The experimental flow rates of glycerin/water and air used to produce the syngas for combustion were used with the numerical model to calculate the species produced from reformation at all loads. These species can be used in a stoichiometric balance to find the amount of air that would result in complete syngas combustion. Equation 27 is used for complete combustion of the reformed glycerin/water:

$$(0.8C_3H_8O_3 + 0.2H_2O) + 2.8(O_2 + 3.76N_2) \rightarrow 2.4CO_2 + 3.4H_2O + 10.528N_2 \quad (27)$$

Completing the molar balance of this equation shows that for every mol of glycerin/water provided, 13.328 moles of air are required. Using the molar weight of glycerin/water and air (77.2 g/mol and 28.97 g/mol, respectively) the mass air to fuel ratio (A/F) of 5.001 can be found for stoichiometry (i.e., perfect combustion). Next, the recorded values of fuel and air flow rates for both the propane and glycerin/water tests are used to find the experimental A/F ratio. The equivalence ratio (ϕ) can then be calculated by dividing the stoichiometric A/F ratio by the experimental A/F ratio. An equivalence ratio greater than one corresponds to rich combustion (deficient oxygen) and an equivalence ratio less than one corresponds to lean combustion (excess oxygen). Table 13 shows the A/F ratio and equivalence ratio for propane and glycerin/water at all generator loads.

Table 13 - Air to fuel ratio and equivalence ratio for propane and glycerin/water at all generator loads.

	Propane			Glycerin/Water		
	$(A/F)_s$	A/F	ϕ	$(A/F)_s$	A/F	ϕ
No Load	15.60	15.19	1.027	5.001	3.222	1.552
One Load	15.60	15.18	1.028	5.001	3.096	1.615
Two Loads	15.60	15.21	1.026	5.001	3.047	1.641

Analysis of the results shows that propane combustion is achieved near stoichiometry as intended. The initial efforts by the previous student working on this project dialed in the flow rates and adjusted the Woodward Air-to-Fuel and Throttle Valves in order to achieve stoichiometry for propane [47]. As a result, the combustion of the syngas resulting from the reformation of glycerin/water is significantly rich. This is because the large disparity between the air-to-fuel ratios between the two fuels should require adjustment of the these valves; i.e., 15.6 versus 5.001. Therefore, carbon monoxide and hydrocarbon emissions are significantly higher for glycerin/water combustion, as indicated in Table 12, because there is not sufficient oxygen to complete combustion. Additionally, the carbon dioxide emissions are lower for glycerin/water combustion since the carbon was not fully converted to CO_2.

Finally, NO_x emissions are lower for glycerin/water combustion due to the lack of air needed for the NO_x dissociation reactions and the additional components in the syngas acting as EGR. EGR is a diluent that reduces the combustion temperature, subsequently decreasing the production of NO_x through the thermal NO mechanism. These results all follow well-established trends with equivalence ratio [21].

In order to more efficiently burn the syngas in the engine, adjustments should be made in order to achieve stoichiometric combustion. The current setup does not link the throttle valve to the LabVIEW program controlling combustion. Purchasing a new throttle valve that is capable of dynamic changes to A/F ratios and coupling to LabVIEW during testing would help solve the issue of rich syngas combustion. Moreover, a lambda sensor should be placed in the exhaust line in order to monitor oxygen content. This can be linked to the throttle valve in LabVIEW in order to provide closed-loop feedback control.

4.6 Application with Biodiesel Production

As biodiesel production continues to increase worldwide, the levels of waste glycerin will grow. Some large-scale biodiesel production facilities have the capabilities to sell the glycerin after extensive purification, but this option can be energy intense and costly. A decreasing cost of crude glycerin has created concerns with its viability as a commodity for the biodiesel industry. Additionally, many smaller biodiesel facilities are required to pay to have the waste glycerin removed, further diminishing the economic benefits of biodiesel. One option to utilize the waste glycerin is to couple the synthesis gas generator rig directly with the production of biodiesel.

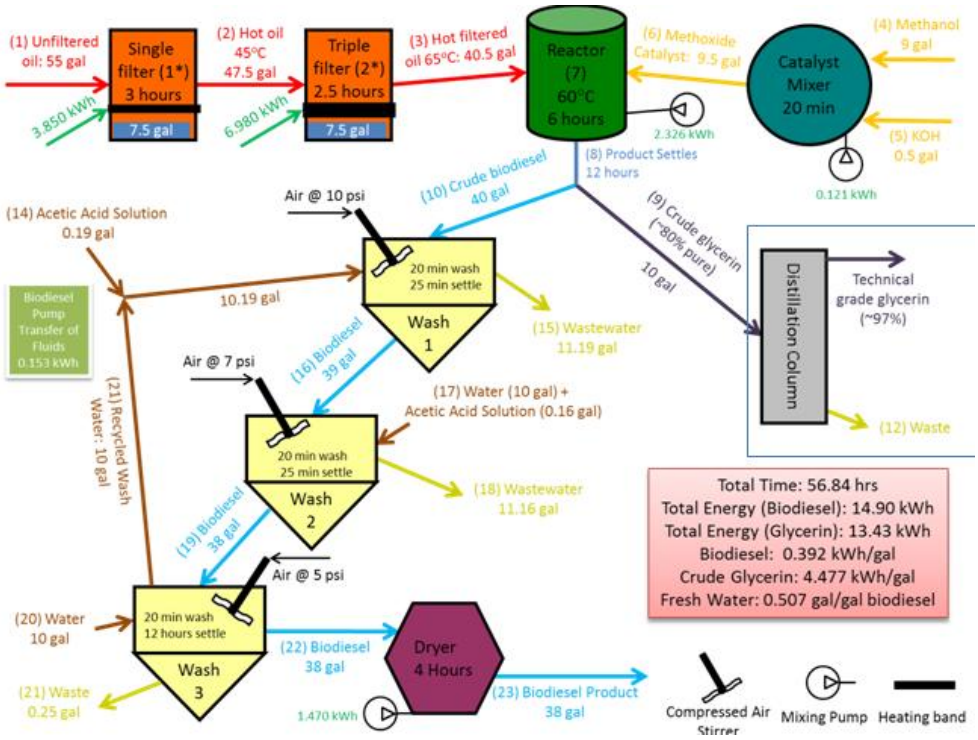

Figure 64 - Power requirements for the entire biodiesel production process at the University of Kansas

In order to determine the size of a biodiesel production facility that can be powered by the glycerin reformation setup, one must analyze a biodiesel production process in order to determine the energy requirements. At the University of Kansas, students run a biodiesel production facility (KU Biodiesel Initiative) that converts the waste cooking oil on campus into biodiesel and crude glycerin as illustrated in Figure 64. Current efforts are underway at installing a distillation column in order to purify the glycerin to technical grade quality, similar to the glycerin supplied by REG used in this effort. Each stage of the biodiesel production process is indicated in Table 14 with the energy required and time at each stage. The continuous energy requirements of each stage were calculated by dividing the energy used by the time at each stage.

Table 14 – Energy requirements and glycerin/water flow rates at each stage of the biodiesel production process.

Phase	Energy Used [kWh]	Time [hr]	Continuous Energy Needed [kW]	Glycerin Flow Rate [gal/hr]	Glycerin Required [gal]
Oil Filter Stage 1	3.850	3.000	1.283	4.285	12.855
Oil Filter Stage 2	6.980	2.500	2.792	4.641	11.603
Reactor Pump	2.326	6.000	0.388	4.075	24.450
Catalyst Mixer Pump	0.121	0.333	0.363	4.069	1.356
Fluid Transfer Pumps	0.153	1.000	0.153	4.019	4.019
Dryer Pump	1.470	4.000	0.368	4.070	16.280
Total	14.900				70.563

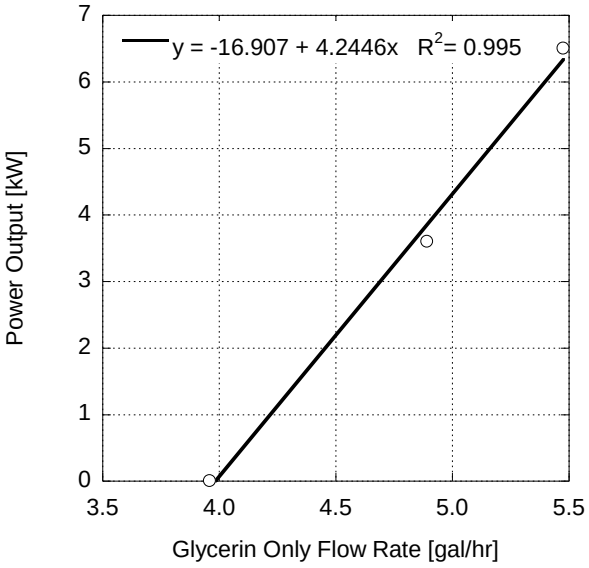

Figure 65 - Extrapolation of energy production as a function of optimized glycerin/water flow rate.

Using the flow rates of glycerin/water and power generation from the REG tests in Section 4.4 (most applicable to this direct plant coupling) and calculating the glycerin only component removing water from the analysis, a trend line of power versus glycerin only flow rate was determined in Figure 65. It is important to note that these flow rates were adjusted using the equivalence ratio calculations (i.e., flow rates divided by equivalence ratio) from Section 4.5 in order to indicate the best case scenario

of minimum glycerin usage for complete combustion. The trend line equation was then used to calculate the required glycerin flow rate to provide continuous energy to complete each phase of the biodiesel production process.

As the results indicate in Table 14 in comparison to Figure 64, approximately seven times the available glycerin is needed in order to produce the required power for the biodiesel production process. While optimization of the entire system and energy recovery of the waste heat from the engine will be studied in order to help heat the oil reactor, it is expected that more glycerin is needed than can be supplied in a continuous manner at a plant. However, the unique setup employed does allow for the replacement of propane to the reformer with (currently) inexpensive natural gas. Therefore, future efforts are targeted at optimizing the hydrogen emanating from the reformer using natural gas, glycerin, and even a hybrid natural gas/glycerin reformer. Of note, nickel is a preferred catalyst for natural gas reforming [48]. This will allow the biodiesel production facility to utilize two low cost feedstocks as a function of availability.

4.7 Conclusion

As petroleum prices continue to rise, alternative energy solutions are becoming much more widely used. Biodiesel is one alternative energy source that has dramatically risen in the last several years. In order for biodiesel to become an alternative to petroleum, an analysis of its economic uses is essential. Utilizing the waste byproduct of biodiesel production greatly improves its economic viability. The unique setup at the University of Kansas converts the waste glycerin from biodiesel production into a hydrogen rich synthesis gas for combustion in an engine generator system. This system helps recover some of the energy needed to produce biodiesel. This thesis describes the details behind the operation and testing of the synthesis gas generator system.

The second chapter gave a complete description of the synthesis gas generator rig and all of the important components. Additionally, an operating manual was provided that details the procedure for

pure propane combustion in the engine, propane reformation and its subsequent combustion and glycerin/water reformation and its subsequent combustion. The operating procedure of the rig also contained information for data acquisition for post processing and analysis.

The third chapter provided a literature review of glycerin reformation. This chapter also detailed the production of the numerical model used for propane reforming. Engine tests were completed to find the baseline fuel requirements to operate the engine at different load settings. Successful combustion of reformed propane provided a proof of concept test and led to calibration methods for glycerin/water reformation by calculating the heat transfer coefficient for the reformer.

The fourth chapter discussed the literature review regarding the catalytic material preparation for the reformer and the production of the catalyst. The numerical model was then adjusted for glycerin/water mixtures through an iterative procedure using the heat transfer calculations from the previous chapter. Results from the numerical model were compared to gas chromatography tests completed at all of the possible load settings of the reformer. Combustion of reformed glycerin/water was then completed for power generation at all three loads. Analysis of the emissions produced from pure propane and reformed glycerin/water combustion was completed using a Semtech DS portable emissions analyzer. Results of the emissions tests indicated that reformed glycerin/water combustion occurs in a rich environment and will need to be adjusted for future tests. Finally, an extrapolation of the combustion results provided a useful application of the work with biodiesel production.

References

[1] *International Energy Outlook 2010.* DOE/EIA; Energy Information and Administration: Washington, D.C.

[2] C. Carraretto, A. Macor, A. Mirandola, A. Stoppato, S. Tonon
Biodiesel as alternative fuel: experimental analysis and energetic evaluations Energy, 29 (2004), pp. 2195–2211

[3] Yusuf, N.N.A.N., S.K. Kamarudin, and Z. Yaakub, *Overview on the current trends in biodiesel production.* Energy Conversion and Management, 2011. **52**(7): p. 2741-2751.

[4] *Regulation of Fuels and Fuel Additives: Changes to Renewable Fuel Standard Program; Final Rule*, E.P. Agency, Editor March 26, 2010, Federal Register. p. 14669-15320.

[5] Greene, D. L., J. L. Hopson, et al. (2006). "Have we run out of oil yet? Oil peaking analysis from an optimist's perspective." Energy Policy 34(5): 515-531.

[6] FAO – Food and Agriculture Organization of the United Nations, 2007. Bioenergy Growth Must be Carefully Managed.

[7] Janaun, J. and N. Ellis, *Perspectives on biodiesel as a sustainable fuel.* Renewable & Sustainable Energy Reviews, 2010. **14**(4): p. 1312-1320.

[8] Araujo, V. K. W. S., S. Hamacher, et al. (2010). "Economic assessment of biodiesel production from waste frying oils." Bioresource Technology **101**(12): 4415-4422

[9] C. Carraretto, A. Macor, A. Mirandola, A. Stoppato, S. Tonon. (2004) “Biodiesel as alternative fuel: experimental analysis and energetic evaluations.” Energy, 29: 2195–2211.

[10] Stelmachowski, M., *Utilization of Glycerol, a By-Product of the Transestrification Process of Vegetable Oils: A Review.* Ecological Chemistry and Engineering, 2011. **18**(1): p. 9-30.

[11] Gui, M.M., K.T. Lee, and S. Bhatia, *Feasibility of edible oil vs. non-edible oil vs. waste edible oil as biodiesel feedstock.* Energy, 2008. **33**(11): p. 1646-1653.

[12] Ahmad, S., D. Papadias, *Hydrogen from Glycerol: A feasibility Study*, U.S.D.o. Energy, Editor 2010: http://www.hydrogen.energy.gov/pdfs/review10/pd003_ahmed_2010_o_web.pdf.

[13] Chiu, C.-W., et al., *Removal of Residual Catalyst from Simulated Biodiesel's Crude Glycerol for Glycerol Hydrogenolysis to Propylene Glycol.* Industrial & Engineering Chemistry Research, 2005. **45**(2): p. 791-795.

[14] Werpy, T., Petersen, G., Aden, A., Bozell, J, Holladay, J, White, J., Manheim, Amy, Elliot, D., Lasure, L. Jones, S., Gerber, M., Ibsen, K., Lumberg, L., and Kelley, S., *Top Value Added Chemicals from Biomass: Volume 1 - Results of Screening for Potential Candidates from Sugars and Synthesis Gas*, U.S.D.o.E.E.E.a.R. Energy, Editor 2004.

[15] Pandey, R. K., A. Rehman, et al. (2012). "Impact of alternative fuel properties on fuel spray behavior and atomization." Renewable and Sustainable Energy Reviews 16(3): 1762-1778.

[16] Zhang, Y., et al., (2003) “Biodiesel production from waste cooking oil: 1. Process design and technological assessment.” Bioresource Technology, 89(1): 1-16.

[17] Kinoshita, E., et al., (2004) “Combustion Characteristics for Diesel Engines with Emulsified Biodiesel Without Adding Emulsifier.”

[18] Crnkovic, P. M., C. Koch, et al. (2012). "Determination of the activation energies of beef tallow and crude glycerin combustion using thermogravimetry." Biomass and Bioenergy 44(0): 8-16

[19] Bohon, M. D., B. A. Metzger, et al. (2011). "Glycerol combustion and emissions." Proceedings of the Combustion Institute 33(2): 2717-2724.

[20] Özgür, D.Ö. and B.Z. Uysal, (2011) “Hydrogen production by aqueous phase catalytic reforming of glycerine.” Biomass & Bioenergy. 35(2): 822-826.

[21] Cecrle, E., et al., (2012) “Analysis of the effects of reformate (hydrogen/carbon monoxide) as an assistive fuel on the performance and emissions of used canola-oil biodiesel.” International Journal of Hydrogen Energy. 37(4): 3510-3527.

[22] Lin, Y.-C. (2013). "Catalytic valorization of glycerol to hydrogen and syngas." International Journal of Hydrogen Energy **38**(6): 2678-2700.

[23] Heywood, J.B., (1988) “Internal combustion engine fundamentals.”

[24] Cecrle, E., C. Depcik, et al. (2012). "Investigation of the Effects of Biodiesel Feedstock on the Performance and Emissions of a Single-Cylinder Diesel Engine." Energy & Fuels 26(4): 2331-2341.

[25] FAO – Food and Agriculture Organization of the United Nations, 2007. “Bioenergy Growth Must be Carefully Managed.”

[26] Araujo, V. K. W. S., S. Hamacher, et al. (2010). "Economic assessment of biodiesel production from waste frying oils." Bioresource Technology 101(12): 4415-4422.

[27] Nichele, V., et al., (2012) “Glycerol steam reforming for hydrogen production: Design of Ni supported catalysts.” Applied Catalysis B: Environmental. 111-112: 225-232.

[28] Wang, X., et al., (2010) “Hydrogen production by glycerol steam reforming with/without calcium oxide sorbent: A comparative study of thermodynamic and experimental work.” Fuel Processing Technology. 91(12): 1812-1818.

[29] Sehested, J., J. A. P. Gelten, et al. (2004). "Sintering of nickel steam-reforming catalysts: effects of temperature and steam and hydrogen pressures." Journal of Catalysis 223(2): 432-443.

[30] Bottino, A., et al., (2006) “Steam reforming of methane in equilibrium membrane reactors for integration in power cycles.” Catalysis Today. 118(1/2): 214-222.

[31] Adhikari, S., S.D. Fernando, and A. Haryanto, (2009) 'Hydrogen production from glycerol: An update." Energy Conversion and Management. 50(10): 2600-2604.

[32] Yang, G., et al., (2011) "Thermodynamic analysis of hydrogen generation via oxidative steam reforming of glycerol." Renewable Energy: An International Journal. 36(8): 2120-2127.

[33] Authayanun, S., et al., (2010) "Thermodynamic study of hydrogen production from crude glycerol autothermal reforming for fuel cell applications." International Journal of Hydrogen Energy. 35(13): 6617-6623.

[34] Glenn Research Center, NASA Chemical Equilibrium with Applications, http://www.grc.nasa.gov/WWW/CEAWeb/

[35] Chen, T., W. G. Wang, et al. (2011). "Evaluation of carbon deposition behavior on the nickel/yttrium-stabilized zirconia anode-supported fuel cell fueled with simulated syngas." Journal of Power Sources **196**(5): 2461-2468.

[36] Dou, B., et al., (2010) "Steam reforming of crude glycerol with in situ CO2 sorption." Bioresource Technology. 101(7): 2436-2442.

[37] Gutiérrez Ortiz, F. J., P. Ollero, et al. (2011). "Thermodynamic study of the supercritical water reforming of glycerol." International Journal of Hydrogen Energy **36**(15): 8994-9013.

[38] Cheng, C. K., S. Y. Foo, et al. (2011). "Steam reforming of glycerol over Ni/Al2O3 catalyst." Catalysis Today **178**(1): 25-33.

[39] Liu, Y., R. Farrauto, et al. (2013). "Autothermal reforming of glycerol in a dual layer monolith catalyst." Chemical Engineering Science 89(0): 31-39.

[40] Cheng, C. K., S. Y. Foo, et al. (2010). "H2-rich synthesis gas production over Co/Al2O3 catalyst via glycerol steam reforming." Catalysis Communications **12**(4): 292-298.

[41] Cheng, C. K., S. Y. Foo, et al. (2011). "Carbon deposition on bimetallic Co–Ni/Al2O3 catalyst during steam reforming of glycerol." Catalysis Today **164**(1): 268-274.

[42] Pompeo, F., G. Santori, et al. (2010). "Hydrogen and/or syngas from steam reforming of glycerol. Study of platinum catalysts." International Journal of Hydrogen Energy **35**(17): 8912-8920.

[43] Chiodo, V., S. Freni, et al. (2010). "Catalytic features of Rh and Ni supported catalysts in the steam reforming of glycerol to produce hydrogen." Applied Catalysis A: General **381**(1–2): 1-7.

[44] Iriondo, A., V. L. Barrio, et al. (2010). "Glycerol steam reforming over Ni catalysts supported on ceria and ceria-promoted alumina." International Journal of Hydrogen Energy **35**(20): 11622-11633.

[45] Wang, S. and G. Q. Lu (1998). "Reforming of methane with carbon dioxide over Ni/Al2O3 catalysts: Effect of nickel precursor." Applied Catalysis A: General **169**(2): 271-280.

[46] Kim, P., H. Kim, et al. (2006). "Effect of nickel precursor on the catalytic performance of Ni/Al2O3 catalysts in the hydrodechlorination of 1,1,2-trichloroethane." Journal of Molecular Catalysis A: Chemical **256**(1–2): 178-183.

[47] Cecrle, E.D., *Controls and Measurements of KU Engine Test Cells for Biodiesel, SynGas, and Assisted Biodiesel Combustion*, in *Mechanical Engineering*. 2011, University of Kansas: Lawrence, Kansas.

[48] Bartholomew, C. and R. Farrauto, *Fundamentals of Industrial Catalytic Processes*2006, Hoboken, NJ: John Wiley and Sons.